

# Fault and Fracture Networks in the Otway Basin, Victoria; Implications for Structural Permeability

Thesis submitted in accordance with the requirements of the University of  
Adelaide for an Honours Degree in Geology

Joshua Matthew Sage  
November 2013



THE UNIVERSITY  
*of* ADELAIDE

## **ABSTRACT**

Over 1900 naturally occurring fractures were recorded in the field, from outcrop of the Eumeralla Formation in the Otway Basin, Victoria, Australia. Two distinctive fracture sets were identified with strike orientations of N-S and NE-SW. Natural fractures were further characterised as open or closed. A total of 623 open fractures in two dominant sets were observed at surface, with mean strikes of N-S and WNW-ESE. A total of 892 closed fractures (generally cemented) in two dominant sets were also observed at surface, also with mean strikes of N-S and WNW-ESE. Further investigation showed that despite a majority of fractures being optimally aligned with the present-day stress field, they remained closed.

Six discrete fracturing events were interpreted in total; Two Cretaceous bedding perpendicular Mode 1 sets; a late Cenozoic vertical Mode 1 set; a late Cenozoic bedding parallel set; a Miocene continuous crack-seal related set; and finally an Early Cretaceous Fault related set, reactivated during the Miocene.

Thin sections revealed multiple generations of fracture cement inferring a crack-seal history or that mineral cement renders the fractures stress insensitive. Failure of fractures to reactivate and remain open to fluid flow in the favourable stress conditions of the Otway Basin has potential to adversely affect and limit the secondary permeability of the system. This also validates the hypothesis that the in-situ stress regime is not always the dominant factor in the propensity for a fracture to be open to fluid flow.

## **KEYWORDS**

Otway Basin, structural permeability, Eumeralla Formation, fracture mechanics, fault.

**TABLE OF CONTENTS**

Abstract.....	1
Keywords.....	1
List of Figures and Tables .....	4
Introduction .....	8
Background.....	10
Geological Setting .....	10
Diagenesis.....	16
Geomechanical Background.....	17
Stress Field Direction .....	17
Horizontal and Vertical Stress Magnitudes .....	18
Pore Pressures.....	19
Rock Strength (Host Rock and Fracture Fill).....	20
Mechanical Stratigraphy.....	21
Methods .....	22
Observations and Results .....	23
Fracture Orientations at Field Sites in the Otway Basin .....	26
Moonlight Head.....	26
Castle Cove.....	26
Cape Otway .....	26
Crayfish Bay.....	27
Marengo.....	27
Skenes Creek .....	27
Wongarra .....	27
Smythes Creek.....	27
Cape Patton.....	28
Cumberland River .....	28
Lorne.....	28
Satellite Comparison .....	28
Fracture Fills and Porosity in the Otway Basin from Thin Section Microscopy .....	31
Mechanical Stratigraphy and Variations in Lithology .....	34
Discussion.....	41
Variation in Fracture Patterns around Local Structures .....	41
Fold at Cape Otway and Associated Fracture Pattern .....	41
Fracture Orientations across the Wild Dog Shear Zone .....	44
Fractures Associated with the Castle Cove Fault .....	46

General Field Trends of Fracture Sets .....	49
Tilt Corrected Fracture Sets.....	49
Implications of Fractures in the Otway Basin: From Past to Present.....	51
Mechanical Stratigraphy of the Eumeralla Formation .....	51
Fracture Generation History .....	52
Implications for Structural Permeability .....	55
Conclusions .....	64
Acknowledgments .....	66
References .....	67
Appendix A: Extended Methods .....	72
Field Mapping .....	72
Structural Data Collection .....	77
Structural Analysis .....	77
Structural Permeability .....	84
Slide Preparation .....	86
Petrology.....	87
Porosity.....	90
Wyllie Time Average Calculations .....	93
Appendix B: Face Maps and transects .....	94
Appendix C: Satellite Images .....	115
Marengo.....	116
Skenes Creek .....	117



**LIST OF FIGURES AND TABLES**

Figure 1. Location map of the Otway Basin, Victoria, Australia. Locations of wells referred to in this study are also shown (Olangolagh-1, Minerva-1 and Bellarine-1).... 12

Figure 2. Stratigraphic column for the Otway Basin (after Krassay *et al.* (2004)), including lithostratigraphy (Geary & Reid 1998) and basin phases and super-sequences (Krassay *et al.* 2004)..... 13

Figure 3. Three-dimensional Mohr Diagram with Griffith-Coulomb failure envelope overlain, showing possible fracture planes within the stress regime and the associated change in pore pressure ( $\Delta P_p$ ) required for that plane to fail (after Dewhurst *et al.* 2002). The position of the fracture plane (solid black circle in the grey shaded area) is dependent on the relative orientation of the plane and the principle stresses. The change in pore pressure is used to determine the propensity for that plane to fail. .... 20

Figure 4. Map showing field sites studied in the Otway Basin, Victoria, Australia, numbered 1 to 11. Insets are rose diagrams (with numbers corresponding to field site on map) which show the strike directions of all fracture planes measured. Large-scale structures and lithological information adapted from Duddy (1994). .... 25

Figure 5. Rose diagrams comparing fracture strikes measured at outcrop and inferred from satellite imagery (for satellite images see Appendix C). a) Rose diagram of strikes of all closed fractures taken from Marengo. b) Rose diagram of strikes of all open fractures inferred from satellite imagery of Marengo. c) Rose diagram of strikes of all fracture planes taken from Marengo. d) Rose diagram of strikes of all fractures inferred from satellite imagery of Marengo. .... 29

Figure 6. Rose diagrams comparing fracture strikes measured at outcrop and inferred from satellite imagery (for satellite images see Appendix C). a) Rose diagram of strikes of all closed fractures taken from Skenes Creek. b) Rose diagram of strikes of all open fractures inferred from satellite imagery of Skenes Creek. c) Rose diagram of strikes of all fracture planes taken from Skenes Creek. d) Rose diagram of strikes of all fractures inferred from satellite imagery of Skenes Creek. .... 30

Figure 7. a) Photomicrograph of calcite vein fill from Cape Otway, Victoria, Australia, showing various calcite grains with sets of twins (Sample JS-07). b) Example of Type I (thin twins) twins from the Northern Subalpine Chain, France (figure adapted from Ferrill *et al.* (2004)). c) Example of Type II twins (tabular thick twins) from the Northern Mountain thrust sheet in the Great Valley, Central Appalachian Valley and Ridge Province (figure adapted from Ferrill *et al.* (2004)). .... 31

Figure 8. Photomicrographs of calcite vein fills at Moonlight Head. Dashed red line represents fracture/host rock boundary. Other coloured lines represent median lines of crack-seal events (green represents first event, blue represents second event, orange represents third event) a) Section of Sample JS-01 showing at least one (possibly two) crack-seal events. b) Section of Sample JS-02 showing a more complex crack-seal history with at least three crack-seal events. .... 32

Figure 9. Photomicrographs of thin sections of samples from the Otway Basin used for porosity calculations. a) Porosity was calculated to be 7.15 % for Sample JS-04 from Moonlight Head. b) Porosity was calculated to be 0.36% for Sample JS-07 from Cape Otway. .... 33

Figure 10. a) Fracture densities in the Eumeralla Formation at different sites in the Otway Basin compared with the maximum depth at which the site had been buried. The

average fracture density from the Eumeralla Formation interval from Bellarine-1 has been included from Tassone *et al.* (in press). b) Fracture densities ranges within different lithologies shown by average grain sizes..... 37

Figure 11. Section of face map drawn at Cape Patton. Note very fine grained/silt, finely laminated and finely bedded layers interbedded with fine to medium grained, thickly bedded, well-rounded and well-sorted volcanogenic sands. (For complete map see Appendix B) ..... 38

Figure 12. Section of face map drawn at Marengo. Note conglomerate lens with fine grained clasts inside a coarse grained matrix, clasts up to 10 cm, sub-angular to rounded. Lens is hosted in fine grained, thickly bedded but finely laminated volcanogenic sands. (For complete map see Appendix B)..... 39

Figure 13. Section of face map drawn at Moonlight Head. Note medium to coarse grained, thickly bedded (20 to 30 cm), less finely laminated (2 to 5 mm) well-rounded and well-sorted volcanogenic sands, interbedded with cross bedded conglomerate bearing lenses (20 to 30 cm) with clasts (1 to 10 cm) within a coarse grained sand matrix. Clasts appear to be those of similar fine to medium grained units. (For complete map see Appendix B) ..... 40

Figure 14. Data collected from Cape Otway. a) Fracture pattern associated with folding with accompanying stereographic projection of the orientations of the coordinate system (a, b and, c), fracture planes (black great circles) and the bedding (red great circle) (adapted from Twiss & Moores 2007). Fracture pattern observed at Cape Otway appeared very similar to this typical fold fracture pattern. b) Fracture planes of open fractures observed at Cape Otway (black great circles) and poles to fracture planes (black open squares). Red great circle represents bedding. c) Fracture planes of calcite filled fractures observed at Cape Otway (black great circles) and poles to fracture planes (black dots). Red great circle represents bedding ..... 42

Figure 15. Rose diagrams showing a) All fracture plane strikes at Cape Otway and b) All fracture plane strikes at Crayfish Bay. Note that radial intervals are not at the same scale. .... 45

Figure 16. Structural data from Castle Cove. a) All fracture planes measured ~14 m from the Castle Cove fault (black great circles) and poles to fracture planes (black dots). b) All fracture planes measured ~173 m from the Castle Cove fault (black great circles) and poles to closed fracture planes (black dots) and poles to open fracture planes (black squares). c) Rose diagram of all fracture strikes measured ~14 m from the Castle Cove fault. D) Rose diagram of all fracture strikes measured ~173 m from the Castle Cove fault..... 47

Figure 17. Photograph of orthogonal fracture relationship to monoclinial folding of Eumeralla Formation adjacent to the Castle Cove Fault, Castle Cove, Victoria. Photograph looking north. .... 48

Figure 18. Stereonet of unfolded bedding data at sites along the Otway Coast. a) Cape Otway, average fracture planes of three separate fracture sets identified in calcite filled fractures (black dashed great circles), average bedding from site where data were collected (red great circle) and fracture plane orientation after bedding is unfolded (solid black great circles). Angles between Fracture Sets 1 and 2 are 87.2° and 92.8°. b) Skenes Creek, average fracture planes of two separate fracture sets identified in fractures (black dashed great circles), average bedding from site where data were collected (red great circle) and fracture plane orientation after bedding is unfolded (solid black great circles). Angles between Fracture Sets 1 and 2 are 84.9° and 95.1°. and c)

Cumberland River, average fracture planes of two separate fracture sets identified in fractures (black dashed great circles), average bedding from site where data were collected (red great circle) and fracture plane orientation after bedding is unfolded (solid black great circles). Angles between Fracture Sets 1 and 2 are 83.1° and 96.9°. ..... 50

Figure 19. Schematic thermal history for sites along the Otway Ranges (Calculated from vitrinite reflectance data and apatite fission track analysis (AFTA) with major events including the mid-Cretaceous cooling and the late Tertiary cooling (Adapted from Duddy (2003)). Temperature at which Type I and Type II calcite twins is also plotted as well as interpreted ages for fracture sets in the field site (dashed lines show areas of lower confidence). ..... 54

Figure 20. Shale unit average sonic transit time vs. shale unit midpoint depth below ground level/seabed plot for shale units of the Eumeralla Formation, including the normal compaction trend zone of uncertainty (grey band) (adapted from Tassone *et al.* (in press). Superimposed is the value for the shale unit average sonic transit time for Sample JS-01 (Cape Otway) calculated from the samples porosity and typical shale values from Rider and Kennedy (2011) using the ‘Wyllie Time Average’ equation (Wyllie *et al.* 1956). ..... 56

Figure 21. Rose diagrams showing a) strikes of all natural fractures from the field area and b) all natural fractures within the Eumeralla Formation from well Bellarine 1 (grey circles represent discontinuous fractures, grey triangles represent continuous fractures and grey squares represent full well bore fractures) (Tassone *et al.* in review). Note that radial intervals are not at the same scale. .... 58

Figure 22. Rose diagrams showing a) strikes of all fractures (black circles represent poles to fracture planes) ~173 m from the Castle Cove Fault, b) strikes of all fractures (black circles represent poles to fracture planes) ~14 m from the Castle Cove Fault and c) all natural fractures within the Eumeralla Formation from well Minerva 1 (grey circles represent discontinuous fractures, grey triangles represent continuous fractures and grey squares represent full well bore fractures) (Tassone *et al.* in review). Note that radial intervals are not at the same scale. .... 58

Figure 23. Plots of fracture susceptibility for reactivation under the Otway Basin stress conditions at 1 km depth in a strike-slip fault stress regime, with a maximum horizontal stress orientation of 144 (Tassone *et al.* in review). Delta P represents the value of pore pressure increases (in MPa) required to move the Mohr Circle to failure. High values (blue) are the furthest from the failure envelope, and therefore represent a low likelihood of reactivation. Low values (red) are the closest to the failure envelope and require the smallest change in pore pressure, and are thus at high likelihood of reactivation. These values also represent orientations of new faults/fractures to form. Poles to fracture planes (represent by x) are included on each plot and are representative of the fracture type in the title. .... 61

Figure 24. Differential hardness between host rocks and fracture fills in the Otway Basin. a) Hardened calcite fracture cements at Moonlight Head, showing preferential weathering of host rock compared to fracture cement. b) Hardened FE-rich alteration halos around some open fractures showing preferential weathering unaffected host rock and to varying extents the fracture itself. .... 63

Table 1. Stress gradients for the strike slip fault stress regime described in the Otway Basin (Tassone 2013). .....	19
Table 2. Fracture data collected from 11 sites in the Otway Basin. ....	23
Table 3. Breakdown of fracture data collected from each of the 11 sites in the Otway Basin. ....	23
Table 4. Fracture sets interpreted from data from each of the 11 sites in the Otway Basin. ....	24
Table 5. Fracture density data, average bedding and lithological variations at field sites in the Otway Basin, Victoria, Australia. Maximum burial temperatures were determined from vitrinite reflectance data by Duddy (1994). ....	35

## INTRODUCTION

The orientation and magnitude of the in-situ stress field, types of cementation within fractures, the rock strength of both fracture fills and wall rock and surrounding pore-fluid pressures in both fracture zone and surrounding rock are all factors that affect the propensity for a fracture to be open to fluid flow. Although it is well understood that the optimal angle between  $\sigma_1$  and the fracture plane for slip is  $\sim 30^\circ$  (Anderson 1951a), the cumulative effects of all these factors are poorly constrained within sedimentary basins. Therefore, the extent of fluid flow through fractures is not well known.

Current exploration for permeable subsurface reservoirs of hydrocarbon, geothermal and water systems within sedimentary basins uses resistivity image logs, which generate pseudo-images of the borehole wall, to identify fractures (e.g. King *et al.* 2008, Bailey *et al.* 2012). Fractures that appear resistive on image logs are identified as being closed to fluid flow as they are filled with cement and no conductive fluids (i.e. drilling muds) will exist within the fractures (King *et al.* 2008). Conductive fractures are identified as being open, as they are thought to be filled with conductive drilling muds (King *et al.* 2008). However, this approach does not take into account the resistivity properties of mineral cements within these fractures. Quartz, a highly resistive mineral, has been observed in many cases to bridge fractures during precipitation but leave permeability intact (Lander *et al.* 2002, Laubach *et al.* 2004). Siderite cements are highly conductive, indicating at first pass they are open to fluid flow on image logs but are actually filled, and therefore, are impermeable.

Identifying an analogue for the connectivity and density of fractures and orientations of open and closed fractures with respect to the in-situ stress field at depth will result in faster and more accurate methods of exploration. This would be of huge importance for the discovery of unconventional hydrocarbon resources, geothermal energy production and safe and effective sites for CO<sub>2</sub> sequestration.

The degree to which fractures are open to fluid flow is poorly known in the Otway Basin. Thus, the aim of this work is to use exposures of the Eumeralla Formation as a natural laboratory to study natural fractures in the Otway Basin.

Mapping fractures in the field will determine the interconnectivity of fractures, the fracture types and the cement fills. Using rock outcrop of the Eumeralla Formation in the Otway Basin as an analogue, these various fracture fills and patterns will then be compared to naturally occurring fractures identified on image logs and in satellite imagery. This will not only validate the use of this geophysical/remote sensing technique for fracture network identification, as well as their propensity to be open to fluid flow, but will also enhance the image log methods for fracture identification in the future where only image logs are available (e.g. in offshore regions around Australia).

## **BACKGROUND**

### **Geological Setting**

The Otway Basin is located along the southern margin of Australia (Figure 1). It is an extensional basin that formed during rifting from the late Jurassic to early Cretaceous (Krassay *et al.* 2004). This rifting resulted in the complete separation of the Australian and Antarctic continents (Willcox & Stagg 1990). This NW-SE trending basin encompasses both onshore and offshore regions of Victoria and South Australia, as well as parts of offshore Tasmania (Krassay *et al.* 2004) (Figure 1). The Otway Basin contains up to 13 km of post-Jurassic sediments that overlie deformed Cambro-Ordovician basement rocks (Krassay *et al.* 2004) (Figure 2). The basin is continuous with the Sorrell Basin to the south-east, however; the northern, north-eastern and eastern extents of the basin are bound by Palaeozoic and Proterozoic basement (Moore *et al.* 2000, Krassay *et al.* 2004).

Seven major tectonic phases have been recognised in rocks of the Otway Basin, which characterise the driving mechanisms responsible for the complex history of rifting, compression, subsidence and inversion of the basin (Figure 2) (Krassay *et al.* 2004). The initial rifting phase, occurred between the Late Jurassic to Early Cretaceous and resulted in a localised onshore deep lacustrine sequence, with high preservation of organic matter and little coarse clastic material (Krassay *et al.* 2004). A series of graben and half-graben structures were also formed during this initial stage (Krassay *et al.* 2004). A second major phase of this initial rifting changed the existing transgressive quiescent sequence of sediments to a sequence reflecting increased rates of rifting, with an influx of coarse clastics and fluvial channel sandstones (Krassay *et al.* 2004). Initial

rifting was then followed by a period of thermal subsidence from the mid-Cretaceous that was the major control on sedimentation (Krassay *et al.* 2004).

A significant period of basin reorganisation then followed in the mid-Cretaceous (Duddy 1994, Krassay *et al.* 2004). Compressional stresses oriented NW-SE resulted in folding, uplift and subsequent erosion that affected the entire basin to varying degrees, with the most major effect being the separation of the Otway Basin and the Torquay Sub-basin by the uplift of the Otway Ranges (Krassay *et al.* 2004). This event also marked a period of reduction of the geothermal gradient, determined from vitrinite reflectance data (Duddy 1997). A renewed rifting phase, confined to continental extension, in almost the same orientation as the initial rifting phase then occurred in the Late Cretaceous (Krassay *et al.* 2004).

A second period of subsidence and regional slow spreading from the Late Cretaceous to the middle Eocene marked the fifth phase of the tectonostratigraphic history of the Otway Basin (Krassay *et al.* 2004). A subsequent third period of subsidence coupled with regional fast spreading in the southern ocean from the middle to late Miocene marked the sixth phase (Norvick & Smith 2001). The final phase includes Pliocene to Pleistocene compression, inversion and uplift with subsequent erosion and associated volcanism (Krassay *et al.* 2004).



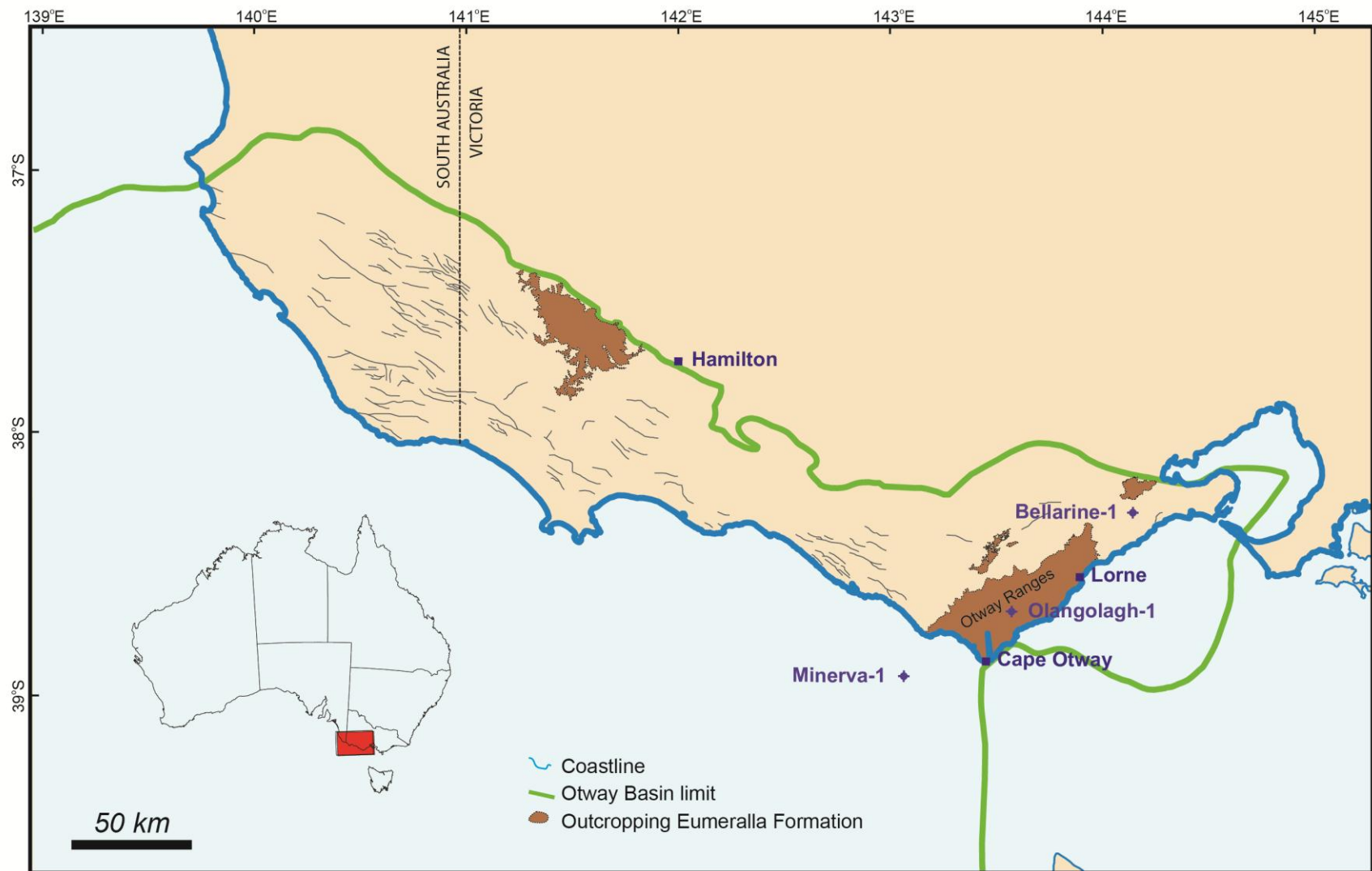


Figure 1. Location map of the Otway Basin, Victoria, Australia. Locations of wells referred to in this study are also shown (Olangolagh-1, Minerva-1 and Bellarine-1).

# Fault and Fracture Networks in the Otway Basin

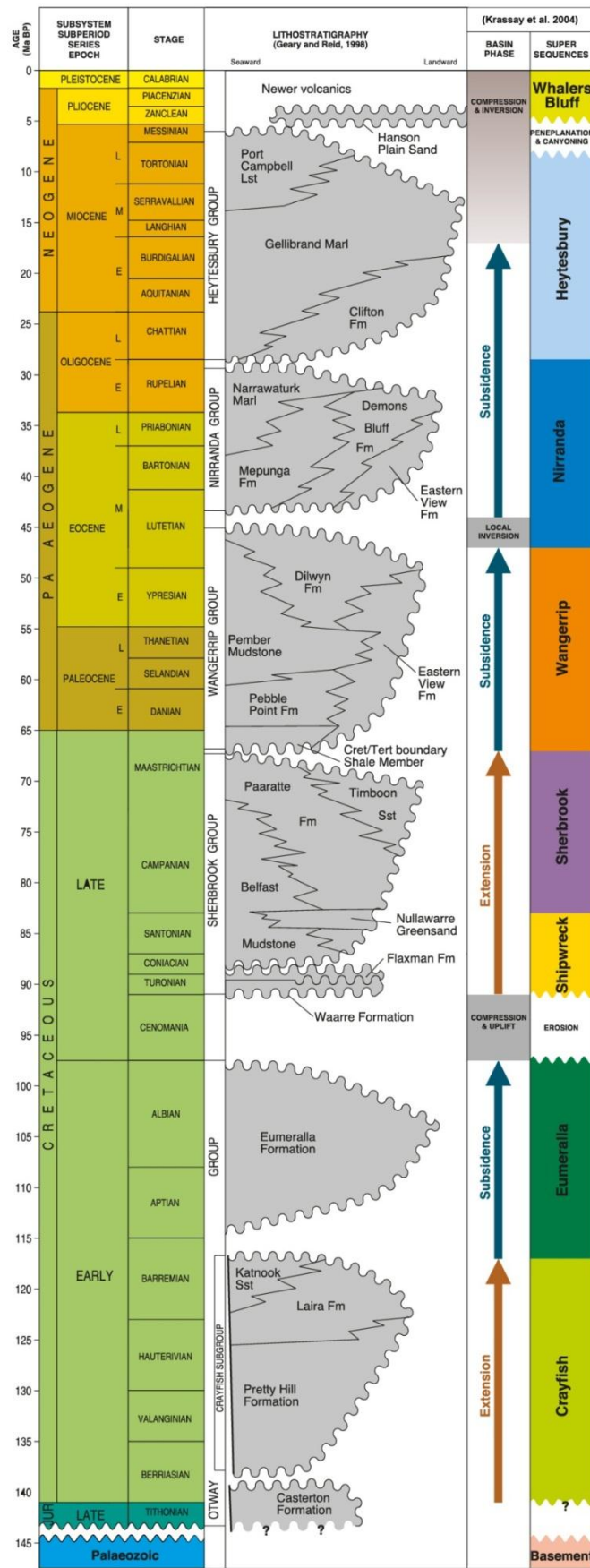


Figure 2. Stratigraphic column for the Otway Basin (after Krassay *et al.* (2004)), including lithostratigraphy (Geary & Reid 1998) and basin phases and super-sequences (Krassay *et al.* 2004).

The orientation of rift depocentres varies across the Otway Basin, with W to NW trending depocentres in the western troughs (Robe and Penola), and NE trending depocentres in the east (Torquay Sub-basin) (Krassay *et al.* 2004). It is argued that the changing trends of these depocentres are due to local response to primary differences between the rheological properties of the basement of the Delamerian and Lachlan fold belts (Miller *et al.* 2002).

Since the Miocene, the basin has been under a reverse fault stress regime, which has resulted in fault reactivation, folding and localised basin inversion (Edwards *et al.* 1996, Krassay *et al.* 2004, Holford *et al.* 2011, Tuitt *et al.* 2011). The two most apparent effects of this compressional event are the Strzelecki and Otway Ranges, with significant uplift and deformation (Perincek & Cockshell 1995). Onshore volcanism is also evident in the basin, predominantly onshore, between eastern Victoria and south eastern South Australia (Krassay *et al.* 2004).

The basin is of significant importance to petroleum exploration within Australia, with commercial gas discoveries in the Penola Trough, Shipwreck Trough and the Port Campbell area, as well as other shows throughout the basin (Tassone *et al.* 2011). Recent exploration, both onshore and offshore, has focused on unconventional plays (Holford *et al.* 2011, Tassone *et al.* in review). The basin has also been proposed as a potential region for geological storage of carbon dioxide (CO<sub>2</sub>), with the Naylor Field already being tested as a demonstration site for this (Vidal-Gilbert *et al.* 2010). There has also been interest in the basin for its potential for geothermal energy, with drilling

undertaken in South Australian regions of the Otway Basin (Beardsmore 2010), and exploration in south-west Victoria (Barnett 2009).

The Late Jurassic to Early Cretaceous Otway Group has a thickness of up to 7,300 m and is the primary source rock for petroleum generation (Krassay *et al.* 2004). However, exploration of this unit has had limited success (Duddy 1997). Although the rocks of the Otway Group are primary source rocks within the Otway Basin, mid-Cretaceous inversion of Early Cretaceous structures in the east of the basin effectively ended hydrocarbon generation in these areas (Duddy 1997).

The only surface exposure of the rift-related Cretaceous Otway Group is the Eumeralla Formation (Figure 2). The Eumeralla Formation is a thick sequence of non-marine, volcanogenic sandstone channel deposits as well as inter-channel sandstones, mudstones and shales, with volcanogenic clastic components derived mainly from volcanism of the same age (Duddy 2003). Therefore, this formation is used to undertake this study of fracture patterns at surface in outcrop, which can be compared with fracture sets seen at depth in the same unit using image logs and/or core data.

A marked reduction in the geothermal gradient (Duddy 1997), and unloading during uplift of the Otway Group sediments (Krassay *et al.* 2004) may indicate that Mode I tensile fractures will be the prevailing fracture type seen in the basin. Tensile fractures created by unloading and subsequent uplift are a common occurrence in sedimentary basins (e.g. Engelder 1985, Gross *et al.* 1995, Laubach *et al.* 2009). Changes in the

stress regime due to removal of overburden and thermal-elastic contraction of the rock column are the likely cause (Engelder 1985).

## **Diagenesis**

Diagenesis of the Eumeralla Group sediments began soon after burial, with different diagenetic processes evident from <10 m to >1.5 km (Duddy 2003, Tassone 2013).

Initial diagenesis began at <10 m with dissolution of the predominantly unstable volcanogenic olivine and orthopyroxene (Duddy 2003). This dissolution subsequently coated remaining grains with smectite and chlorite clays, reducing porosity and permeability at very shallow depth (Duddy 2003). Diagenesis at less than a few hundred metres saw precipitation of pore filling calcite and siderite cements, forming concretions (containing clinopyroxene, plagioclase and amphibole) (Duddy 2003). These concretions were then further altered in a 1.2 to 1.5 km thick zone at the top of the Eumeralla Formation where zeolites precipitated, forming a zone with porosities from ~15 to 35 % (Duddy 2003). At burial depths greater than this zone, laumontite precipitation was pervasive and reduced primary porosity to less than ~10%, porosity was then almost completely destroyed by the replacement of swelling chlorite clays (Duddy 2003).

This diagenesis has had pervasive and profound effects on both the porosity and permeability of the Otway group (Duddy 2003, Tassone 2013). The extensive work by Duddy (2003) identified the diagenesis of volcanogenic sediments of the Otway Group, particularly those of the Eumeralla Formation, as a major problem to reservoir quality.

## Geomechanical Background

### STRESS FIELD DIRECTION

Based on Andersonian faulting theory in the Earth's crust the three principle stress axes ( $\sigma_1 > \sigma_2 > \sigma_3$ ) can be resolved into a vertical stress axis ( $\sigma_v$ ), a maximum horizontal stress axis ( $\sigma_H$ ) and a minimum horizontal stress axis ( $\sigma_h$ ) (Anderson 1951a).

In order to determine the orientation of horizontal stress components, inferences can be made from borehole failures, including borehole breakouts and drilling-induced tensile fractures (DITFs) (Bell 1996a). As the orientation of the two horizontal stresses are perpendicular to one another, it is therefore only necessary to determine either  $\sigma_H$  or  $\sigma_h$  (Bell 2003). Borehole breakouts are laterally elongated sections within a well where a cave-in has occurred on opposing sides of the wellbore due to the propagation of shear fractures (Kirsch 1898, Babcock 1978). Elongation occurs perpendicular to  $\sigma_H$ , and propagates parallel to  $\sigma_h$ . Drilling-induced tensile fractures occur parallel to  $\sigma_H$  and represent a tensile failure of rock forming the borehole wall (Bell 1996a).

As the propagation direction of fractures within a rock column is reliant on the magnitude and orientation of the of the principle stresses, there will be a close relationship between fracture patterns and the regional structure formed in the same deformational event (Bell 1996a). Therefore, a good understanding of the structural and tectonic history of a region is required in order to determine the direction and timing of propagation of different fracture sets.

The orientation of  $\sigma_H$  in the eastern Otway Basin is 144 (Reynolds *et al.* 2003, Nelson *et al.* 2006, Tassone *et al.* in press). The magnitude of the stress regime has been documented as both a reverse fault stress regime and a strike slip fault stress regime (Denham *et al.* 1981, Jones *et al.* 2000, Krassay *et al.* 2004, Nelson *et al.* 2006, Tassone *et al.* 2011, King *et al.* 2012b).

### HORIZONTAL AND VERTICAL STRESS MAGNITUDES

According to work by Dickinson (1953), which used the average density of  $2.3\text{g/cm}^3$  for sedimentary rocks, average vertical stress ( $\sigma_v$ ) gradients for sedimentary basins were determined to be approximately 22.6 MPa/km, and have since been commonly used. Further work by Tingay *et al.* (2003) demonstrated that  $\sigma_v$  can vary greatly between basins, and therefore should be accurately determined for a given area. The vertical stress gradient ( $\sigma_v$ ) for the eastern Otway Basin was determined to be  $\sim 25.8$  MPa/km (Tassone 2013) (Table 1). This value is higher than the average that might be assumed using Dickinson (1953).

The minimum horizontal stress ( $\sigma_h$ ) magnitude can be measured using leak-off test (LOT) data (Bell 1996a, 1996b). Leak-off tests involve stimulating fractures in a well bore by increasing hydraulic pressure in an isolated well section (Bell 1996a). Fractures formed strike parallel to  $\sigma_2$ , which in the case of a strike slip fault regime is  $\sigma_H$  and in a reverse fault regime is  $\sigma_h$  (Bell 1996a). The magnitude of  $\sigma_H$  however, cannot be directly measured and must be estimated from relationships with  $\sigma_h$  and rock strength (Bell 1996a).

A strike slip fault stress regime has been defined from stress magnitude data for the eastern Otway Basin (Tassone 2013) (Table 1). However, this strike slip fault stress regime is inconsistent with neotectonic structures which indicate a reverse fault stress regime (Denham

*et al.* 1981, Dickinson *et al.* 2001, Hillis *et al.* 2008, King *et al.* 2012b). This inconsistency is an ongoing debate for the Otway Basin and other southern Australian margin basins which also show this discrepancy between measured stress magnitudes and neotectonic structures (e.g. Nelson *et al.* 2006, Hillis *et al.* 2008, Holford *et al.* 2011, King *et al.* 2012b).

**Table 1. Stress gradients for the strike slip fault stress regime described in the Otway Basin (Tassone 2013).**

	<b>Strike Slip Fault Stress Regime</b>
$\sigma_v$	25.8 MPa/km
$\sigma_H$	37.2 MPa/km
$\sigma_h$	19.36 MPa/km

## PORE PRESSURES

Any three dimensional stress field can be shown using 3-D Mohr Circles on a Mohr Diagram (Figure 3), where the normal and shear stresses are represented on the horizontal and vertical axes (Twiss & Moores 2007). Each circle is defined by a pair of principle stresses, and is a graph of the surface stress parallel to one of the principle axes (Twiss & Moores 2007). Rock properties are displayed on Mohr Diagrams as a failure envelope, typically Griffith-Coulomb failure (Brace 1960, Secor 1965, Zang & Stephansson 2010). If the Mohr Circle intersects the failure envelope, then shear or tensile failure will result depending on the point of the envelope at which intersection occurs (Figure 3). As stress states change, the Mohr circle will move with respect to the failure envelope. One of the primary factors influencing the potential failure of a rock is pore pressure of fluids, with increases in pore pressure moving rocks closer to failure by shifting them towards their failure envelope (Sibson 1996). For a given fracture plane, the integrity of that plane, and hence, the propensity of that plane to fail, is determined by the change in pore pressure ( $\Delta P_p$ ) necessary to bring the circle into contact with the failure envelope (Dewhurst *et al.* 2002) (Figure 3). When  $\Delta P_p$  is low (i.e. a small  $P_p$  increase towards the failure envelope), then a fracture is highly likely to reactivate, and where



$\Delta P_p$  is high (i.e. a large  $P_p$  increase towards the failure), then there is a low likelihood of reactivation (Mildren *et al.* 2005).

Well bore pore pressures (WBPP) in the eastern Otway Basin were found to be 10.88 MPa (slightly overpressured) (Tassone 2013).

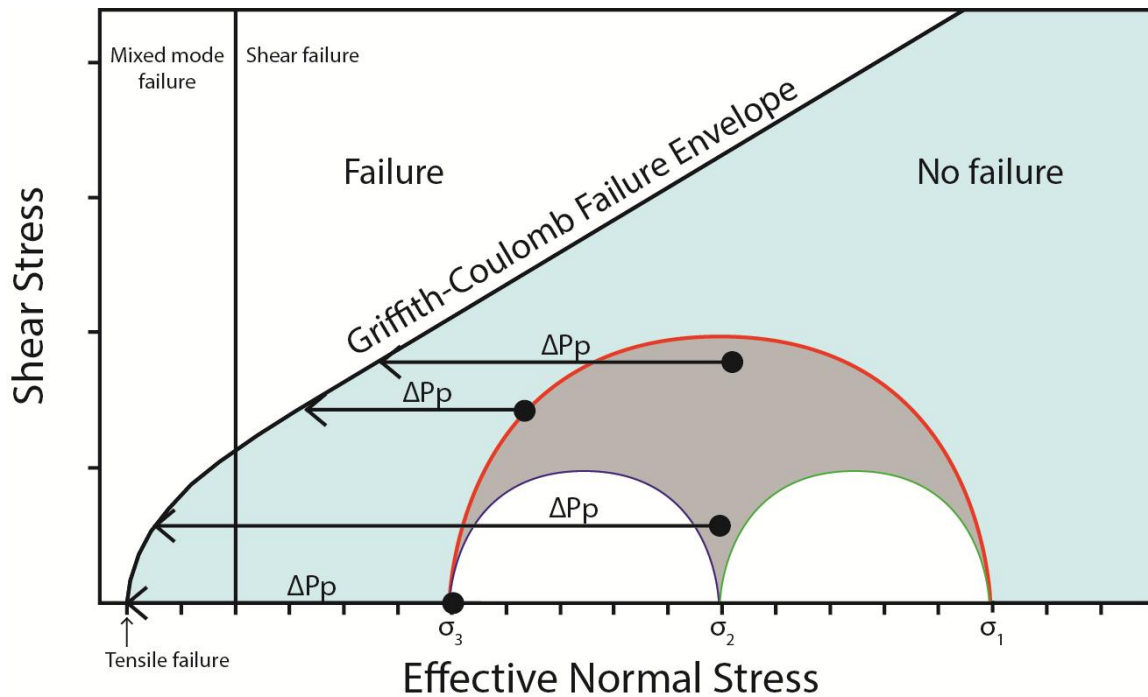


**Figure 3. Three-dimensional Mohr Diagram with Griffith-Coulomb failure envelope overlain, showing possible fracture planes within the stress regime and the associated change in pore pressure ( $\Delta P_p$ ) required for that plane to fail (after Dewhurst *et al.* 2002). The position of the fracture plane (solid black circle in the grey shaded area) is dependent on the relative orientation of the plane and the principle stresses. The change in pore pressure is used to determine the propensity for that plane to fail.**

### ROCK STRENGTH (HOST ROCK AND FRACTURE FILL)

Mechanical rock properties, including internal angle of friction ( $\phi$ ), cohesion ( $C_0$ ), unconfined compressive strength (UCS) and coefficient of friction ( $\mu$ ) are all important properties that determine rock strength (Barton 1976, Byerlee 1978, Dewhurst *et al.* 2002, Chang *et al.* 2006). These mechanical rock properties can be obtained from laboratory experiments, including uni-axial and tri-axial compressive tests (Zoback 2010) and also by using empirical relationships (Chang *et al.* 2006).

Mechanical rock property tests on rocks from the Otway Basin are rare with only one sample from the Eumeralla Formation tested (Dewhurst *et al.* 2002, Tassone 2013). Due to the complexity of this formation (composition, compaction and diagenetic history), the sample tested is insufficient to derive accurate mechanical properties specific to the entire formation (Tassone 2013). Elastic rock properties for the Eumeralla Formation were also empirically derived from well data from the Eumeralla Formation, including Poisson's Ratio at ~0.27 GPa and Young's Modulus at 6.0 GPa (Tassone 2013).

At present the critically limiting factor for assessing the likelihood of fault seal reactivation is a lack of geomechanical data for naturally occurring fault rocks (Dewhurst *et al.* 2002).

Compared with the amount of geomechanical data available for clay-rich gouges and cataclasites from fault zones, little data exists for failure criteria of intact fault rocks (Dewhurst *et al.* 2002).

## MECHANICAL STRATIGRAPHY

Mechanical stratigraphy is the subdivision of rock into intervals based on the distinct mechanical properties of the each lithological unit (Corbett *et al.* 1987, Laubach *et al.* 2009). It has been shown that fracture distribution can exhibit no systematic patterns in wells (King *et al.* 2008). However, variations in concentrations of fractures have been observed within particular formations within sedimentary basins (e.g. Gross 1995, Gross *et al.* 1995, King *et al.* 2008) as well as the partitioning of brittle failure modes (i.e. Mode 1, 2 and 3 fractures) between different layers (e.g. the Monterey Formation; Gross 1995). This is likely the result of various mechanical properties of these strata that influence the rate of growth of fractures (Gross 1995, Gross *et al.* 1995, Laubach *et al.* 2009). Mechanical properties that affect Mode

1 tensile fractures (the main fracture type expected to be seen in this study in the Otway Basin) include tensile strength, brittleness, elastic stiffness, the thickness of rock layers and the interfaces between different lithologies (Laubach *et al.* 2009). Stratigraphy has an effect on fracture occurrence, style, size and spatial arrangements (Laubach *et al.* 2009). Thus, considering the lithological variations in stratigraphic sequence is vital to studying the fracture networks within a sedimentary basin.

### **METHODS**

Data for this study were acquired by a variety of techniques, chiefly through field work, as well as microscopic analysis and structural data analysis software. Transects of between 15 m and 40 m (measuring fracture planes as they cross the line of the transect) and face maps (detailed cross-sections, with scales from 1:10 to 1:30) covering 2 m<sup>2</sup> to 24 m<sup>2</sup> (see Appendix A for full details) were completed at various field sites along the Victorian coast at outcrops of the Eumeralla Formation in the Otway Basin (Figure 4). JRS Suite© (provided by Ikon Science) and Stereonet 8 (Allmendinger *et al.* 2012) were used to construct rose diagrams, stereonet and fracture susceptibility plots from structural data collected at these sites.

Thin sections of rock samples collected in the field were also used to provide detailed petrology of rocks and fracture cements. Digital photos from these thin sections were used for the image analysis technique using JMicroVision© V1.27 (Roduit 2013) to determine porosity of the host rock.

## OBSERVATIONS AND RESULTS

Over 1900 naturally occurring fractures were recorded at 11 field sites in the Otway Basin at outcrop of the Eumeralla Formation (Figure 4). Fractures were further characterised as open or closed and siderite or calcite filled (where observable). Fracture data for the entire field area are shown in (Table 2); a breakdown of fracture data by site is shown in (Table 3). Five fracture sets were then defined by their similar orientations and fracture fills (Table 4).

**Table 2. Fracture data collected from 11 sites in the Otway Basin.**

<b>Fracture Type</b>	<b>Number</b>	<b>Mean strike orientations(s)</b>
<b>All</b>	1943	N-S & NE-SW
<b>Open</b>	623	N-S & ESE-WNW
<b>Closed</b>	892	N-S & ESE-WNW
<b>Siderite Filled</b>	534	N-S, ESE-WNW & NNE-SSW
<b>Calcite Filled</b>	128	N-S, NW-SE & NE-SW

**Table 3. Breakdown of fracture data collected from each of the 11 sites in the Otway Basin.**

<b>Field Site Location</b>	<b>Total Fractures</b>	<b>Open Fractures</b>	<b>Closed Fractures</b>	<b>Siderite Filled Fractures</b>	<b>Calcite Filled Fractures</b>
<b>Moonlight Head</b>	68	8	60	51	9
<b>Castle Cove</b>	458	73	362	225	55
<b>Cape Otway</b>	74	45	29	0	29
<b>Crayfish Bay</b>	40	30	7	6	1
<b>Marengo</b>	247	138	109	100	1
<b>Skenes Creek</b>	128	67	61	34	4
<b>Wongarra</b>	552	76	89	8	10
<b>Smythes Creek</b>	23	16	7	4	3
<b>Cape Patton</b>	53	36	17	16	0
<b>Cumberland River</b>	188	76	110	81	12
<b>Lorne</b>	112	58	41	9	4

**Table 4. Fracture sets interpreted from data from each of the 11 sites in the Otway Basin.**

<b>Fracture Set</b>	<b>Nature</b>	<b>Orientation</b>	<b>Fault Regime</b>	<b>Fracture Characteristics</b>	<b>Cements</b>
<b>1</b>	Perpendicular to Bedding	Rotating from NNW-SSE to N-S, Originally vertical	Normal Fault or Reverse Fault	Open & closed fractures	Calcite & Siderite (Closed only)
<b>2</b>	Perpendicular to Bedding	Rotating from ENE-WSW to E-W, Originally vertical	Normal Fault or Reverse Fault	Open & closed fractures	Calcite & Siderite (Closed only)
<b>3</b>	Vertical	ESE-WNW, Vertical	Reverse Fault	Open & Closed fractures	Calcite (Closed only)
<b>4</b>	Bedding Parallel	Varies with bedding	Reverse Fault	Closed fractures	Siderite(All)
<b>5</b>	Crack Seal	-	Reverse Fault	Closed fractures	Calcite (All)
<b>Castle Cove</b>	Fault Parallel	NE-SW, Steeply dipping	Normal Fault or Reverse Fault	Closed fractures	Calcite (All)

# Fault and Fracture Networks in the Otway Basin

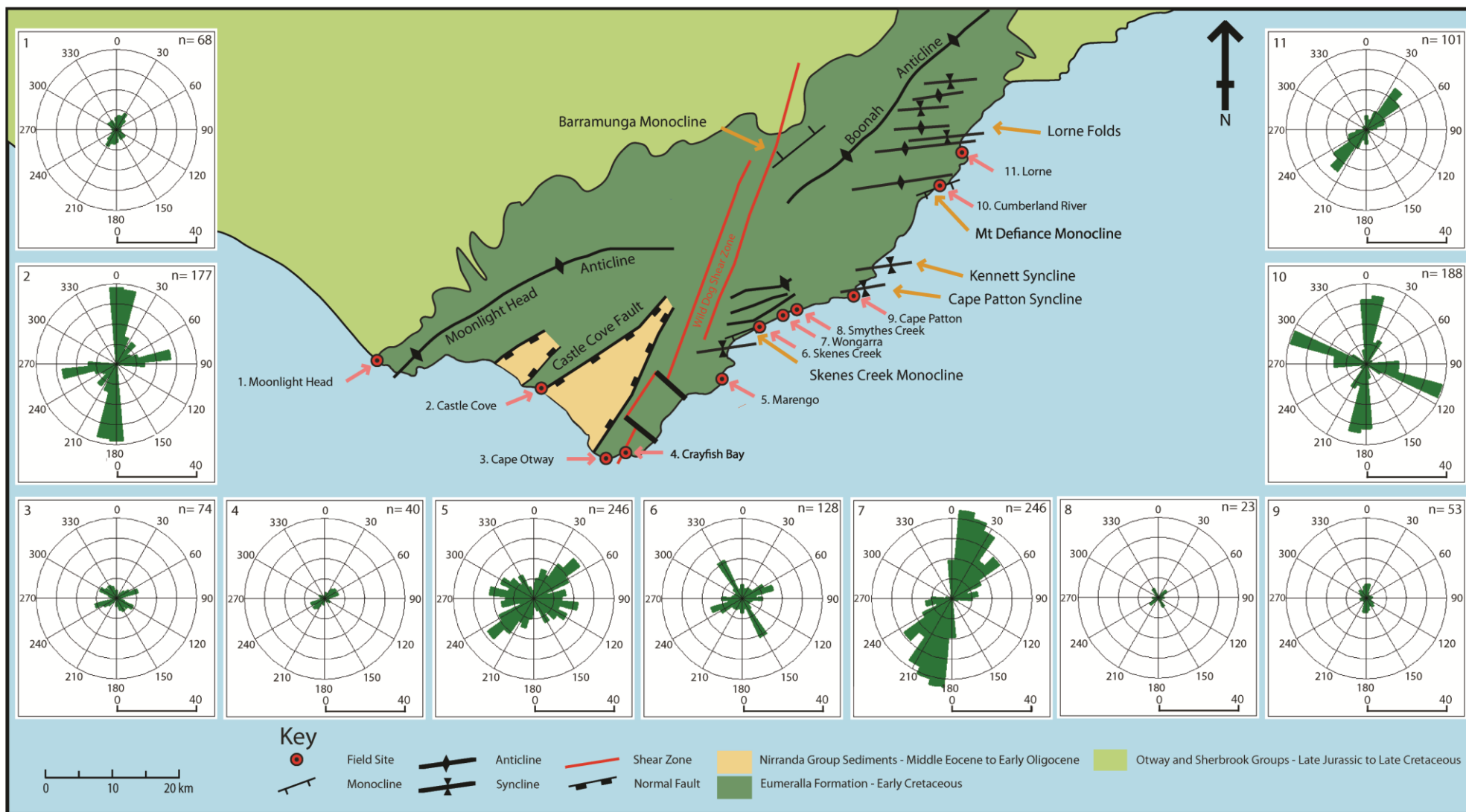


Figure 4. Map showing field sites studied in the Otway Basin, Victoria, Australia, numbered 1 to 11. Insets are rose diagrams (with numbers corresponding to field site on map) which show the strike directions of all fracture planes measured. Large-scale structures and lithological information adapted from Duddy (1994).

## **Fracture Orientations at Field Sites in the Otway Basin**

### **Moonlight Head**

Two dominant fracture sets were observed at Moonlight Head. The first and most obvious fracture set was oriented NNE-SSW, the second more minor set was oriented NW-SE (Figure 4). Fractures have highly variable dip angles from shallow to steep. Fracture fills were very common in this area, with siderite filling the majority of fractures but also some calcite fractures observed (Table 3). The majority of fractures at this location appeared closed in outcrop.

### **Castle Cove**

Two dominant fracture sets were observed at Castle Cove. The first and most obvious fracture set was oriented N-S, the second set was oriented ENE- WSW (Figure 4). The majority of fractures were moderately to steeply dipping. Fracture fills were very common in this area, with siderite filling approximately half of all fractures, and also minor calcite (Table 3). The majority of fractures at this location appeared closed at surface.

### **Cape Otway**

Two dominant fracture sets oriented ENE-WSW and WNW-ESE and one minor fracture set oriented NNW-SSE were observed at Cape Otway (Figure 4). All fractures were moderately to steeply dipping. Only calcite existed here as a fracture fill, making up all of the closed fractures observed (Table 3).

### Crayfish Bay

The dominant fracture set observed at Crayfish Bay was ENE-WSW (Figure 4). Fractures had variable dip angles from shallow to steep. This site had few calcite and siderite filled fractures, with the majority of fractures appearing open at surface (Table 3).

### Marengo

Dominant fracture sets at this location were oriented NE-SW and WNW-ESE (Figure 4). Fractures had highly variable dip angles, with both very steep and very shallow dip angles observed. Fractures measured from satellite imagery also showed two dominant fracture sets with similar orientations to those measured in the field (Figure 5).

### Skenes Creek

Two dominant fracture sets oriented NNW-SSE and ENE-WSW were recorded at Skenes Creek (Figure 4). Fractures had highly variable dip angles, with both very steep and very shallow dip angles observed. The numbers of open versus closed fractures was comparable (Table 3). Fractures measured from satellite imagery also showed two dominant fracture sets with similar orientations to those measured in the field (Figure 6).

### Wongarra

Fractures at Wongarra were predominantly striking NE-SW (Figure 4). Few dip angles were recorded but all were steeply dipping.

### Smythes Creek

Two dominant fracture sets were observed at Smythes Creek oriented NE-SW and NNW-SSE (Figure 4), with the majority of fractures being open (Table 3). All fractures were either steeply or shallowly dipping, with no moderately dipping fractures recorded.



### Cape Patton

Two dominant fracture sets were observed at Cape Patton oriented N-S and NNW-SSE (Figure 4), with the majority of fractures being open (Table 3) and also steeply dipping.

### Cumberland River

Cumberland River showed two dominant fracture sets oriented N-S and ESE-WNW (Figure 4). The majority of fractures were near vertical.

### Lorne

Lorne showed a dominant fracture trend of NE-SW (Figure 4). Few dips were recorded but all were moderately to steeply dipping. Open and closed fracture fills were of similar occurrence, however, filled fractures were not as frequent (Table 3).

## **Satellite Comparison**

The Marengo and Skenes Creek field sites were chosen to do an analysis of fracture orientations gathered from satellite imagery due to good resolution of satellite images and size of wave cut platform on which fractures could be identified. These sites were also easily accessible to conduct transects in the field for comparison.

In the case of the Marengo data, a similarity can be seen with the dominant strikes of the fracture sets between the field data and the satellite data, with two main sets striking NE-SW and WNW-ESE (Figure 5). However the satellite image interpreted data under represents the number of fractures striking NE-SW. When broken down into closed and open fractures (Figures 5a and 5b respectively), a number of the under-represented fractures are closed fractures.

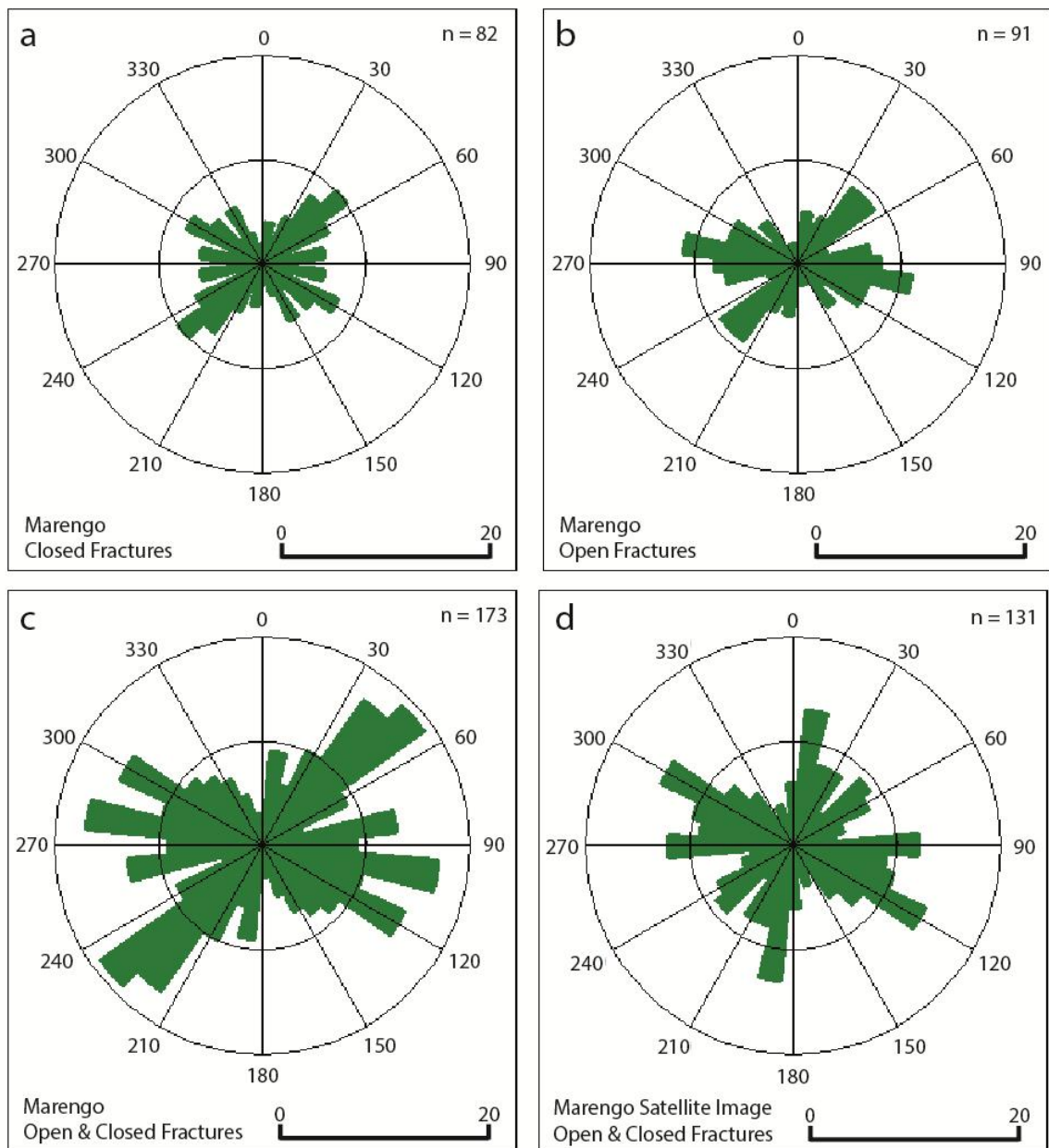


**Figure 5. Rose diagrams comparing fracture strikes measured at outcrop and inferred from satellite imagery (for satellite images see Appendix C). a) Rose diagram of strikes of all closed fractures taken from Marengo. b) Rose diagram of strikes of all open fractures inferred from satellite imagery of Marengo. c) Rose diagram of strikes of all fracture planes taken from Marengo. d) Rose diagram of strikes of all fractures inferred from satellite imagery of Marengo.**

In the case of Skenes Creek, a similarity can be seen with the dominant strikes of the fracture sets between field data and the satellite data, with two main sets striking ENE-WSW and WNW-ESE (Figure 6). At Skenes Creek, the ENE-WSW striking satellite data seems to be over represented compared to that from outcrop.

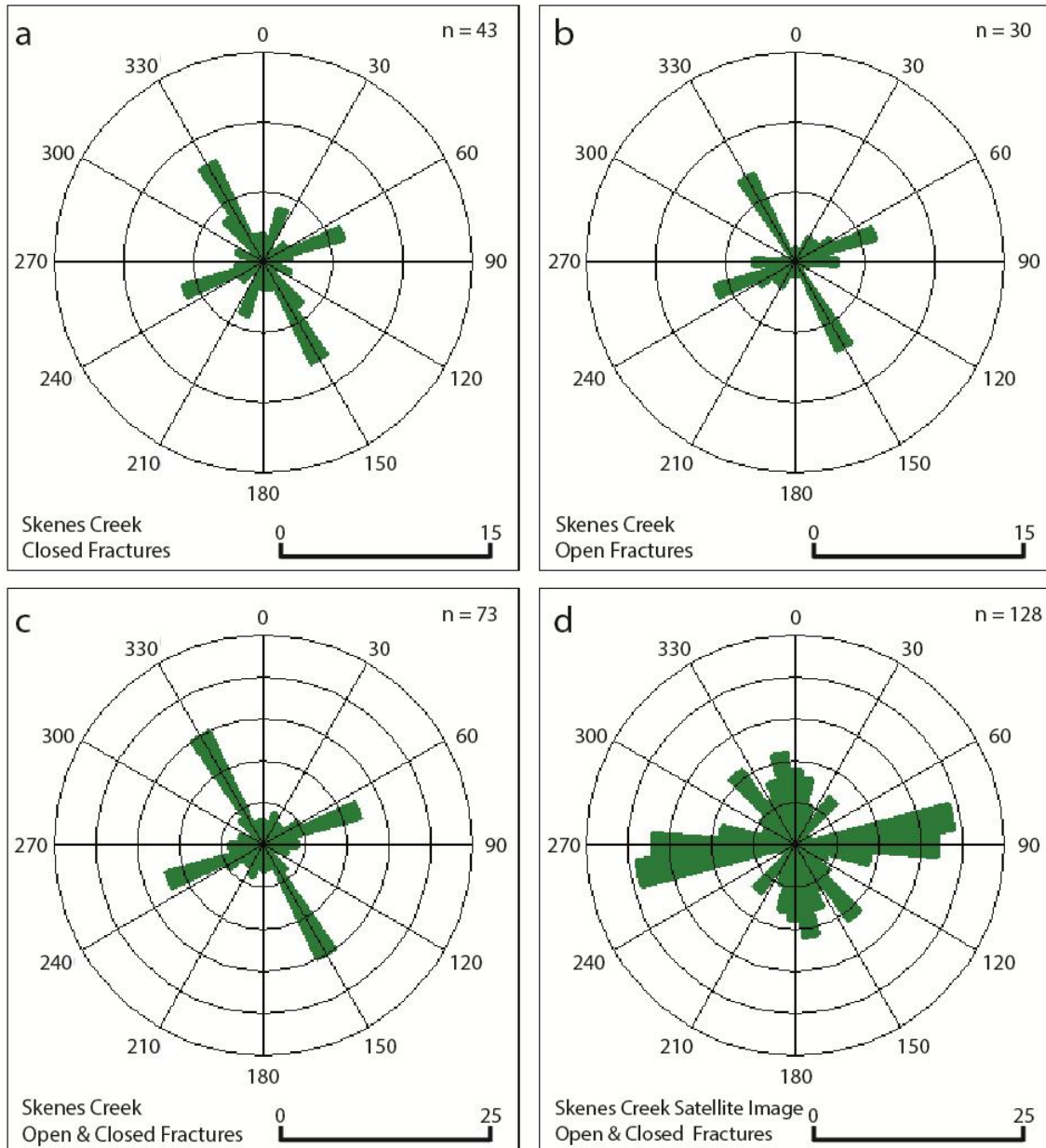


**Figure 6. Rose diagrams comparing fracture strikes measured at outcrop and inferred from satellite imagery (for satellite images see Appendix C). a) Rose diagram of strikes of all closed fractures taken from Skenes Creek. b) Rose diagram of strikes of all open fractures inferred from satellite imagery of Skenes Creek. c) Rose diagram of strikes of all fracture planes taken from Skenes Creek. d) Rose diagram of strikes of all fractures inferred from satellite imagery of Skenes Creek.**

## Fracture Fills and Porosity in the Otway Basin from Thin Section Microscopy

Thin sections were prepared from samples taken from Cape Otway and Moonlight Head (locations and descriptions are given in Figure 1 and Appendix A, respectively). Multiple thin calcite twins were observed in calcite crystals within fracture cements observed at Cape Otway (Sample JS-07) (Figure 7a). Twins were observed in the majority of grains, with orientations of twin sets varying between grains (with some showing up to three sets within a single grain (Figure 7a). Twins in Sample JS-07 (Figure 7a) were similar thickness to those in Figure 7b but more closely spaced (Figure 7).

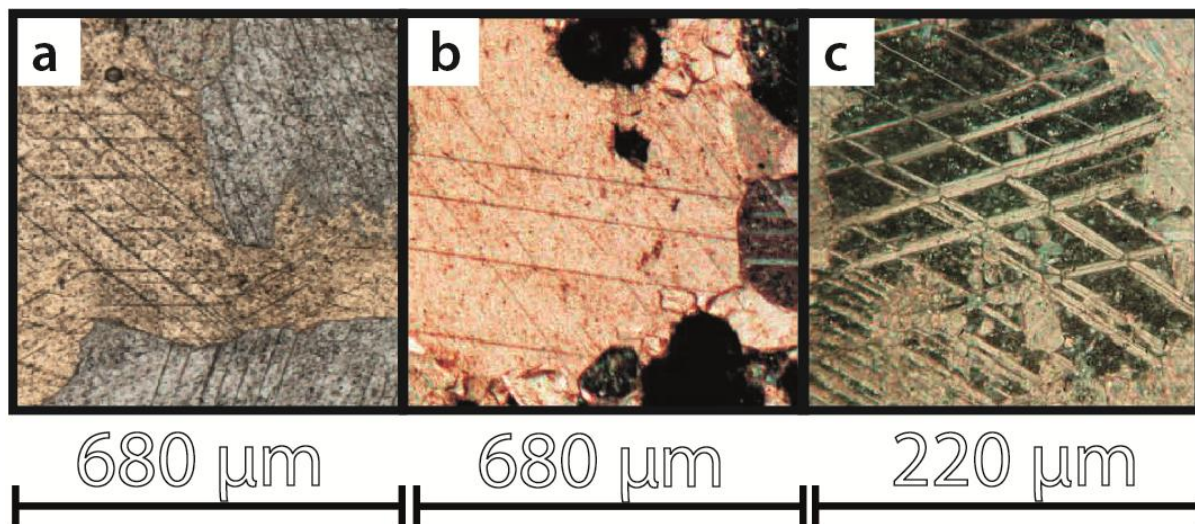


**Figure 7.** a) Photomicrograph of calcite vein fill from Cape Otway, Victoria, Australia, showing various calcite grains with sets of twins (Sample JS-07). b) Example of Type I (thin twins) twins from the Northern Subalpine Chain, France (figure adapted from Ferrill *et al.* (2004)). c) Example of Type II twins (tabular thick twins) from the Northern Mountain thrust sheet in the Great Valley, Central Appalachian Valley and Ridge Province (figure adapted from Ferrill *et al.* (2004)).

Calcite cement fills in Samples JS-01 and JS-02 revealed several phases of crack-seal deformation at Moonlight Head, where two discrete fracture fills are separated by one median line, which is equivalent to one crack seal event (Figure 8). Crack-seal is simple in Sample JS-01 (Figure 8a). However, Sample JS-02 records a more complex history, with multiple crack-seal events evident (Figure 8b).



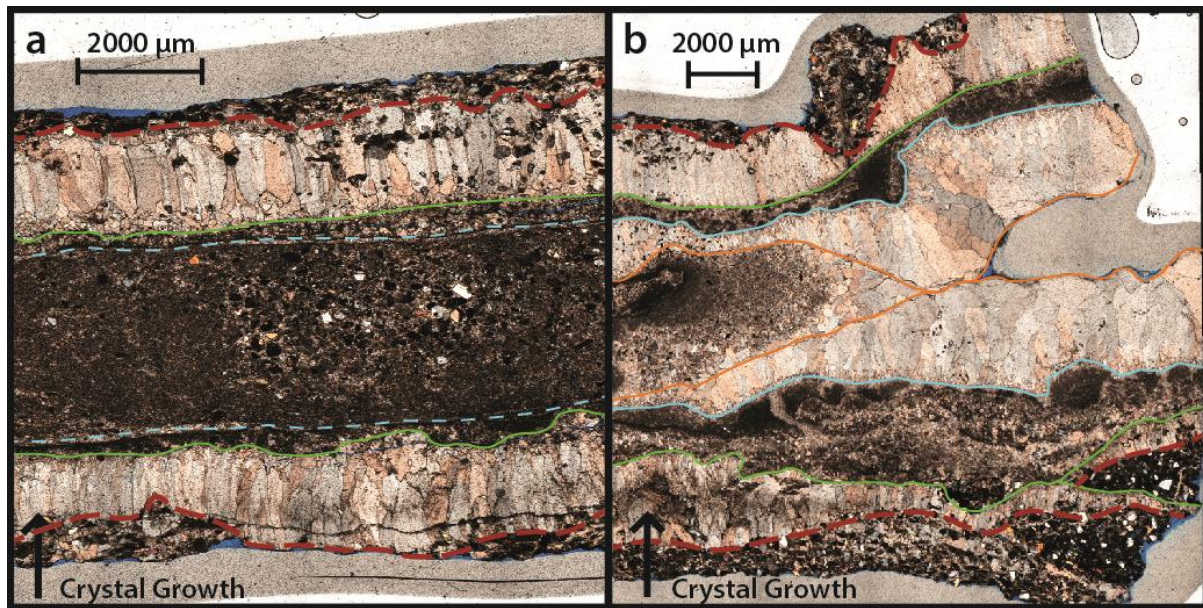


**Figure 8. Photomicrographs of calcite vein fills at Moonlight Head. Dashed red line represents fracture/host rock boundary. Other coloured lines represent median lines of crack-seal events (green represents first event, blue represents second event, orange represents third event) a) Section of Sample JS-01 showing at least one (possibly two) crack-seal events. b) Section of Sample JS-02 showing a more complex crack-seal history with at least three crack-seal events.**

Porosity calculations were undertaken on sections of samples from Moonlight Head (Sample JS-04) (Figure 9a) and from Cape Otway (Sample JS-07) (Figure 9b). These locations were used due to their burial history and lithological differences with Cape Otway having deeply buried siltstones and Moonlight Head having shallowly buried medium grained sandstones. Samples were impregnated with blue epoxy resin (appearing blue on thin sections) as part of the slide manufacturing process, in order to determine porosity. Using the image analysis technique on JS-04 and JS-07 with JMicroVision<sup>®</sup>, porosities of 7.15% and 0.36%, respectively, were determined.



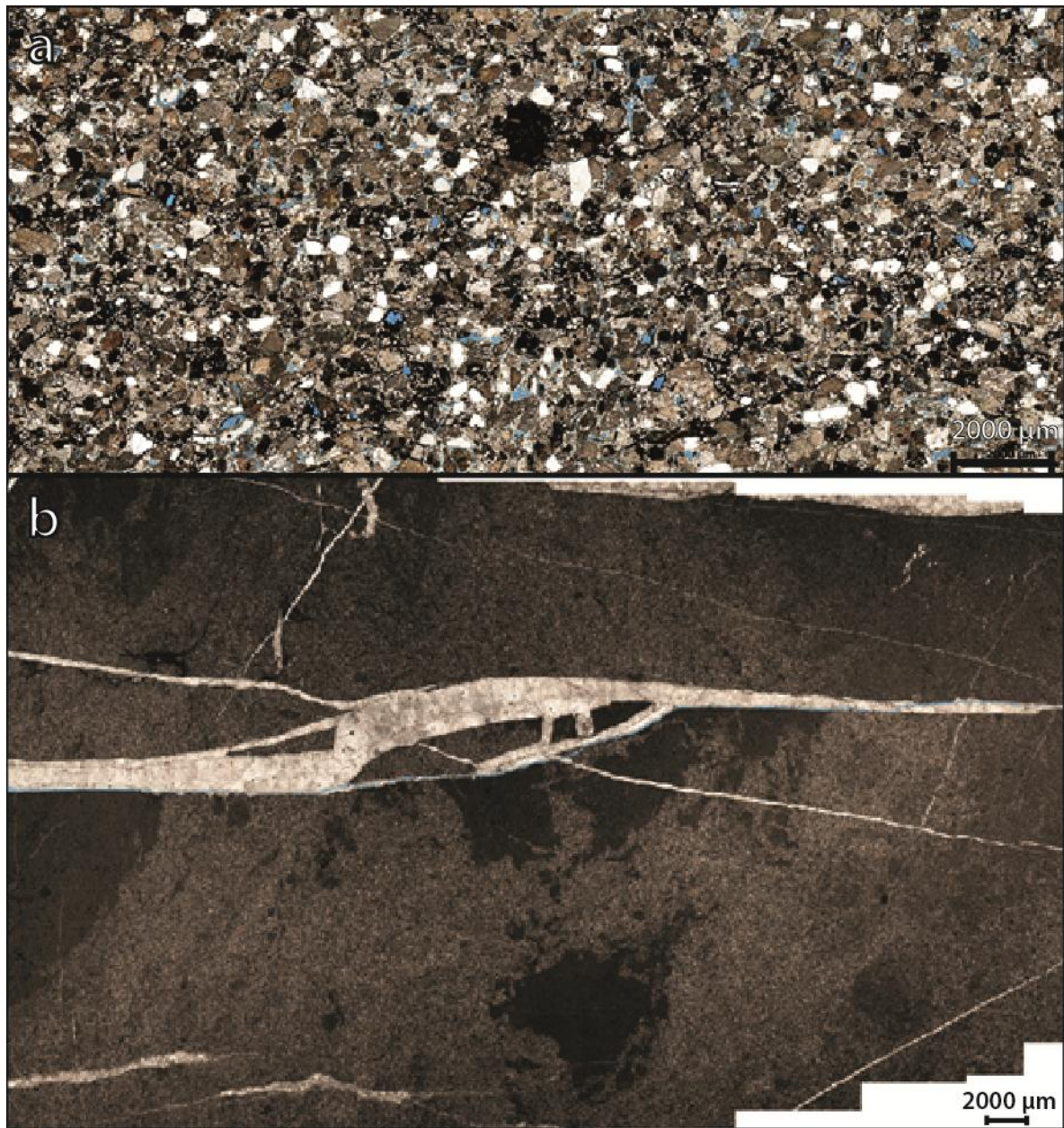


**Figure 9. Photomicrographs of thin sections of samples from the Otway Basin used for porosity calculations. a) Porosity was calculated to be 7.15 % for Sample JS-04 from Moonlight Head. b) Porosity was calculated to be 0.36% for Sample JS-07 from Cape Otway.**

### **Mechanical Stratigraphy and Variations in Lithology**

Due to the lithological variance within the Eumeralla Formation, fracture patterns observed in the field were also quite variable. Therefore, detailed lithological observations were taken at every field site to compare fracture patterns with rock type (Table 4).

The data in Table 4 show a varying degree of fracture densities within the Eumeralla Formation at outcrop in the Otway Basin. Fracture densities were an order of magnitude higher at Cape Otway within the finest grained and deepest buried sediments observed (Figure 10a). From these data, it can be seen that lithological variation has a strong control on the fracture density within the Eumeralla Formation (Figure 10b).

**Table 5. Fracture density data, average bedding and lithological variations at field sites in the Otway Basin, Victoria, Australia. Maximum burial temperatures were determined from vitrinite reflectance data by Duddy (1994).**

Location (total transect length)	Lithological variations	Bedding (dip/dip Direction)	Number of fractures (Fractures/m)			Number of Siderite Filled Fractures (Fractures/m)	Number of Calcite Filled Fractures (Fractures/m)	Maximum burial T (°C)
			Open	Closed	Total			
<b>Moonlight Head (20 m)</b>	Fine to very fine volcanogenic sandstone. Well-rounded and well-sorted. Thickly bedded (10 to 20 cm) but finely laminated (1 to 2 mm) with cross-bedding. Sequence coarsens up over ~20 m to medium grained volcanogenic sandstone. Also well-	42/330	36 (1.8)	27 (1.35)	63 (3.15)	24 (1.2)	3 (0.15)	~50
<b>Moonlight Head - Conglomerate Beds (3 m)/Medium Grained Beds (12 m)/Fine Grained beds (5 m)</b>	rounded and well-sorted. Thickly bedded (20 to 30 cm) and less finely laminated (2 to 5 mm) interbedded with cross bedded conglomerate lenses (20 to 30 cm) with clasts (1 to 10 cm) within a coarse grained sand matrix. Sequence is moderately to well fractured, with preferential fracturing occurring between medium to coarse grained lithologies and conglomerate bearing lenses.		5 (1.66)/ 36 (3)/ 22 (4.4)					
<b>Cape Patton</b>	Medium grained light grey volcanogenic sandstones. Well-	18/076	64 (4.2)	8 (0.5)	72 (4.5)	8 (0.5)	0 (0)	~50
<b>Cape Patton - Medium Grained Beds (11)/Silt Beds (4 m)</b>	rounded and well-sorted. Thickly bedded (up to 1 m) with interbedded silt and fine sand layers (20 to 30 cm) with very fine laminations (1 mm).		22 (2)/ 50 (12.5)					
<b>Marengo (90 m)</b>	Fine dark grey volcanogenic sandstones. Well-rounded and well-sorted. Thickly bedded yet finely laminated, with cross bedding and scour and fill surfaces. Well fractured with numerous Fe-rich alteration halos around fractures. A large conglomerate channel with sub-angular to rounded, fine grained	20/016	112 (1.24)	53 (0.58)	165 (1.83)	41 (0.45)	0 (0)	~100
<b>Marengo - Conglomerate (1 m)</b>	clasts (up to 10 cm) inside a coarser grained matrix. Few interbedded thin (1 to 2 cm) coal rich lenses.		0 (0)					



## Fault and Fracture Networks in the Otway Basin

<b>Skenes Creek (120 m)</b>	Fine to very fine dark grey volcanogenic sandstones. Cross bedding and scour and fill channels. Coal beds (width up to 20 cm) with small clasts (1 to 2 cm) are interbedded with conglomerate layers (up to 1 m) with large clasts (5 to 10 cm) in medium sand matrix. Sequence coarsens upwards, with distinctive honeycomb weathering pattern in coarse grained beds. Moderately fractured with numerous Fe-rich alteration halos around fractures. Large concretions of Fe-rich cemented sands, with closed fractures radiating outwards from the concretions.	20/125	67 (0.56)	61 (0.51)	128 (1.07)	34 (0.28)	4 (0.03)	~105
<b>Castle Cove (48 m)</b>	Fine to very fine dark grey volcanogenic sandstones. Well-rounded and well-sorted. Moderately fractured with numerous Fe-rich alteration halos around fractures. Large concretions of Fe-rich concreted sands with closed fractures radiating outwards from the concretions. Several distinct interbedded lenses of slightly coarser coal rich lithology. Soft sediment deformation (flame structures) and cm-scale faulting in some intervals.	16/148 (173 m from fault), 30/128 (14 m from fault)	30 (0.63)	147 (3.06)	177 (3.69)	88 (1.83)	52 (1.08)	~100-120
<b>Crayfish Bay (70 m)</b>	Fine to very fine dark grey volcanogenic sandstones. Well-rounded and well-sorted. Moderately fractured with numerous Fe-rich alteration halos around fractures. Large concretions of Fe-rich cemented sands, with closed fractures radiating outwards from the concretions. Several distinct interbedded lenses of slightly coarser coal rich lithology.	28/240	30 (0.43)	10 (0.14)	40 (0.57)	5 (0.07)	1 (0.01)	~100-130
<b>Cumberland River (90 m)</b>	Fine dark grey volcanogenic sandstones. Well-rounded and well-sorted. Very well defined cross bedding (beds 5 to 10 cm) with fine laminations. Some minor coal lenses (1 to 2 cm). Very well fractured and very little variation in lithology along the transect.	10/113	78 (0.87)	90 (1.22)	188 (2.09)	81 (0.9)	12 (0.13)	~156
<b>Cape Otway (4 m)</b>	Very fine volcanogenic siltstone. Very well-rounded and very well-sorted. Highly fractured with numerous calcite filled veins. Very finely laminated, with fine beds (0.5 to 2 cm) observed.	30/009	128 (32.0)	41 (10.25)	169 (42.25)	0 (0)	24 (6.0)	>350

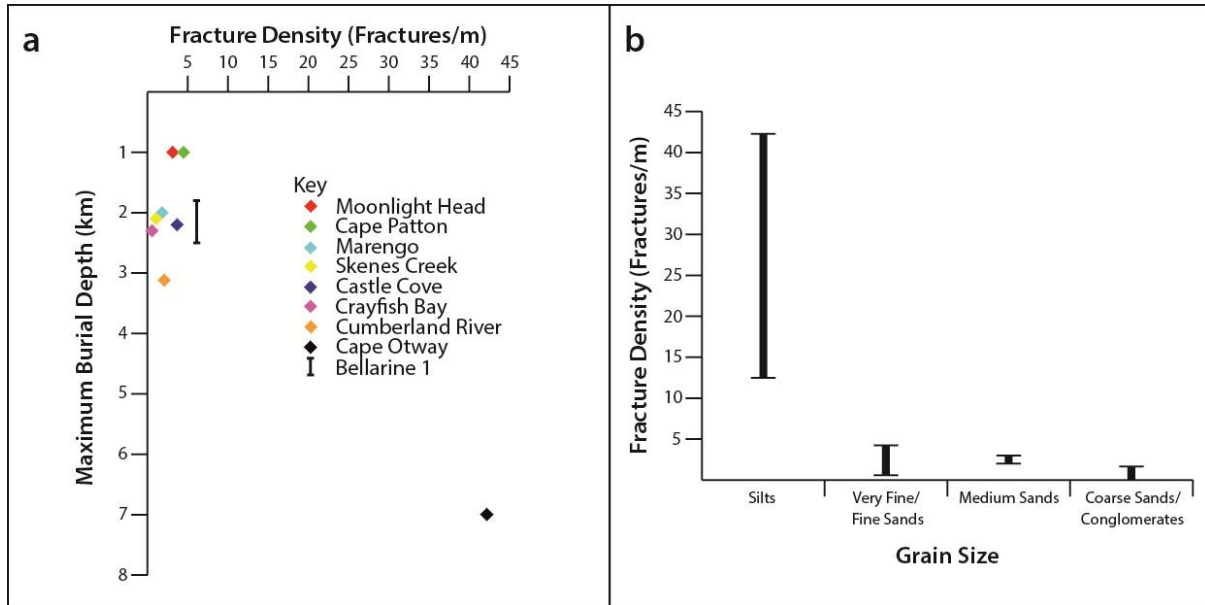


**Figure 10. a) Fracture densities in the Eumeralla Formation at different sites in the Otway Basin compared with the maximum depth at which the site had been buried. The average fracture density from the Eumeralla Formation interval from Bellarine-1 has been included from Tassone *et al.* (in press). b) Fracture densities ranges within different lithologies shown by average grain sizes.**

The total fracture density is highest in the silt-sized grain lithologies, which also show the highest variation in fracture densities (Figure 10b). There is a marked drop in fracture densities between silt-sized grain lithologies and very fine sand lithologies, with a general decrease in fracture density with increasing grain size (Figure 10b).

In the case of Cape Patton (Figure 11) it is clearly seen that a marked increase in fractures can be seen from the coarse grained sand beds to the very fine grained shale beds. In both Figures 12 and 13 many fractures terminate at the boundaries of thick coarse grained conglomerate lenses. However, in Figure 13 a small number of much larger siderite filled fractures propagate throughout the entire section, unaffected by the change in lithology.

Section of Cape Patton face map

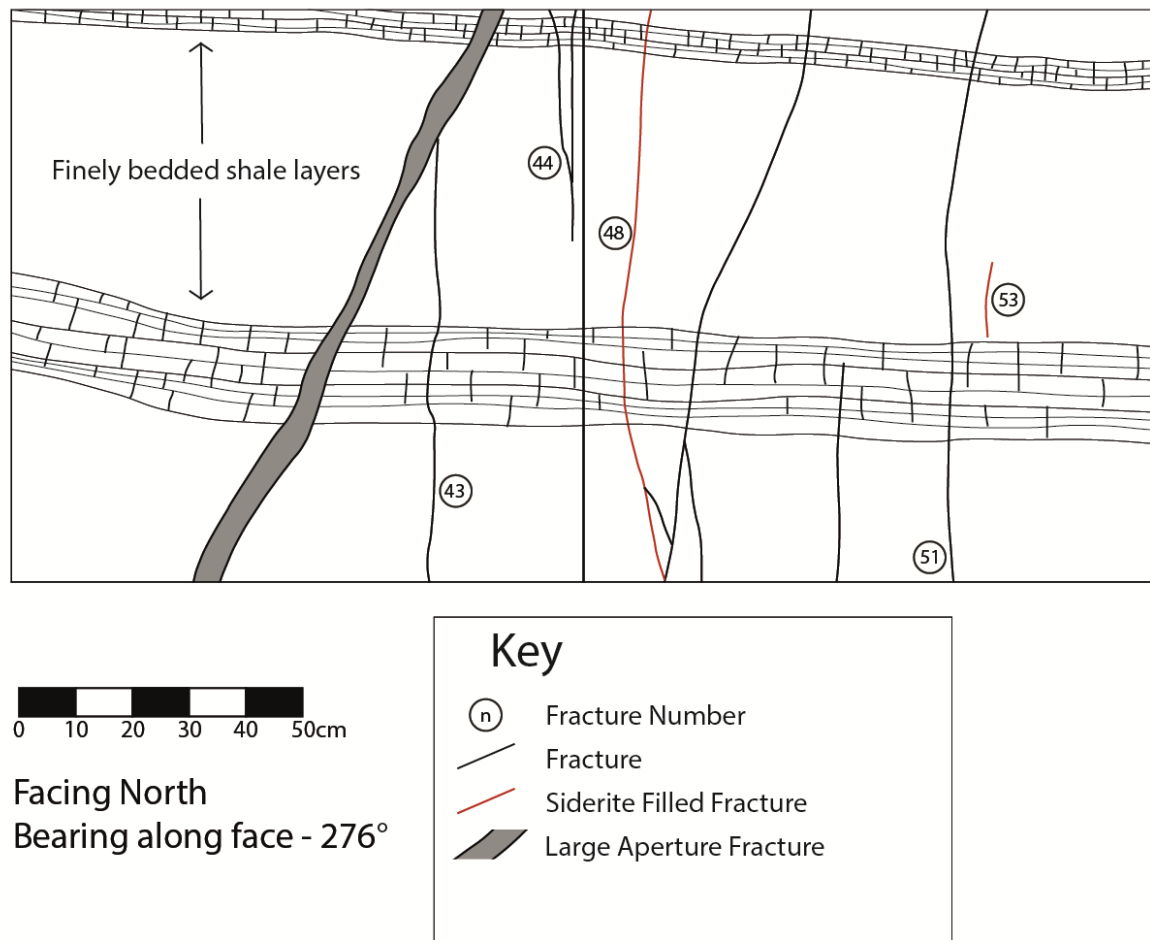
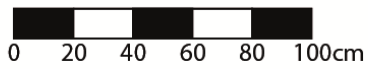
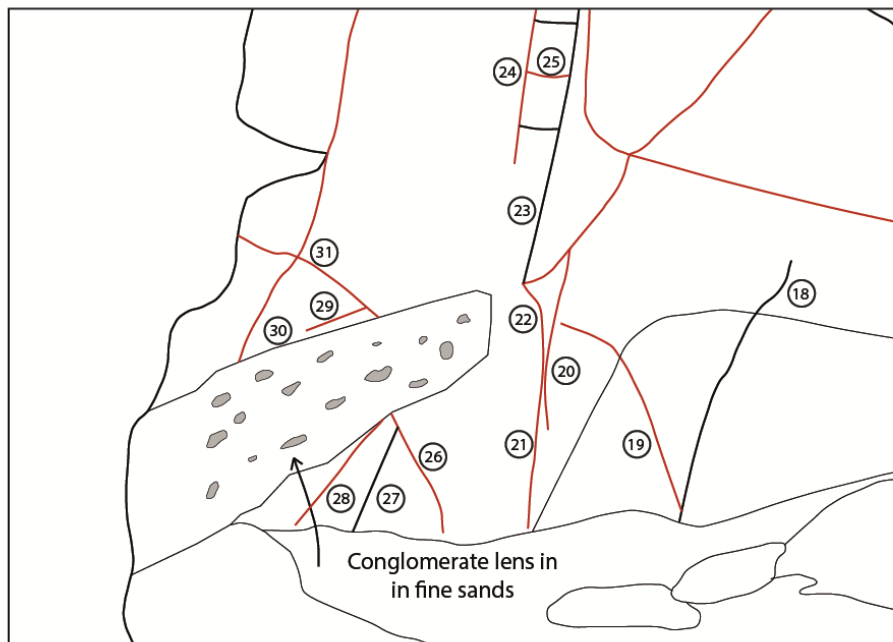


**Figure 11. Section of face map drawn at Cape Patton. Note very fine grained/silt, finely laminated and finely bedded layers interbedded with fine to medium grained, thickly bedded, well-rounded and well-sorted volcanogenic sands. (For complete map see Appendix B)**

Section of Marengo face map 1



Facing West  
Bearing along face - 305°

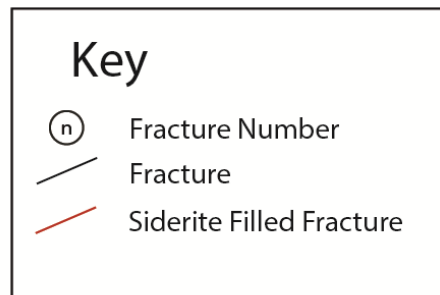
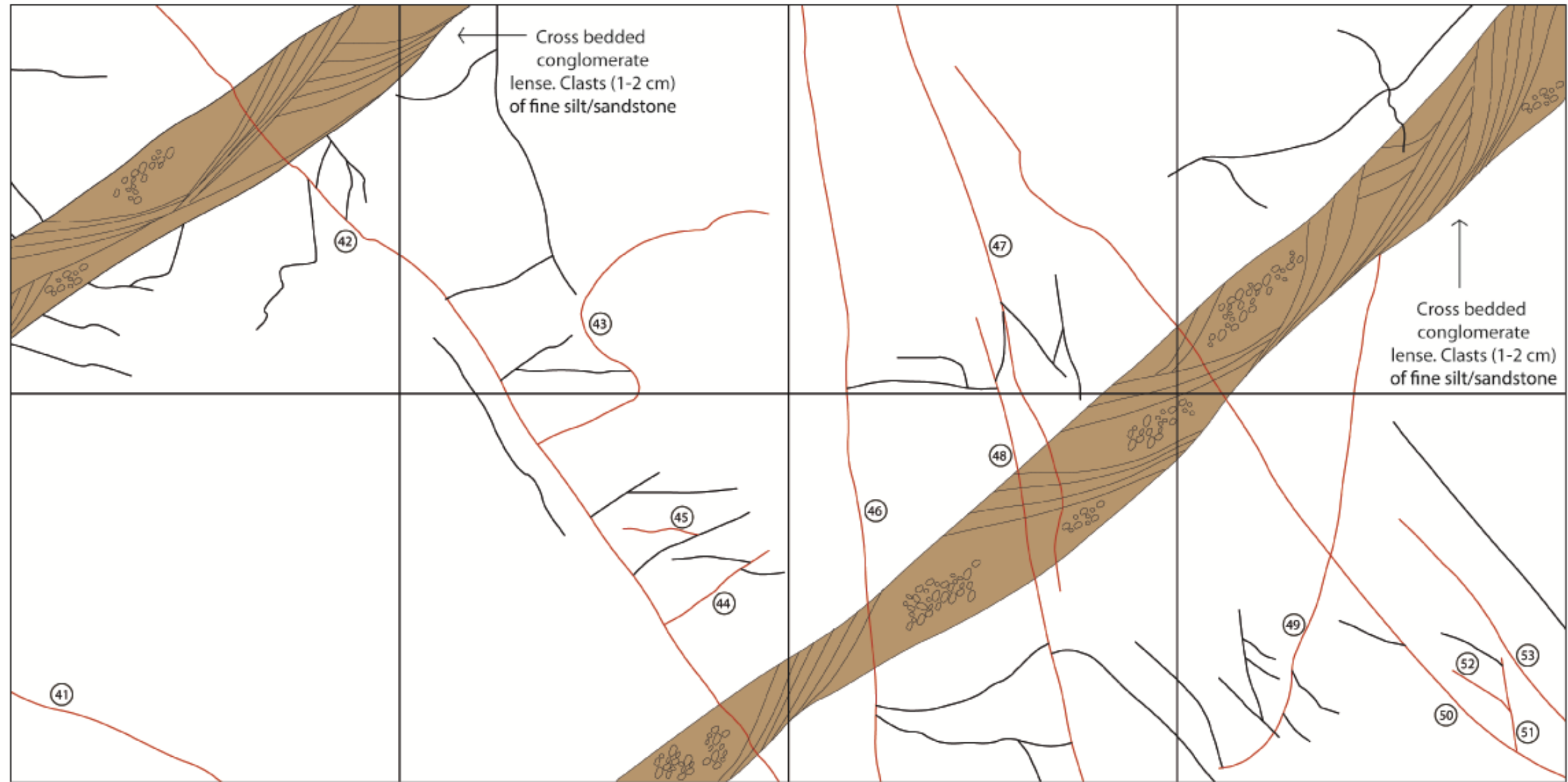


**Figure 12. Section of face map drawn at Marengo. Note conglomerate lens with fine grained clasts inside a coarse grained matrix, clasts up to 10 cm, sub-angular to rounded. Lens is hosted in fine grained, thickly bedded but finely laminated volcanogenic sands. (For complete map see Appendix B)**

Moonlight Head face map 2- C-D (Map 3 of 3)



C

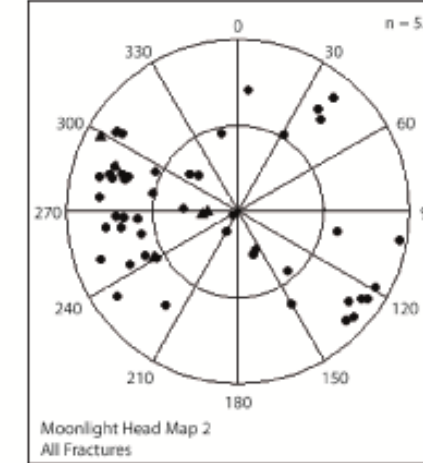
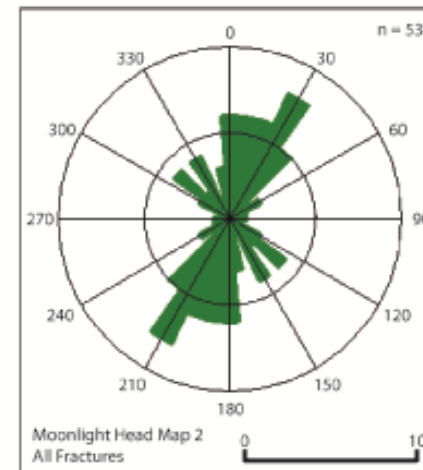
Transect Start S 38° 45.285'  
E 143° 12.762'  
Transect End S 38° 45.288'  
E 143° 12.771'



Facing North  
Bearing along face - 127°

Key

- (n) Fracture Number
- Fracture
- Siderite Filled Fracture



D

Figure 13. Section of face map drawn at Moonlight Head. Note medium to coarse grained, thickly bedded (20 to 30 cm), less finely laminated (2 to 5 mm) well-rounded and well-sorted volcanogenic sands, interbedded with cross bedded conglomerate bearing lenses (20 to 30 cm) with clasts (1 to 10 cm) within a coarse grained sand matrix. Clasts appear to be those of similar fine to medium grained units. (For complete map see Appendix B)

## **DISCUSSION**

### **Variation in Fracture Patterns around Local Structures**

Local structures appear to have significant effects on the fracture patterns observed at sites in the Otway Basin. By observing fracture patterns seen at individual sites and comparing them with other sites across local structures and with published examples, the mechanisms responsible for the creation of such patterns can be better understood.

### **FOLD AT CAPE OTWAY AND ASSOCIATED FRACTURE PATTERN**

Outcrop at Cape Otway provides one of the best examples in the field area to compare how local structures can potentially affect fracture networks. Figure 14a shows a fracture pattern typically associated with folding (Twiss & Moores 2007). This same fracture pattern was observed at Cape Otway and is potentially related to the broad, low amplitude fold seen at this location.

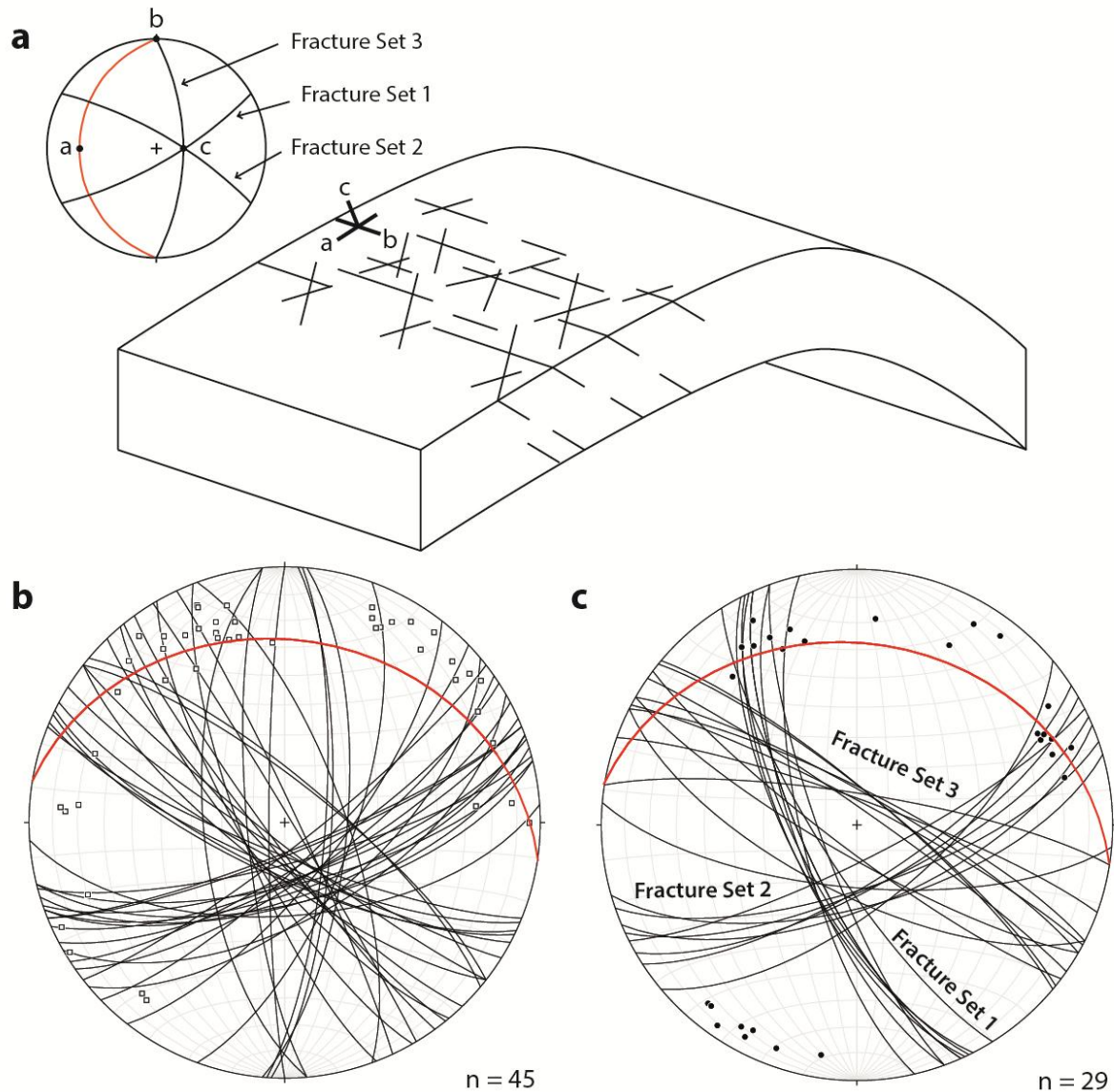


**Figure 14. Data collected from Cape Otway. a) Fracture pattern associated with folding with accompanying stereographic projection of the orientations of the coordinate system (a, b and, c), fracture planes (black great circles) and the bedding (red great circle) (adapted from Twiss & Moores 2007). Fracture pattern observed at Cape Otway appeared very similar to this typical fold fracture pattern. b) Fracture planes of open fractures observed at Cape Otway (black great circles) and poles to fracture planes (black open squares). Red great circle represents bedding. c) Fracture planes of calcite filled fractures observed at Cape Otway (black great circles) and poles to fracture planes (black dots). Red great circle represents bedding.**

Fractures measured at Cape Otway were located on the north-western limb of a NE- SW trending fold, with both open and calcite filled fractures identified (Figure 14b and 14c respectively). The orientations of the calcite filled fractures approximate the idealised fracture pattern associated with folding (Figure 14a); where Fracture Sets 1 and 2 form a conjugate

pair with their bisecting angle parallel to  $\sigma_1$ /shortening direction and perpendicular to  $\sigma_2$ /fold hinge and Fracture Set 3 striking parallel to the fold hinge and bedding (Figure 14a).

The occurrence of calcite fill in Fracture Sets 1, 2 and 3 in this pattern suggests that calcite fracture fill was coeval with the formation of these fractures. Later fractures initiated and opened and were not filled with calcite. Thus, calcite rich fluid was in the system for a short period of time.

During the Miocene the previous extensional stress regime in the Otway Ranges changed to a compressional stress regime. This formed a series of NE trending features including anticlines, synclines and monoclines (Edwards *et al.* 1996). Existence of the NE trending Cape Otway fold is consistent with previous work and associated calcite fill would then be interpreted to be of Miocene age.

Although fractures from Cape Otway appear to describe these same geometries on a stereographic projection (Figure 14b & 14c), a fold interpreted from these data should strike WNW-ESE, and not NE-SW as the Cape Otway fold does. If this is the case then the interpretation that these fractures are fold related and of Miocene age is incorrect. Given that the pattern observed at this location does approximate an idealised fold related fracture pattern, a pattern that could be observed in data from image logs for example, erroneous interpretations are conceivable where access to outcrop or other supporting data are not available.

Calcite twins observed in fracture fills from this area were also analysed and compared with published examples. Twins in deformed calcite at temperatures below 170°C are usually type



I (thin twins), appearing under optical microscope as only thin black lines (Ferrill *et al.* 2004). These twins are commonly less than one micron (1  $\mu\text{m}$ ) thick (Ferrill *et al.* 2004).

When comparing the calcite twins from sample JS-07 (Figure 7a), to the type I (thin twins) and type II (tabular thick twins) (Figures 7b and 7c, respectively), it is likely that twins in JS-07 are type I (thin twins). This implies that the temperature conditions during formation of calcite filled fractures at Cape Otway did not exceed 170°C. Although this does not help define timing of fracture generation, any fracture fill must have been precipitated and deformed at temperatures of equal to or less 170°C. It is likely then that fracture fills are post the mid-Cretaceous event described by Duddy (1994), before which, the maximum paleotemperatures exceeded 350°C in this location.

#### FRACTURE ORIENTATIONS ACROSS THE WILD DOG SHEAR ZONE

As discussed by Duddy (2002), the highly uplifted structural block, which includes Cape Otway sediments and the area around well Olangolagh-1, exists immediately west of the Wild Dog Shear Zone (Figure 4). Towards the east of this system the Eumeralla Formation crops out at Crayfish Bay, with the distance between Crayfish Bay and Cape Otway representing an uplift difference of 4 km (Duddy 2002). This area provides a great opportunity to study the differences in fracture patterns over short distances where a major structure exists as well as areas with a change in uplift history.

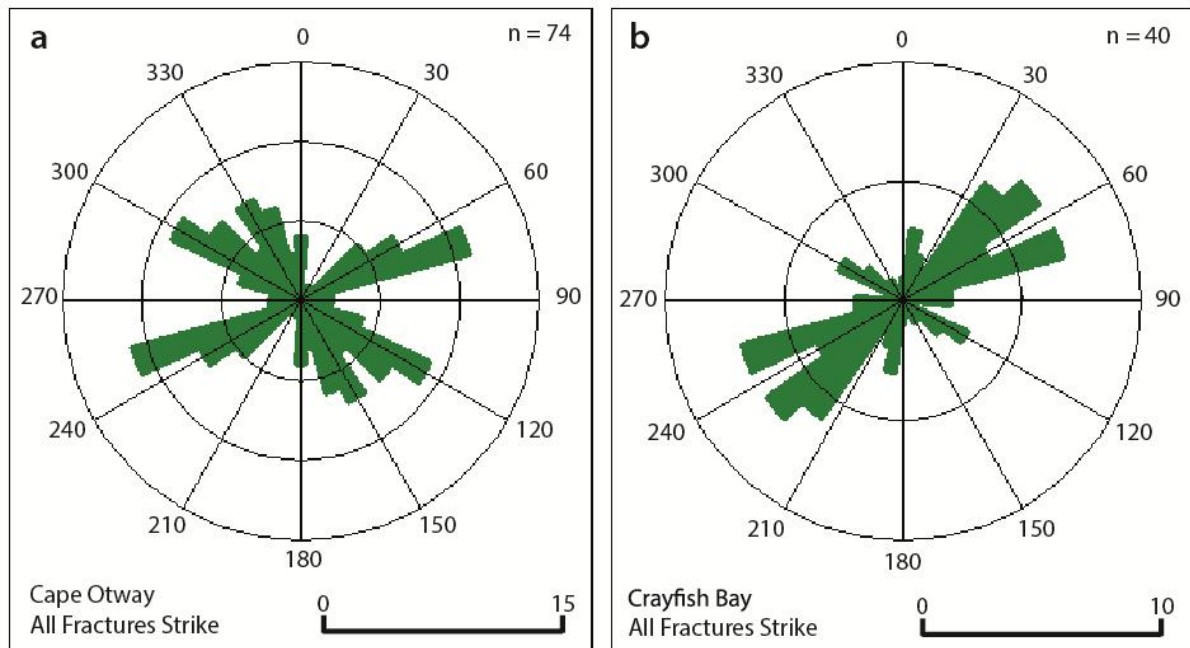


**Figure 15.** Rose diagrams showing a) All fracture plane strikes at Cape Otway and b) All fracture plane strikes at Crayfish Bay. Note that radial intervals are not at the same scale.

At Cape Otway two major fracture sets were observed (ENE-WSW and WNW-ESE) and one minor set (NNW-SSE) (Figure 15a). When fracture patterns are compared across the Wild Dog Shear Zone, with the vastly different burial depths of the two areas, it was observed that there was no representation of a NNW-SSE fracture set at Crayfish Bay (Figure 15b). Given the lateral proximity of Cape Otway and Crayfish Bay, fracture set generation is most likely due to the differential burial depths. Therefore, generation of the NNW-SSE fracture set occurred only at the Cape Otway interval when it was at greater depth.

## FRACTURES ASSOCIATED WITH THE CASTLE COVE FAULT

The Castle Cove Fault is a NE-SW striking fault that was inverted during the Miocene to form a monoclinial structure (Edwards *et al.* 1996). The structure dips steeply (up to 90°) to the NW, with the footwall to the SE (Carter 1958, Duddy 2002), indicating that the Castle Cove Fault is a result of inversion of an earlier rift fault (Tassone *et al.* in press). Overlying Eocene sediments are also folded within the monocline indicating that inversion and folding of this structure must have occurred post-Eocene in the late Cenozoic (Duddy 2002, Tassone 2013).

Fracture orientations at Castle Cove demonstrate a distinct rotation from fractures adjacent to the Castle Cove Fault that strike NE-SW to fractures observed ~170 m away from the fault that strike NNW-SSE (Figure 16). Given the NE-SW orientation of the Castle Cove Fault, it is likely that fractures adjacent to the fault are directly related to the initial formation of the fault or reactivation of the fault itself, given their similar orientation. Thus, forming a damage zone around the fault that lessens with distance away from the fault, as shown by the change in fracture density adjacent to the fault (~4.5 fractures/m) to that seen away from the fault (~3.69 fractures/m) (Table 4).

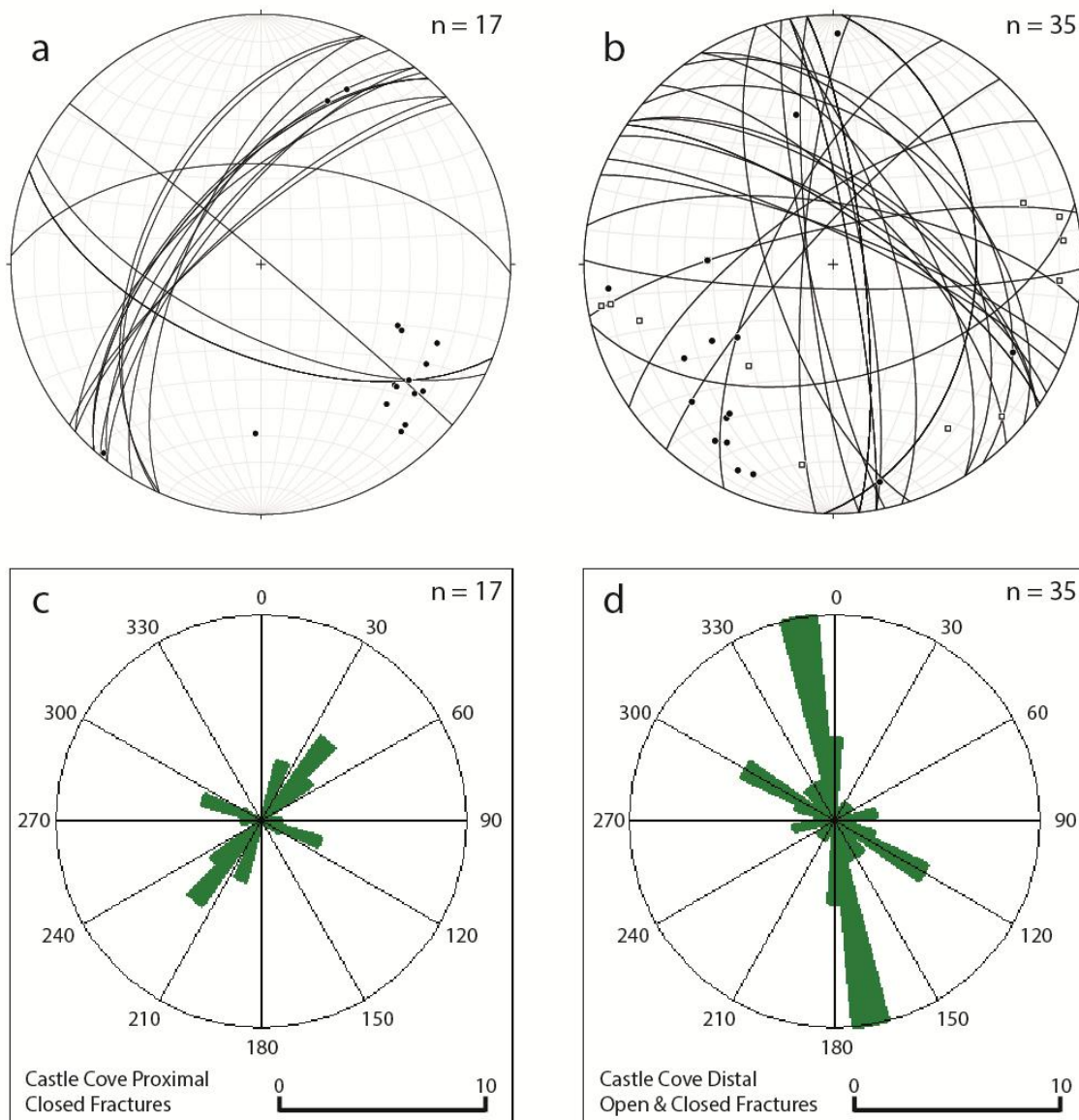


**Figure 16. Structural data from Castle Cove. a) All fracture planes measured ~14 m from the Castle Cove fault (black great circles) and poles to fracture planes (black dots). b) All fracture planes measured ~173 m from the Castle Cove fault (black great circles) and poles to closed fracture planes (black dots) and poles to open fracture planes (black squares). c) Rose diagram of all fracture strikes measured ~14 m from the Castle Cove fault. D) Rose diagram of all fracture strikes measured ~173 m from the Castle Cove fault.**

However, it is argued by Tassone (2013) that the majority of fractures seen at Castle Cove largely remain perpendicular to bedding regardless of their proximity to the fault, becoming horizontal at the hinge of the monocline where the bedding is vertical. This infers that fractures observed at this location were initiated prior to reactivation and folding, and have

thus been realigned during the Miocene inversion. Although data presented in Figure 16 do not clearly support this relationship, Figure 17 shows the trend of fractures remaining perpendicular to bedding adjacent to the fault. Therefore, a subsequent set of NE-SW closed fractures next to the Castle Cove Fault are inferred to have formed contemporaneously with the fault reactivation (Castle Cove Set), with bedding perpendicular fracture sets formed prior to this event (Sets 1 and 2).



**Figure 17. Photograph of orthogonal fracture relationship to monoclinical folding of Eumeralla Formation adjacent to the Castle Cove Fault, Castle Cove, Victoria. Photograph looking north.**

## General Field Trends of Fracture Sets

### TILT CORRECTED FRACTURE SETS

Figure 18 shows the average planes of different fracture sets interpreted from three sites in the Otway Basin. From south to north an apparent clockwise rotation of orthogonal Fracture Sets 1 and 2 occurs. When bedding is unfolded these orthogonal fracture sets plot, in all cases, as vertical fracture sets. This is consistent with observations by Tassone (2013) at Castle Cove, where fractures were seen to remain perpendicular to bedding despite large-scale monoclinical folding in the vicinity of the Castle Cove Fault.

Although there is consistency in the fracture patterns at these four sites, unfolding bedding to compare fracture sets assumes that all fracture sets were created prior to the folding event(s). Thus, the consistency of Fracture Sets 1 and 2 indicate that at least one major fracturing event occurred prior to folding. Given that major folding occurred during and since the Miocene, Fracture Sets 1 and 2 can be inferred to have formed prior to the Miocene.

The interpretation of data from Cape Otway presented in Figure 18a is contrary to the fold related fracture patterns presented in Figure 14. However, due to the consistent pattern of orthogonal Fracture Sets 1 and 2 at other sites along the coast (Figures 18b and 18c), the interpretation that fractures were vertical opening Mode I type (where  $\sigma_1$  was vertical, and fracture opening was perpendicular to  $\sigma_3$  (Anderson 1951b, Sibson 1995)) were formed prior to Miocene inversion is favoured.

The clockwise rotation of the fracture sets from south to north could be the result of small variations in the rotation of the stress field since the Miocene. Given that the present-day



stress directions, determined from petroleum wells, plus neotectonic structures and earthquake focal mechanisms around the Otway Ranges show consistent  $\sigma_H$  orientations, any widespread large rotation is unlikely. This is unless localised stress field deflections occur around small to large scale structures (e.g. Bell 1996b, Gudmundsson *et al.* 2010, King *et al.* 2012a), like that seen at Castle Cove, or between Cape Otway and Crayfish Bay.

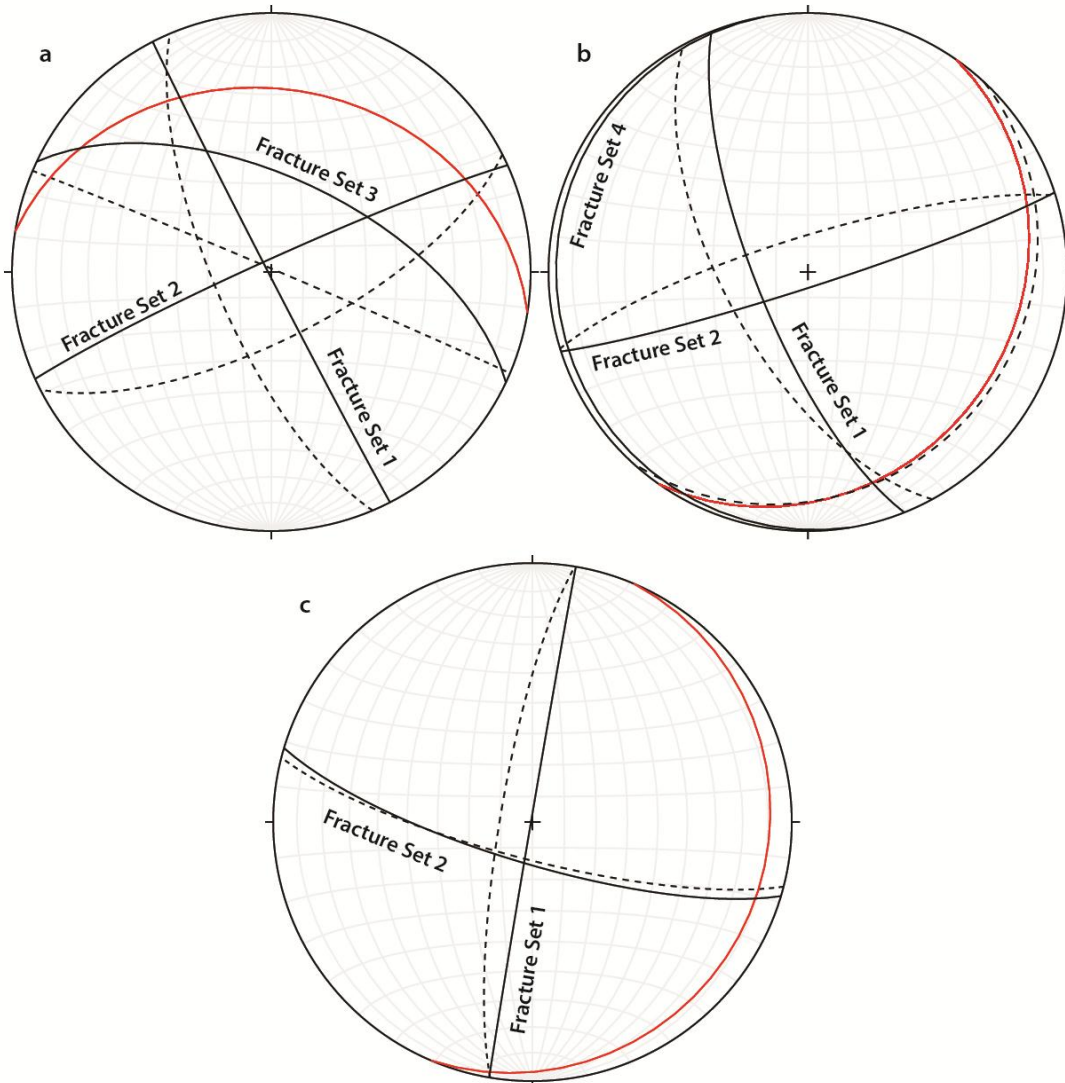


**Figure 18.** Stereonet of unfolded bedding data at sites along the Otway Coast. a) Cape Otway, average fracture planes of three separate fracture sets identified in calcite filled fractures (black dashed great circles), average bedding from site where data were collected (red great circle) and fracture plane orientation after bedding is unfolded (solid black great circles). Angles between Fracture Sets 1 and 2 are  $87.2^\circ$  and  $92.8^\circ$ . b) Skenes Creek, average fracture planes of two separate fracture sets identified in fractures (black dashed great circles), average bedding from site where data were collected (red great circle) and fracture plane orientation after bedding is unfolded (solid black great circles). Angles between Fracture Sets 1 and 2 are  $84.9^\circ$  and  $95.1^\circ$ . and c) Cumberland River, average fracture planes of two separate fracture sets identified in fractures (black dashed great circles), average bedding from site where data were collected (red great circle) and fracture plane orientation after bedding is unfolded (solid black great circles). Angles between Fracture Sets 1 and 2 are  $83.1^\circ$  and  $96.9^\circ$ .

## **Implications of Fractures in the Otway Basin: From Past to Present**

### MECHANICAL STRATIGRAPHY OF THE EUMERALLA FORMATION

It is clear from outcrop of the Eumeralla Formation that fracture density and character is highly dependent on lithology (e.g. Table 4, Figure 10b). Figures 11, 12 and 13 all show specific circumstances where fracture density, length and continuance are affected by a change in lithology at an outcrop scale. In some it has been observed that differences in lithology can have a negative effect on the propagation of fractures, with many fractures within fine-grained sediments terminating at boundaries of very coarse grained intervals (Figures 12 and 13).

Figure 11 shows that fracture densities can dramatically increase from coarser grained intervals into shale intervals. This is contrary to the traditional view that shales deform in a ductile manner. However, shales with densities greater than  $2.5 \text{ g/cm}^3$  behave in a brittle manner (Corcoran & Doré 2002). Using average bulk densities with respect to depth as a proxy for brittleness for the Eumeralla Formation, Tassone *et al.* (in press) showed that well Bellarine-1 (which is representative of the lithology seen in the field area) has high densities and is therefore brittle throughout the entire Eumeralla Formation. This observation explains the increased fracture densities in the shale intervals seen across the field area (Table 4, Figure 10b & Figure 11).

The effect of lithology on fracture density in the Eumeralla Formation is further reinforced by the observations of Tassone *et al.* (in review) who showed that in well Bellarine-1, discontinuous fractures were within zones of changing resistivity, implying that fracture occurrence was strongly controlled by lithology. Fracture densities observed in Tassone *et al.*



(in press) were high, with ~6 fractures per metre recorded. However, this is still somewhat less than the range of high values observed in some lithologies in this study.

## FRACTURE GENERATION HISTORY

Determining the timing of fracture generation is difficult in the Otway Basin due to its complex history of deformation. Nevertheless, fracture generation can still be constrained based around deformational events within the basin.

Commencement of N-S trending extension during the Late Jurassic created accommodation space for the deposition of the Otway Group sediments (Cooper & Hill 1997). Extension gave way to compression and inversion during the mid-Cretaceous (Krassay *et al.* 2004); resulting in as much as 3 km of inversion with localised deformation occurring in the eastern part of the basin (Cooper & Hill 1997). Subsequent NE-SW extension followed in the Late Cretaceous (Schneider *et al.* 2004). Finally, reactivation of Cretaceous faults, folding and new fault development has been occurring continually since the mid-Eocene (Tuitt *et al.* 2011).

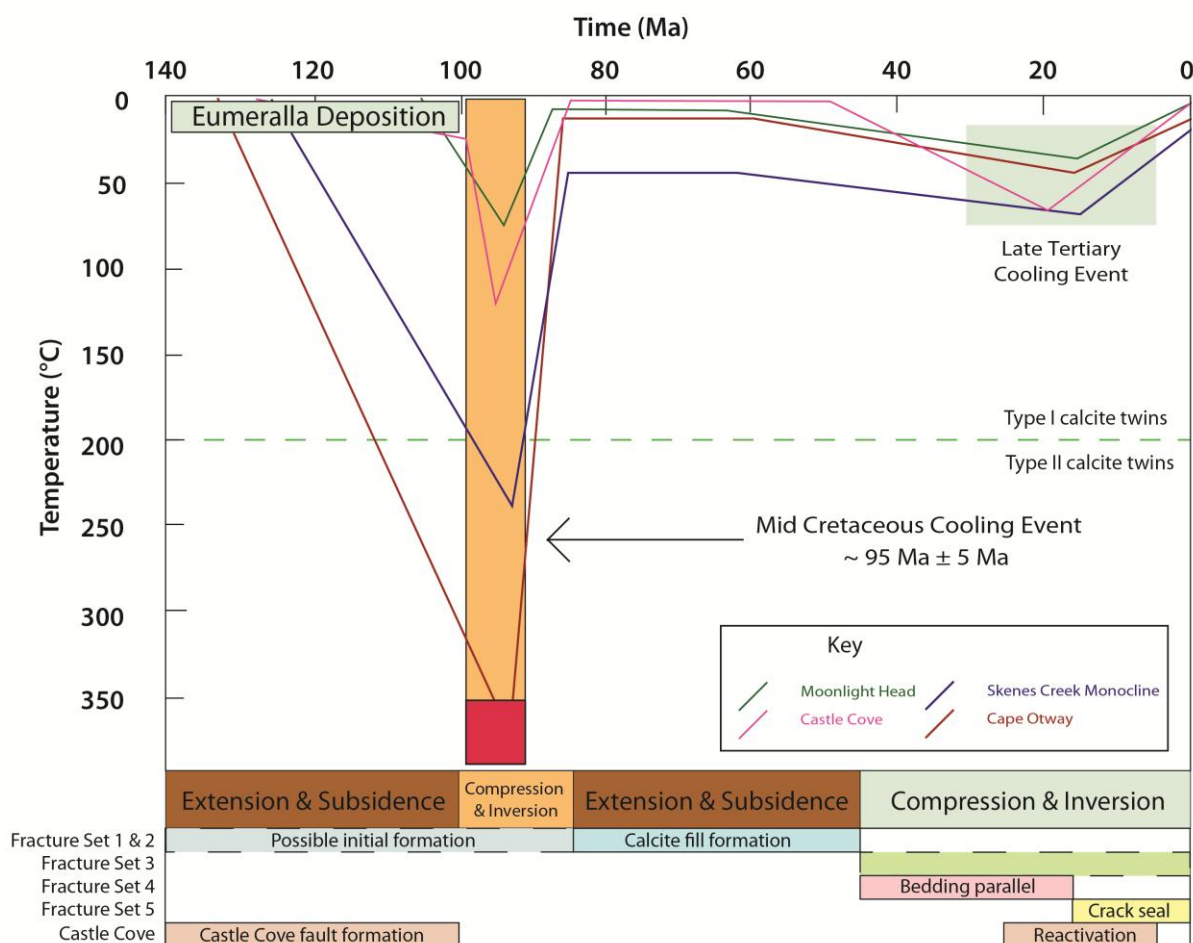
Modelling by English (2012) showed that thermal contraction due to cooling is an important mechanism through which vertical tensile fractures are formed. English (2012) indicated this mechanism is highly dependent on exhumation and rock stiffness, and that Mode 1 fractures were more likely to form where uplift occurred in initially overpressured and tectonically relaxed environments. This model shares similarities with the Otway Basin. The Otway Basin demonstrates large, fast cooling events following basin rifting and sag with high geothermal gradients (Duddy 1994, 2003, Tassone *et al.* in press). Evidence from Sibson (1995) indicates that fluid overpressures occur where tectonic regimes change from extension to compression.

Thus, this may have been a source of overpressure in the Otway Basin during two periods in its history: The mid-Cretaceous and the Miocene. If thermal contraction is the cause for widespread fracture sets, this would place them during the mid-Cretaceous cooling or the Miocene inversion and uplift. As shown by the work of (Becker *et al.* 2010) continuous crack seal formation is dependent on the thermoelastic effect, without which, conditions for tensile failure are not met. Continuous crack seal fracture sets (Fracture Set 5) observed at Moonlight Head (Figure 8) provides further evidence towards Miocene inversion and uplift causing fracturing, as no crack seal features were seen in any of the bedding perpendicular sets formed during the mid-Cretaceous inversion at any of the sites in the Otway Basin.

The history of the NE trending Otway Ranges (where the majority of data in this study was collected) is also complex and still under debate. Duddy (2003) argues that the topographic high dates to the mid-Cretaceous. However, Tickell *et al.* (1992) and Hill *et al.* (1995) have argued the Otway Ranges are a much younger, late Cenozoic feature. Revealing the Otway Range's history is also made more difficult by the large geothermal gradient of the Early Cretaceous, limiting the effectiveness of techniques including vitrinite reflectance and apatite fission track analysis (AFTA) (Duddy 1994, Holford *et al.* 2011).

Regardless of whether the uplift of the Otway Ranges was of Cretaceous or Cenozoic age, calcite fill and deformation of Fracture Sets 1 and 2 are interpreted to have occurred post-maximum burial during the Cretaceous, and at paleo-temperatures of less than 170 °C during burial, based on calcite twinning observed at Cape Otway (Figure 7). Vertical Fracture Set 3, seen at Cape Otway, was the most difficult set to constrain, with the best interpretation placing it after Miocene folding given that it has no orthogonal relationship to bedding. Pervasive bedding parallel fractures seen at Skenes Creek (labelled Set 4 in Figure 18b) were

also seen at Marengo (Appendix B), Moonlight Head (Appendix B) and Smythes Creek (Appendix B). Bedding parallel fractures have been shown to form under stress conditions where  $\sigma_1$  is horizontal and  $\sigma_3$  is vertical (e.g. a reverse fault stress regime) (Sibson 1995). This would place this set at the beginning of the Miocene inversion or shortly after (Figure 19). The fracture sets related to faulting observed at Castle Cove are interpreted to have formed during the Miocene inversion (Figure 19).



## IMPLICATIONS FOR STRUCTURAL PERMEABILITY

Compaction and diagenesis have had profound effects on the porosity and permeability of the sediments of the Otway Basin, particularly the Eumeralla Formation (Duddy 2003, Tassone 2013). Porosities from two samples from Moonlight Head and Cape Otway (Figures 9a and 9b respectively) were calculated at 7.15% and 0.36%, respectively, consistent with published values for the Otway Basin (Duddy 2003, Tassone 2013).

Compaction of a sedimentary column during burial is a loss of volume due to mechanical and diagenetic processes, with overall porosity loss mostly irreversible (Corcoran & Doré 2005, Rider & Kennedy 2011, Tassone *et al.* in press). Although temperature does play a part in the reduction of porosity via diagenesis, if the overall geothermal gradient is relatively unaffected by external factors, then porosity loss is primarily controlled by burial depth (Rider & Kennedy 2011).

Using sonic transit times as a proxy for porosity is a common technique and is advantageous because of the wide coverage and availability of data gathered for formation evaluation in petroleum wells (Corcoran & Doré 2005). Sonic transit time is also a good proxy for compaction, and therefore, burial, as porosity is strongly dependent on burial (Hillis *et al.* 1994).

The calculated value of sonic transit time from sample JS-07 (Figure 20) shows that a minimum of 3600 m (and potentially more) uplift of the sediments at Cape Otway must have occurred. This minimum value is consistent with estimates of uplift of at least 6000 m (from vitrinite reflectance data) following maximum burial at  $\sim 104 \pm 7$  Ma (Duddy 1994, 2002).

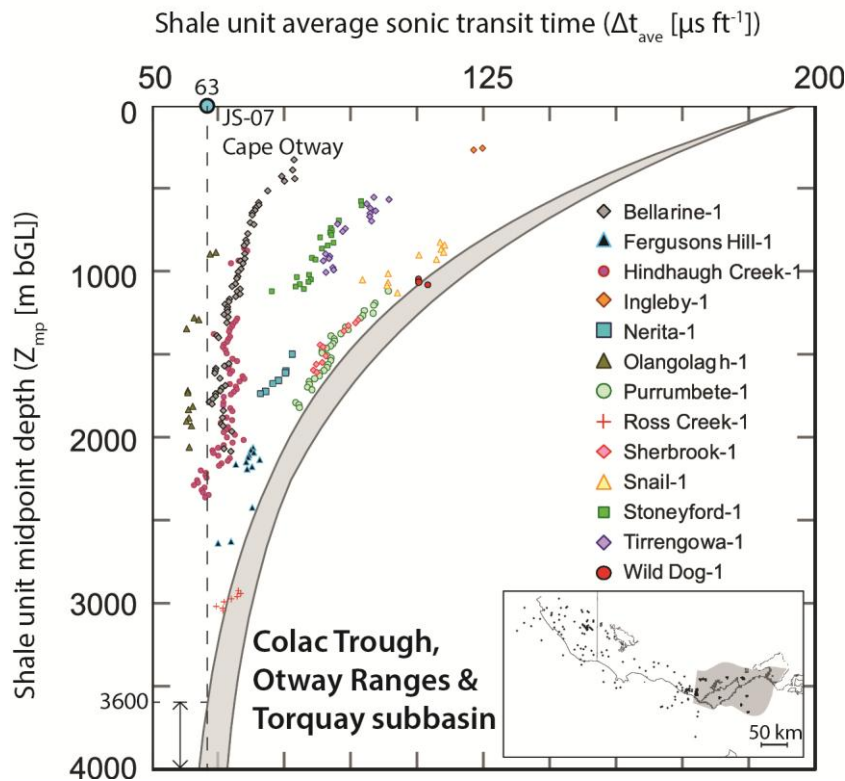


Figure 20. Shale unit average sonic transit time vs. shale unit midpoint depth below ground level/seabed plot for shale units of the Eumeralla Formation, including the normal compaction trend zone of uncertainty (grey band) (adapted from Tassone *et al.* (in press)). Superimposed is the value for the shale unit average sonic transit time for Sample JS-01 (Cape Otway) calculated from the samples porosity and typical shale values from Rider and Kennedy (2011) using the ‘Wyllie Time Average’ equation (Wyllie *et al.* 1956).

Faults, joints and fractures have increasing importance with respect to unconventional hydrocarbon systems, CO<sub>2</sub> sequestration and geothermal energy production. This is particularly true for the Otway Basin given the low porosities and permeability throughout the basin. Therefore, being able to accurately predict fracture densities, fracture character (open, closed and cemented fractures) within a basin is of great importance. The same can also be said for accurate prediction of fold and fault structures and fracture patterns related to these.

In some cases natural fault and fold related fractures have little or no effect on permeability and can even be detrimental to fracture stimulation, due to loss of fluid pressures

(Montgomery *et al.* 2005, Bowker 2007, Jarvie *et al.* 2007). However, many other studies have concluded that fractures associated with these structures do indeed act as effective pathways for fluid flow (e.g. Sibson 1981, Fisher & Knipe 2001, Bjorlykke *et al.* 2005, Vidal-Gilbert *et al.* 2010). Again, it is important for accurate prediction of fracture networks related to local structures. Given the fault associated fracture networks described in this study, as well as potential fold related fracture networks within the Otway Basin, careful consideration is vital when determining the unconventional energy potential around similar structures.

By comparing fracture data from image logs with observed field relations, additional inferences can be made about fracture networks. Figure 21 shows a comparison between all fractures observed in this study and those interpreted using image logs from well Bellarine-1 by Tassone *et al.* (in press). No clear relationship is observed between fractures in this study and fractures identified from Bellarine-1. Tassone *et al.* (in press) discussed that these fractures could be attributed to a strike-slip in-situ stress regime, possibly during mid-Cretaceous inversion. This is plausible for the fracture generation model derived in this study (Figure 19), given that ~NW-SE fracture sets have been seen in several locations around the basin. Also given that Bellarine-1 is located further north east of Cumberland River, these fractures could be interpreted as a further clockwise rotation of Fracture Set 2 in Figure 18.

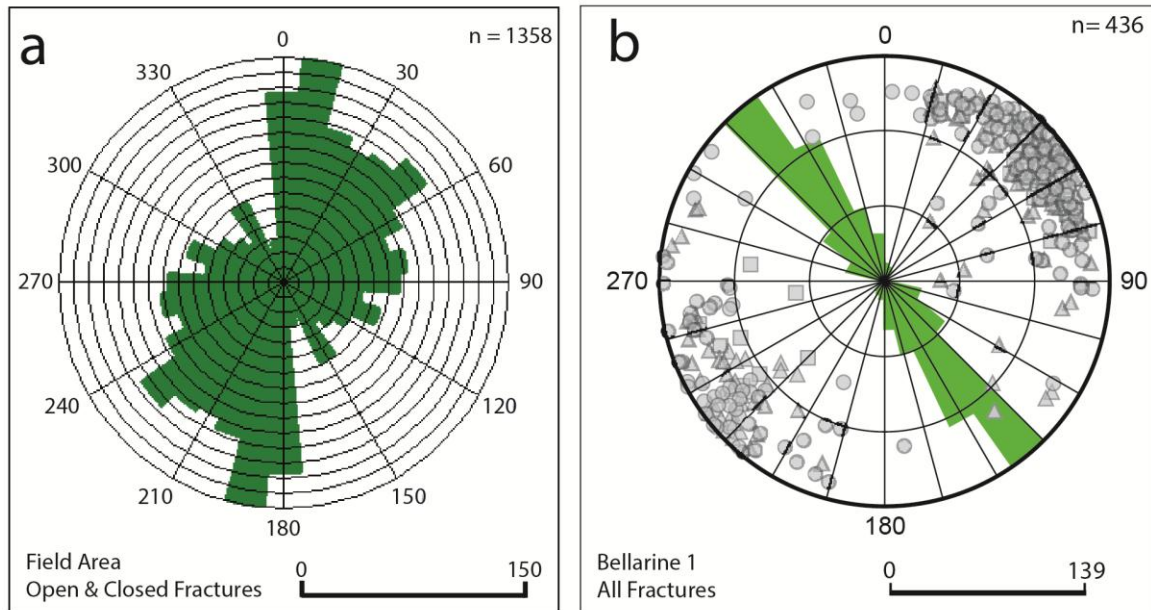


**Figure 21.** Rose diagrams showing a) strikes of all natural fractures from the field area and b) all natural fractures within the Eumeralla Formation from well Bellarine 1 (grey circles represent discontinuous fractures, grey triangles represent continuous fractures and grey squares represent full well bore fractures) (Tassone *et al.* in review). Note that radial intervals are not at the same scale.

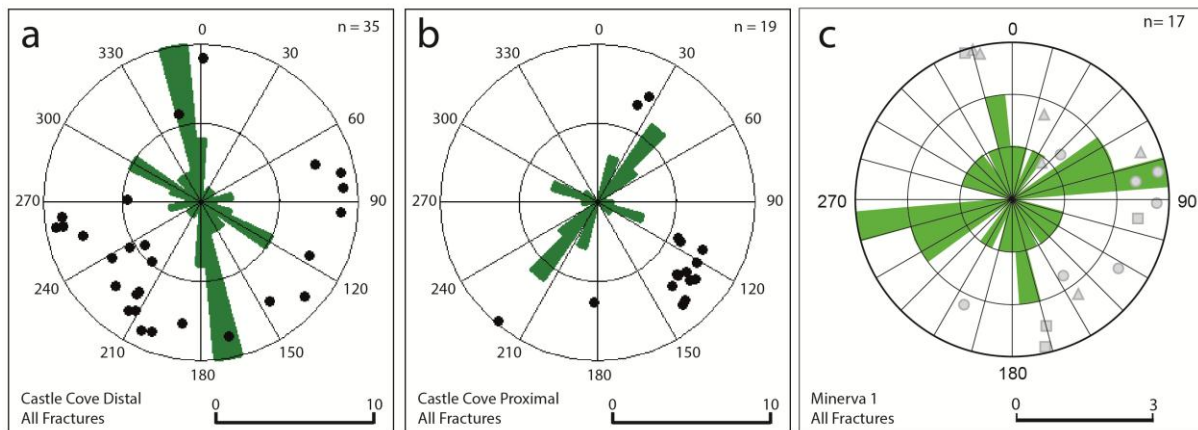


**Figure 22.** Rose diagrams showing a) strikes of all fractures (black circles represent poles to fracture planes) ~173 m from the Castle Cove Fault, b) strikes of all fractures (black circles represent poles to fracture planes) ~14 m from the Castle Cove Fault and c) all natural fractures within the Eumeralla Formation from well Minerva 1 (grey circles represent discontinuous fractures, grey triangles represent continuous fractures and grey squares represent full well bore fractures) (Tassone *et al.* in review). Note that radial intervals are not at the same scale.

The Minerva Anticline is useful as a comparison to the structure at Castle Cove as it is an inverted half graben basin with reactivation of normal faults that have caused folding of overlying sediments (Holford *et al.* 2010). Numerous E-W trending normal faults were also formed during from the during the Late Cretaceous and Paleocene, related to N-S extension

and subsequent E-W to NW-SE compression (Schneider *et al.* 2004). Schneider *et al.* (2004) have also shown that the structure has undergone significant growth from the Miocene to Present-Day, similar to the Castle Cove Fault. The pattern of fracture strikes are similar with one dominant fracture set orientation, and a second less dominant set between 60° and 90° to the dominant set's orientation. The dominant fracture set in Figure 22b, close to the fault zone, is aligned with the orientation of faulting, this relationship is also seen in Figure 21c so it is inferred that the fractures are directly related to previous normal faulting perpendicular to the Minerva Anticline. Considering the relationship between fracture patterns close to the fault and at a distance to the fault at Castle Cove (Figure 22b and 22a, respectively), it may be expected that rotation of fracture sets will occur moving to the south of the Minerva Anticline related faults. However, further data would be required to validate this assumption. This example demonstrates one analogue that can be used to predict sub surface fracture patterns.

The abundance of open fractures seen in outcrop, and the high densities that are seen in particular lithologies, provides a good initial estimate of structural permeability; and potential permeability networks that can be further improved by hydraulic fracture stimulation. This has been demonstrated in the Otway Basin with increased fracture density correlating to increased gas flow in petroleum wells (Tassone *et al.* in press). It has even been shown that cemented natural fractures can be planes of weakness that can still be preferentially reactivated given the right conditions (Jacobi *et al.* 2008, Tassone 2013). Therefore, providing further pathways for fluid flow via the large amount of cemented fractures observed in the basin.



Potential for reactivation of fractures at depth that are similar to fractures seen in outcrop is high under the present-day stress regime in the Otway Basin (Figure 23). If the fracture networks seen in outcrop are representative of the subsurface fracture networks, then the majority of open fractures remain open in the subsurface (Figure 23). The majority of closed, siderite filled and calcite filled fractures are optimally aligned to be reactivated, although likely closed to fluid flow (Figure 23). As previously discussed, cemented fractures, may still act as planes of weakness (Jacobi *et al.* 2008). If this is the case in the Otway Basin, then all fractures optimally aligned to reactivation are potential fluid pathways. Partially filled fractures have also been shown to render fractures in-sensitive to effective stress changes, reducing their likelihood to close even under favourable conditions (Laubach *et al.* 2004). Stress in-sensitive fractures would also help to improve the structural permeability networks within the basin. However, many workers have argued that fracture cements can significantly increase the shear strength of faults and fractures and surrounding rocks (e.g. Nygård *et al.* 2004, Bjorlykke *et al.* 2005), which could potentially render more than half of all fractures observed in this study unlikely to be reactivated.

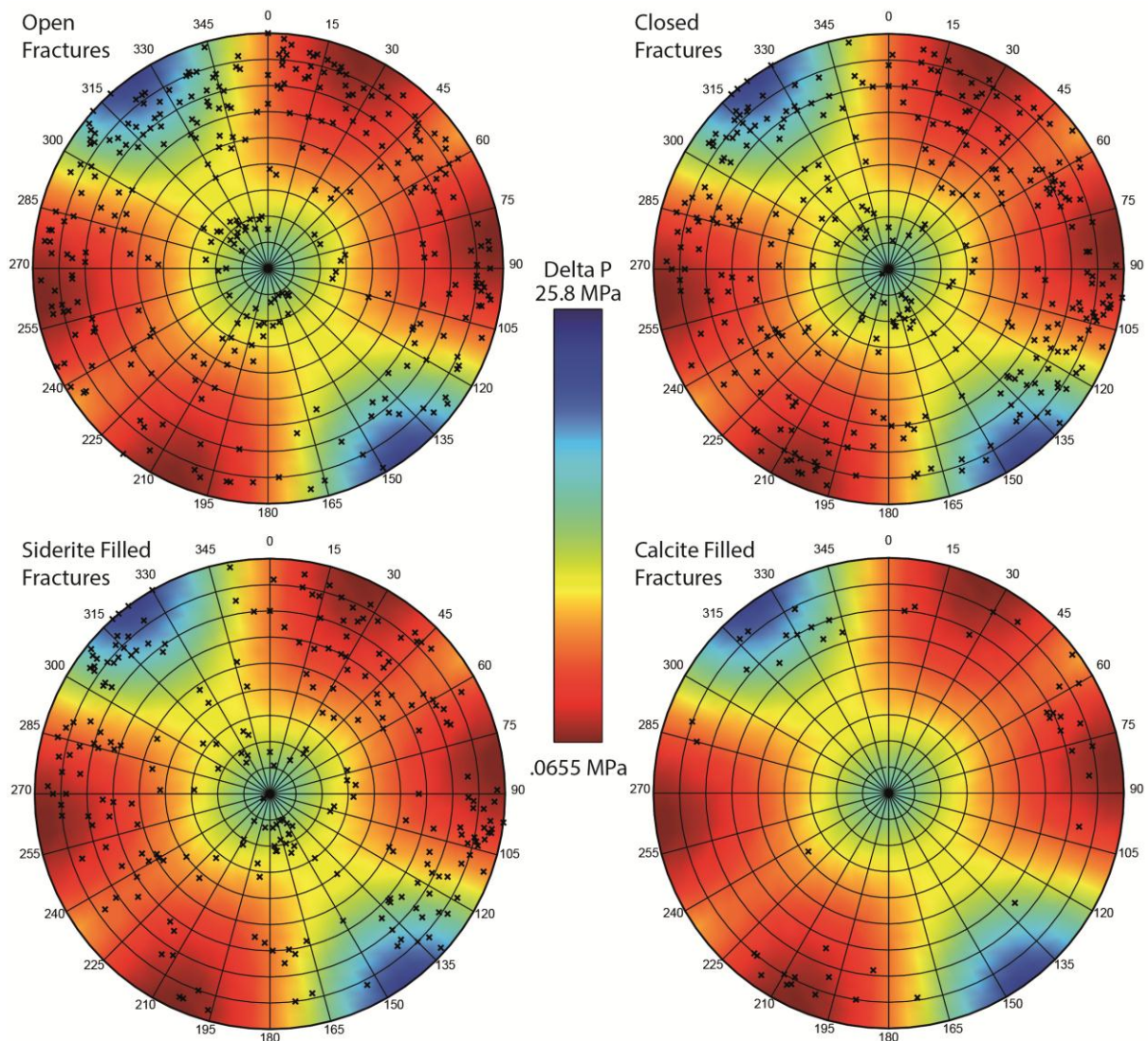


**Figure 23. Plots of fracture susceptibility for reactivation under the Otway Basin stress conditions at 1 km depth in a strike-slip fault stress regime, with a maximum horizontal stress orientation of 144 (Tassone *et al.* in review). Delta P represents the value of pore pressure increases (in MPa) required to move the Mohr Circle to failure. High values (blue) are the furthest from the failure envelope, and therefore represent a low likelihood of reactivation. Low values (red) are the closest to the failure envelope and require the smallest change in pore pressure, and are thus at high likelihood of reactivation. These values also represent orientations of new faults/fractures to form. Poles to fracture planes (represent by x) are included on each plot and are representative of the fracture type in the title.**

When using satellite imagery to identify fracture networks, caution must be exercised when interpreting the results. Fractures which are open at the surface are much more likely to be weathered out and enlarged over time, whereas closed or cemented fractures were seen to be more resistive to weathering. This is particularly the case in the Otway Basin; calcite filled fractures were often observed to be much more resistant to weathering than the surrounding rock, standing proud of the outcrop (Figure 24a). Hardened alteration halos around some open fractures were also observed to be more resistive to weathering (Figure 24b). However, fractures identified on satellite images were highly weathered fractures.

This being said, Figures 5 and 6 show dominant fracture sets were represented accurately with respect to their orientation. Using satellite images compared with additional data sets, including field mapping and image log analysis, enables fracture sets to be mapped over much larger area, including inaccessible areas, with a higher degree of confidence.



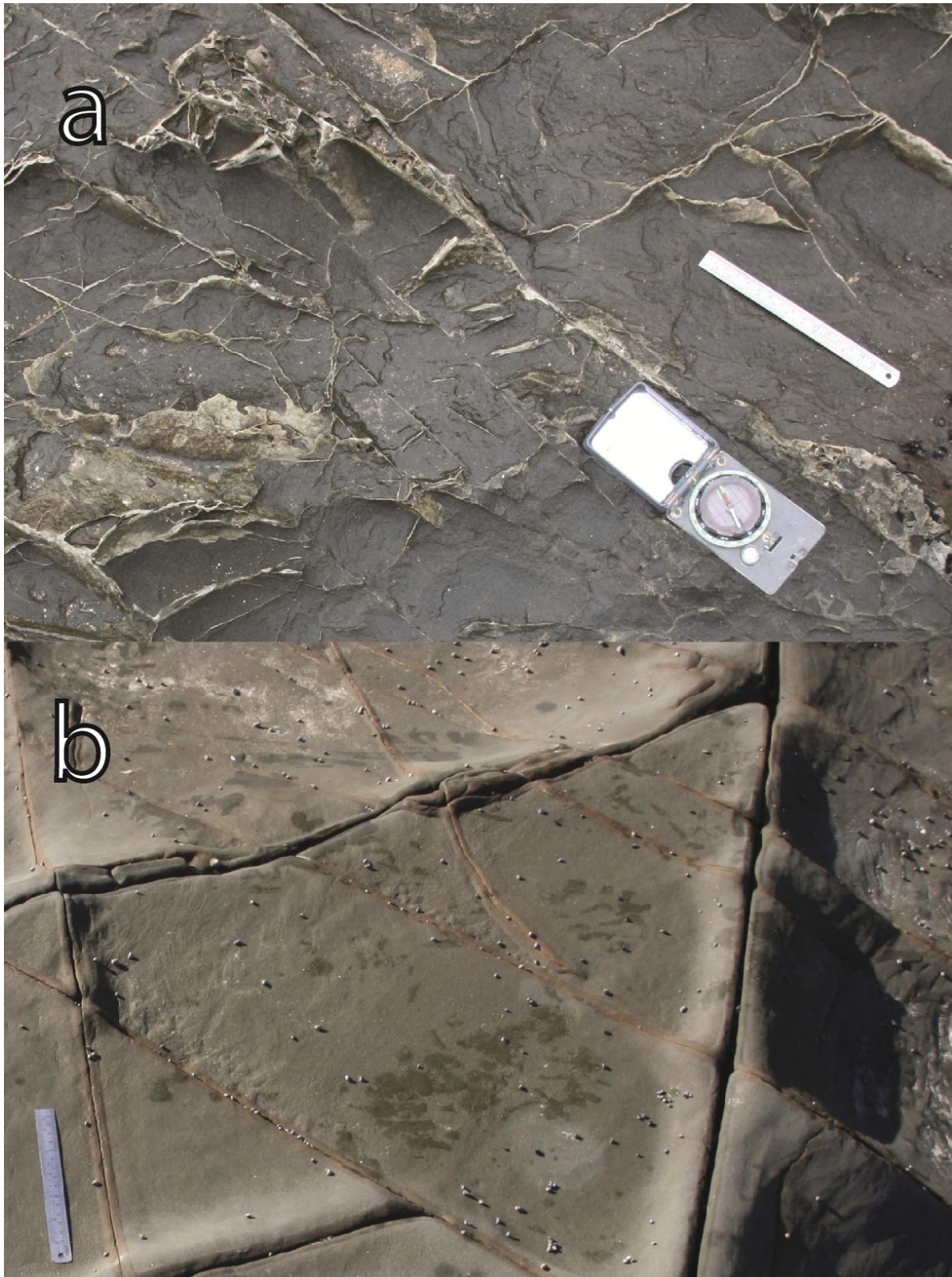


**Figure 24. Differential hardness between host rocks and fracture fills in the Otway Basin. a) Hardened calcite fracture cements at Moonlight Head, showing preferential weathering of host rock compared to fracture cement. b) Hardened FE-rich alteration halos around some open fractures showing preferential weathering unaffected host rock and to varying extents the fracture itself.**

## CONCLUSIONS

Six fracture sets were identified:

- Fracture Set 1 with variable orientations from NNW-SSE to N-S.
- Fracture Set 2 (orthogonal to Fracture Set 1) with variable orientations from ENE-WSW to E-W.
- Fracture Set 3 with an orientation of ESE-WNW.
- Bedding parallel Fracture Set 4, with varying orientation depending on bedding at specific locations.
- Fracture Set 5, recording numerous crack-seal events at Moonlight Head, also with varying orientations.
- Finally the fault related Castle Cove set, with orientations mirroring the NE-SW striking Castle Cove Fault.

Fracture densities within the Eumeralla Formation are heavily dependent on lithology.

Fracture densities were observed to be the highest (up to 42.25 fractures per metre) in the finest grained lithologies with decreasing fracture densities to zero fractures per metre with increasing grain size. Specific targeting of similar fine grained intervals should be considered where increased secondary permeability is required, and coarse-grained units should be targeted where high secondary permeability would be unfavourable.

Localised structures had associated characteristic fracture patterns. This study has shown the similarities and differences between the Castle Cove fault and the Minerva Anticline, which can be used as an analogue for other similar structures in this basin and others. Folding at Cape Otway also provided an example of where already published relationships between fracture patterns and structures could be misinterpreted without all the necessary data

available. The ability to accurately identify fracture patterns associated with local structures with regard to potential trapping mechanisms or fluid pathways must be an important consideration for hydrocarbon exploration, CO<sub>2</sub> sequestration or geothermal energy production.

Just under half of all fractures observed appeared as open fractures in outcrop. Reactivation potential plots indicate that almost all equivalent fractures at depth have a high likelihood of being open to fluid flow. Thus, providing a comprehensive and connected secondary permeability network.

The majority of closed, calcite filled and siderite filled fractures are optimally aligned for reactivation at depth, potentially providing further permeability pathways if fractures are weak and can be reactivated. However, further testing of host rock and fracture fill strengths would need to be undertaken in order to validate this.

Comparison of fracture data from two sites in the Otway Basin with corresponding satellite images characterizes orientations of major fracture sets accurately. Differences between the nature of fractures (open, closed or cement filled) did, however, effect the representation of fractures on satellite images compared with measurements in the field. For example, open fractures appeared to be over represented compared with closed fractures, this being attributed to the preferential weathering of open fractures (which were more prominent on satellite imagery). Using this technique, in conjunction with other fracture identification methods, can provide a better indication of fracture networks over larger areas with better accuracy.

## **ACKNOWLEDGMENTS**

Many thanks go to all those who have been there for me throughout out the year providing the support and knowledge needed to reach this point in my studies. This is particularly the case for my primary supervisor, Dr. Rosalind King, who was always patient and who always made time for me. Also Dr. Simon Holford, my secondary supervisor, for his ongoing support. Thanks to Adam Bailey for his assistance in the field and with all my software issues and Dave Tassone for his help with data collection. Dr. Khalid Amrouch and Dr. Ian Duddy for their specialist advice and assistance. Ben Wade and Adelaide Microscopy for the use of their equipment and the time spent instructing me and solving problems. Special thanks to Ikon Science for their use of JRS Suite© and Pontifex & Associates Pty. Ltd. for making thin sections. Lastly, thanks go to the South Australian Centre for Geothermal Exploration and Research for their generous financial contribution to my studies.

## REFERENCES

- ALLMENDINGER R. W., CARDOZO N. & FISHER D. 2012. *Stereonet 8 v. 8.0.0*.
- ANDERSON E. M. 1951a. *The dynamics of faulting and dyke formation with applications to Britain (2nd Edition)*. Oliver and Boyd, Edinburgh.
- ANDERSON E. M. 1951b. *The dynamics of faulting and dyke formation with applications to Britain (2nd Edition)*. Oliver and Boyd, Edinburgh.
- BABCOCK E. A. 1978. Measurements of subsurface fractures from dipmeter logs. *American Association of Petroleum Geologists Bulletin* **62**.
- BAILEY A. H. E., KING R. C. & BACKE G. 2012. Integration of structural, stress and seismic data to define secondary permeability networks through deep cemented sediments in the Northern Perth Basin. *APPEA Journal* **52**, 455-474.
- BARNETT P. 2009. Statement of Estimated Geothermal Resources For the Koroit Geothermal Power Project, Victoria Geothermal Exploration Permit (GEP) 8. *Hot Rock Limited*.
- BARTON H. 1976. The shear strength of rocks and rock joints. *International Journal of Rock Mechanics and Mining Sciences & Geomechanics Abstracts* **13**, 255-279.
- BEARDSMORE G. 2010. PANAX Geothermal Annual Report. *PANAX Geothermal*.
- BECKER S. P., EICHHUBL P., LAUBACH S. E., REED R. M., LANDER R. H. & BODNAR R. J. 2010. A 48-m.y. history of fracture opening, temperature and fluid pressure: Cretaceous Travis Peak Formation, East Texas Basin. *Geological Society of America Bulletin* **122**, 1081-1093.
- BELL J. S. 1996a. In situ stresses in sedimentary rocks (part 1): Measurement techniques. *Geoscience Canada* **23**.
- BELL J. S. 1996b. In situ stresses in sedimentary rocks (part 2): Applications of stress measurements. *Geoscience Canada* **23**, 135-153.
- BELL J. S. 2003. Practical methods for estimating in situ stresses for borehole stability applications in sedimentary basins. *Journal of Petroleum Science and Engineering* **38**, 111-119.
- BJORLYKKE K., HOEG K., FALEIDE J. I. & JAHREN J. 2005. When do faults in sedimentary basins leak? Stress and deformation in sedimentary basins; examples from the North Sea and Haltenbanken, offshore Norway. *AAPG Bulletin* **89**, 1019-1031.
- BOWKER K. A. 2007. Barnett Shale gas production, Fort Worth Basin: Issues and discussion. *AAPG Bulletin* **91**, 523-533.
- BRACE W. F. 1960. An extension of the Griffith theory of fracture to rocks. *Journal of Geophysical Research* **65**, 3477-3480.
- BYERLEE J. 1978. Friction of rocks. *Pure and applied Geophysics* **116**, 615-626.
- CARTER A. N. 1958. Tertiary foraminifera from the Aire district, Victoria. *Geological Survey of Victoria Bulletin* **55**, 76.
- CHANG C., ZOBACK M. D. & KHAKSAR A. 2006. Empirical relations between rock strength and physical properties in sedimentary rocks. *Journal of Petroleum Science and Engineering* **51**, 223-237.
- COOPER G. T. & HILL K. C. 1997. Cross-section balancing and thermochronological analysis of the Mesozoic development of the eastern Otway Basin. *APPEA Journal* **37**, 390-414.
- CORBETT K., FRIEDMAN M. & SPANG J. 1987. Fracture development and mechanical stratigraphy of Austin Chalk, Texas. *Am. Assoc. Pet. Geol., Bull. (United States)* **71**.
- CORCORAN D. & DORÉ A. 2005. A review of techniques for the estimation of magnitude and timing of exhumation in offshore basins. *Earth-Science Reviews* **72**, 129-168.



- CORCORAN D. V. & DORÉ A. G. 2002. Top seal assessment in exhumed basin settings — some insights from atlantic margin and borderland basins. *In: Andreas G. K. & Robert H. eds., Norwegian Petroleum Society Special Publications*, Vol. Volume 11, pp 89-107, Elsevier.
- DENHAM D., WEEKES J. & KRAYSHEK C. 1981. Earthquake evidence for compressive stress in the southeast Australian crust. *Journal of the Geological Society of Australia* **28**, 323-332.
- DEWHURST D. N., JONES R., HILLIS R. R. & MILDREN S. D. 2002. Microstructural and geomechanical characterisation of fault rocks from the Carnarvon and Otway basins. *APPEA Journal*.
- DICKINSON G. 1953. Geological aspects of abnormal reservoir pressures in Gulf Coast Louisiana. *American Association of Petroleum Geologists Bulletin* **37**, 410-432.
- DICKINSON J., WALLACE M., HOLDGATE G., DANIELS J., GALLAGHER S. & THOMAS L. 2001. Neogene tectonics in SE Australia: implications for petroleum systems. *APPEA Journal* **41**, 37-52.
- DUDDY I. R. 1994. The Otway Basin: Thermal, structural, tectonic and hydrocarbon generation histories. NGMA/PESA Otway Basin Symposium Extended Abstracts, Melbourne (unpubl.).
- DUDDY I. R. 1997. Focussing exploration in the Otway Basin: Understanding timing of source rock maturation. *The APPEA Journal* **37**, 178-191.
- DUDDY I. R. 2002. *The Otway Basin: Geology, sedimentology, diagenesis, AFTA© thermal history reconstruction and hydrocarbon prospectivity*. Geophysics N. C. f. P. G. a. Geotrack International Pty. Ltd, Brunswick West, Victoria.
- DUDDY I. R. 2003. Mesozoic, a time of change in tectonic regime. *In: Birch W. D. ed., Geology of Victoria* (3 edition), pp 239-286, Geological Society of Australia (Victoria Division), Victoria, Australia.
- EDWARDS J., LEONARD J. G., PETTIFER G. R. & McDONALD P. A. 1996. Colac 1:250 000 Map Geological Report
- ENGELDER T. 1985. Loading paths to joint propagation during a tectonic cycle: an example from the Appalachian Plateau, U.S.A. *Journal of Structural Geology* **7**, 459-476.
- ENGLISH J. M. 2012. Thermomechanical origin of regional fracture systems *AAPG Bulletin* **96**, 1597-1625.
- FERRILL D. A., MORRIS A. P., EVANS M. A., BURKHARD M., GROSHONG JR R. H. & ONASCH C. M. 2004. Calcite twin morphology: a low-temperature deformation geothermometer. *Journal of Structural Geology* **26**, 1521-1529.
- FISHER Q. J. & KNIPE R. J. 2001. The permeability of faults within siliciclastic petroleum reservoirs of the North Sea and Norwegian Continental Shelf. *Marine and Petroleum Geology* **18**, 1063-1081.
- GROSS M. R. 1995. Fracture partitioning: Failure mode as a function of lithology in the Monterey Formation of coastal California. *Geological Society of America Bulletin* **107**, 779-792.
- GROSS M. R., FISCHER M. P., ENGELDER T. & GREENFIELD R. J. 1995. Factors controlling joint spacing in interbedded sedimentary rocks: integrating numerical models with field observations from the Monterey Formation, USA. *Geological Society, London, Special Publications* **92**, 215-233.
- GUDMUNDSSON A., SIMMENES T. H., LARSEN B. & PHILIPP S. L. 2010. Effects of internal structure and local stresses on fracture propagation, deflection, and arrest in fault zones. *Journal of Structural Geology* **32**, 1643-1655.

- HILL K. C., HILL K. A., COOPER G. T., O'SULLIVAN A. J., O'SULLIVAN P. B. & RICHARDSON M. J. 1995. Inversion around the Bass Basin, SE Australia. *Geological Society, London, Special Publications* **88**, 525-547.
- HILLIS R., THOMSON K. & UNDERHILL J. R. 1994. Quantification of Tertiary erosion in the inner Moray Firth using sonic velocity data from the Chalk and Kimmeridge Clay *Marine and Petroleum Geology* **11**, 283-293.
- HILLIS R. R., SANDIFORD M., REYNOLDS S. D. & QUIGLEY M. C. 2008. Present-day stresses, seismicity and Neogene-to-Recent tectonics of Australia's 'passive' margins: intraplate deformation controlled by plate boundary forces. *Geological Society, London, Special Publications* **306**, 71-90.
- HOLFORD S., HILLIS R. R., DUDDY I. R., GREEN P. F., STOKER M., TUITT A., BACKÉ G., TASSONE D. R. & MACDONALD J. 2011. Cenozoic post-breakup compressional deformation and exhumation of the southern Australian margin. *APPEA Journal* **51**, 613-638.
- HOLFORD S. P., HILLIS R. R., DUDDY I. R., GREEN P. F., TUITT A. K. & STOKER M. S. 2010. Impacts of Neogene-recent compressional deformation and uplift on hydrocarbon prospectivity of the passive southern Australian margin. *APPEA Journal* **50**, 267-286.
- HOLFORD S. P., TASSONE D. R. & BAILEY A. H. E. Unpublished. Fracture networks in the Otway Basin
- JACOBI D., GLADKIKH M., Lecompte B., HURSAN G., MENDEZ F., LONGO J., ONG S., BRATOVICH M., PATTON G. & SHOEMAKER P. 2008. Integrated petrophysical evaluation of shale gas reservoirs. CIPC/SPE Gas Technology Symposium Joint Conference, Calgary, Alberta, Canada (unpubl.).
- JARVIE D. M., HILL R. J., RUBLE T. E. & POLLASTRO R. M. 2007. Unconventional shale-gas system: the Mississippian Barnett Shale of north-central Texas as one model for thermogenic shale-gas assessment. *AAPG Bulletin* **91**, 475-499.
- JONES R. M., BOULT P., HILLIS R. R., MILDREN S. D. & KALDI J. G. 2000. Integrated hydrocarbon seal evaluation in the Penola Trough, Otway Basin. *APPEA Journal* **40**, 194-212.
- KERR P. F. & ROGERS A. F. 1977. *Optical Mineralogy* (4 edition). McGraw-Hill, University of Minnesota.
- KING R., BACKÉ G., TINGAY M., HILLIS R. & MILDREN S. 2012a. Stress deflections around salt diapirs in the Gulf of Mexico. *Geological Society, London, Special Publications* **367**, 141-153.
- KING R. C., HILLIS R. R. & REYNOLDS S. D. 2008. In situ stresses and natural fractures in the Northern Perth Basin, Australia. *Australian Journal of Earth Sciences* **55**, 685-701.
- KING R. C., HOLFORD S., HILLIS R., BACKÉ G., TINGAY M. & TUITT A. 2012b. Reassessing the In Situ Stress Regimes of Australia's Petroleum Basins. *APPEA Journal*.
- KIRSCH E. G. 1898. Die Theorie der Elastizität und die Bedürfnisse der Festigkeitslehre. *Zeitschrift des Vereines Deutscher Ingenieure* **42**.
- KRASSAY A. A., CATHRO D. L. & RYAN D. J. 2004. A regional tectonostratigraphic framework for the Otway Basin. *Eastern Australian Basins Symposium II: Petroleum Exploration Society of Australia, Special Publication 23*, pp. 239-286.
- LANDER R. H., GALE J. F. W., LAUBACH S. E. & BONNELL L. M. 2002. Interaction between quartz cementation and fracturing in sandstone. *AAPG Annual Convention Program*, p. 98.
- LAUBACH S. E., OLSON J. E. & GALE J. F. W. 2004. Are open fractures necessarily aligned with maximum horizontal stress? *Earth and Planetary Science Letters* **222**, 191-195.
- LAUBACH S. E., OLSON J. E. & GROSS M. R. 2009. Mechanical and fracture stratigraphy. *AAPG Bulletin* **93**, 1413-1426.

- MILDREN S. D., HILLIS R. R. & BOULT P. J. 2005. FAST: A new technique for geomechanical assessment of the risk of reactivation-related breach of fault seals. *AAPG Hedberg Series* **2**, 73-85.
- MILLER J. M., NORVICK M. S. & WILSON C. J. L. 2002. Basement controls on rifting and the associated formation of ocean transform faults—Cretaceous continental extension of the southern margin of Australia. *Tectonophysics* **359**, 131-155.
- MONTGOMERY S., JARVIE D. M., BOWKER K. A. & POLLASTRO R. M. 2005. Mississippian Barnett Shale, Fort Worth Basin, north-central Texas: Gas-shale play with multi-trillion cubic foot potential. *AAPG Bulletin* **89**, 155-175.
- MOORE A. M. G., STAGG H. M. J. & NORVICK M. S. 2000. Deep-water Otway Basin: a new assessment of the tectonics and hydrocarbon prospectivity. *The APPEA Journal* **32**, 66-85.
- NELSON E., HILLIS R., SANDIFORD M., REYNOLDS S. & MILDREN S. 2006. Present-day state-of-stress of southeast Australia. *APPEA Journal* **46**, 283-305.
- NORVICK M. S. & SMITH M. A. 2001. Mapping the plate tectonic reconstruction of southern and southeastern Australia and implications for petroleum systems. *The APPEA Journal* **41**, 15-36.
- NYGÅRD R., GUTIERREZ M., HØEG K. & BJØRLYKKE K. 2004. Influence of burial history on microstructure and compaction behaviour of Kimmeridge clay. *Petroleum Geoscience* **10**, 259-270.
- PERINCEK D. & COCKSHELL C. D. 1995. The Otway Basin: Early Cretaceous rifting to Neogene inversion. *The APPEA Journal* **35**, 451-466.
- REYNOLDS S., COBLENTZ D. & HILLIS R. 2003. Influences of plate-boundary forces on the regional intraplate stress field of continental Australia.
- RIDER M. & KENNEDY M. 2011. *The geological interpretation of well logs* (3 edition). Rider-French Consulting Ltd., Scotland.
- RODUIT N. 2013. *JMicroVision*, Geneva.
- SCHNEIDER C. L., HILL K. C. & HOFFMAN N. 2004. Compressional growth of the Minerva Anticline, Otway Basin, Southeast Australia-Evidence of oblique rifting. *APPEA Journal* **44**, 463-480.
- SECOR D. T. 1965. Role of fluid pressure in jointing. *American Journal of Science* **263**, 633-646.
- SIBSON R. 1981. Fluid flow accompanying faulting: field evidence and models. *Maurice Ewing Series* **4**, 593-603.
- SIBSON R. H. 1995. Selective fault reactivation during basin inversion; potential for fluid redistribution through fault-valve action. *Geological Society, London, Special Publications* **88**.
- SIBSON R. H. 1996. Structural permeability of fluid-driven fault-fracture meshes. *Journal of Structural Geology* **18**, 1031-1042.
- TASSONE D. R. 2013. Otway Basin Unconventional Assessment.
- TASSONE D. R., HOLFORD S. P., DUDDY I. R., GREEN P. F. & HILLIS R. R. in press. Quantifying Cretaceous-Cenozoic exhumation in the Otway Basin, southeastern Australia, using sonic transit time data: Implications for conventional and unconventional hydrocarbon prospectivity. *AAPG Bulletin*, 1-50.
- TASSONE D. R., HOLFORD S. P., KING R. C., TINGAY M. R. P. & HILLIS R. R. in review. New constraints on in situ stresses in the offshore Victorian Otway Basin, southeastern Australia, and their implications towards compressional deformation in passive margin sedimentary basins. *Tectonophysics*.

- TASSONE D. R., HOLFORD S. P., TINGAY M. R. P., TUITT A. K., STOKER M. S. & HILLIS R. R. 2011. Overpressures in the central Otway Basin: the result of rapid Pliocene-Recent sedimentation? *APPEA Journal* **51**, 439-458.
- TICKELL S. J., EDWARDS J. & ABELE C. 1992. *Port Campbell Embayment 1:100 000 geological map. Report 95*. Geological Survey of Victoria.
- TINGAY M. R. P., HILLIS R. R., MORLEY C. K., SWARBRICK R. E. & OKPERE E. C. 2003. Variation in vertical stress in the Baram Basin, Brunei: tectonic and geomechanical implications. *Marine and Petroleum Geology* **20**, 1201-1212.
- TUITT A. K., HOLFORD S. P., HILLIS R. R., UNDERHILL J. R., RITCHIE J. D., JOHNSON H., HITCHEN K., STOKER M. S. & TASSONE D. R. 2011. Continental margin compression: a comparison between compression in the Otway Basin of the southern Australian margin and the Rockall-Faroe area in the NE Atlantic margin. *The APPEA Journal* **51**, 241-257.
- TWISS R. J. & MOORES E. M. 2007. *Structural Geology* (2nd edition). W. H. Freeman, New York.
- VIDAL-GILBERT S., TENTHOREY E., DEWHURST D., ENNIS-KING J., VAN RUTH P. & HILLIS R. 2010. Geomechanical analysis of the Naylor Field, Otway Basin, Australia: Implications for CO<sub>2</sub> injection and storage. *International Journal of Greenhouse Gas Control* **4**, 827-839.
- WILLCOX J. B. & STAGG H. M. J. 1990. Australia's southern margin: a product of oblique extension. *Tectonophysics* **173**, 269-281.
- WYLLIE M. R. J., GREGORY A. R. & GARDNER L. W. 1956. Elastic wave velocities in heterogeneous and porous media. *Geophysics* **21**, 41-70.
- ZANG A. & STEPHANSSON O. 2010. *Stress field of the Earth's crust*. Springer, London.
- ZOBACK M. D. 2010. *Reservoir geomechanics*. Cambridge University Press.

## APPENDIX A: EXTENDED METHODS

### FIELD MAPPING

For this study two methods of fracture measurement were used to collect data.

Where only wave cut platform was accessible, a series of representative parallel transects (from 15 m to 40 m) running across strike of the predominant fractures were made, with a second series of shorter parallel transects (from 10 m to 15 m) running perpendicular to and cross cutting the longer transects. The general pattern of these transects was two parallel transects running roughly E-W and two perpendicular transects running roughly N-S cross cutting both parallel transects. A tape measure was laid out along the transect with its bearing taken in the direction from 0 metres. The GPS location was taken at the beginning and end of each transect. The total length of transects completed was 370 m. A full list of transect locations, GPS readings, lengths and orientations is given in Transect Table 1, Figure Location Map.

Additional transects were done and data acquired at Castle Cove, Wongarra and Lorne by previous workers (Transect Table 2) (Holford *et al.* Unpublished). These data included fracture dip and dip directions or strikes where these were not possible, and also fracture aperture and cement fill.

Where vertical or near vertical faces were encountered at a field site, annotated face maps were drawn of the vertical face. Using grids of 1 metre by 1 metre squares, fracture and other important features of the face were drawn and measured. These grids were usually 2 or 3 metres high, due to the difficult nature of measuring fractures above these heights, and from 6 to 12 metres in length. A tape measure was laid out at the base of the face and with its bearing taken in the direction from 0 metres. The GPS location of the start of the section and the end of the section was also recorded, including the accuracy of the GPS itself. A minimum of 3 metres of accuracy on all GPS readings was taken, where possible. A full list of face map locations, GPS readings, lengths and orientations is given in Face Map Table 3. Additional face maps and data were acquired at Castle Cove, both in the vicinity of the main fault structure and 150 m W from the main fault structure by previous workers (Face Map Table 4) (Holford *et al.* Unpublished). These data included fracture dip and dip directions where possible or strikes, fracture aperture and cement fill.

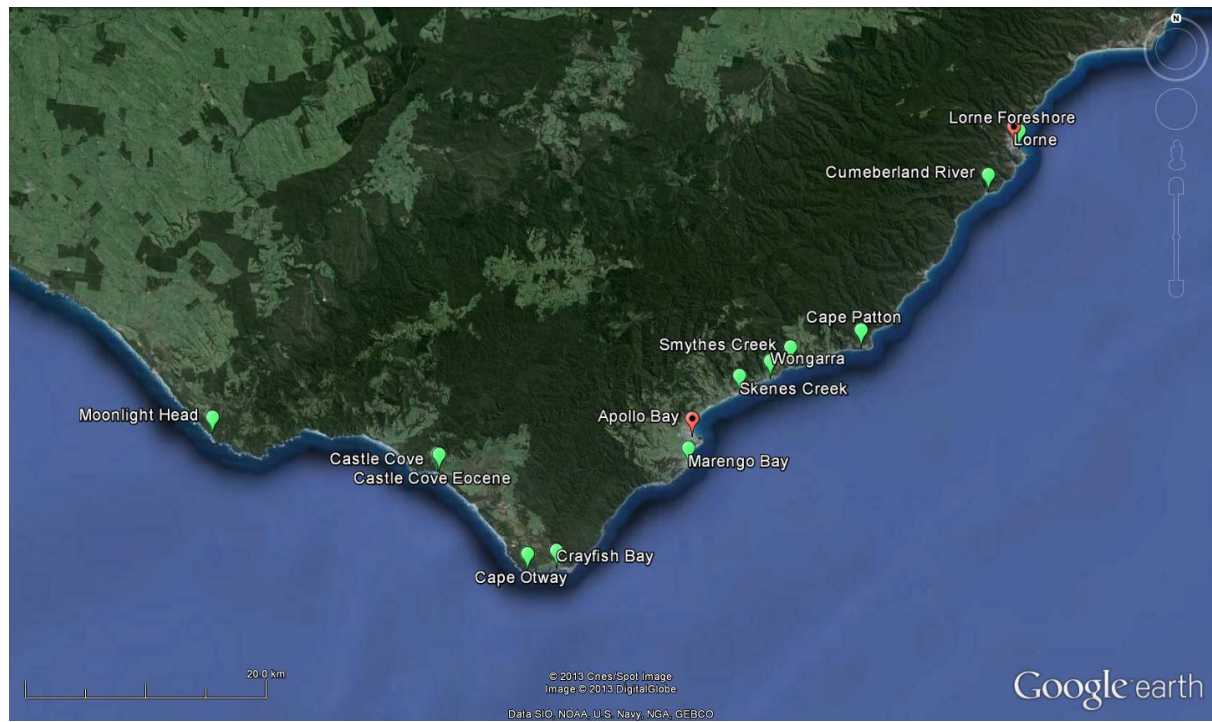


Figure Location Map. Map of all locations where data were recorded in the field area around Apollo Bay.

Transect Table 1. Transect locations for this study, with GPS coordinates, orientation and length.

Transect Location	GPS Start		GPS End		Orientation of Transect	Length of Transect
	Latitude	Longitude	Latitude	Longitude		
Crayfish Bay Transect 1	-38 51.274	143 32.397	-38 51.296	143 32.419	308	35 m
Crayfish Bay Transect 2	-38 51.277	143 32.389	-38 51.290	143 32.404	303	35 m
Marengo Bay Transect 1	-38 46.812	143 39.933	-38 46.802	143 39.594	055	30 m
Marengo Bay Transect 2	-38 46.806	143 39.929	-38 46.797	143 39.947	055	30 m
Marengo Bay Transect 3	-38 46.806	143 39.943	-38 46.801	143 39.935	318	15 m
Marengo Bay Transect 4	-38 46.804	143 39.945	-38 46.797	143 39.941	320	15 m
Skenes Creek Transect 1	-38 43.531	143 42.994	-38 43.531	143 42.984	270	15 m
Skenes Creek Transect 2	-38 43.525	143 42.984	-38 43.525	143 42.984	270	15 m
Skenes Creek Transect 3	-38 43.523	143 42.991	-38 43.531	143 42.989	180	15 m
Skenes Creek Transect 4	-38 43.523	143 42.987	-38 43.530	143 42.985	180	15 m
Skenes Creek Transect 5	-38 43.533	143 42.900	-38 43.534	143 42.890	270	15 m
Skenes Creek Transect 6	-38 43.529	143 42.901	-38 43.529	143 42.890	270	15 m
Skenes Creek Transect 7	-38 43.528	143 42.898	-38 43.536	143 42.896	183	15 m
Skenes Creek Transect 8	-38 43.529	143 42.894	-38 43.537	143 42.893	182	15 m
Cumberland River Transect 1	-38 34.594	143 57.078	-38 34.589	143 57.058	285	30 m
Cumberland River Transect 2	-38 34.598	143 57.080	-38 34.595	143 57.060	278	30 m
Cumberland River Transect 3	-38 34.593	143 57.076	-38 34.601	143 57.077	173	15 m
Cumberland River	-38 34.593	143 57.068	-38 34.598	143 57.069	172	15 m

Transect 4						
------------	--	--	--	--	--	--

Transect Table 2. Transect locations measured by Holford, Tassone and Bailey, 2012, with accompanying GPS coordinates, orientation and length.

Transect Location	GPS Start		GPS End		Orientation of Transect	Length of Transect
	Latitude	Longitude	Latitude	Longitude		
Castle Cove Transect 1	-	-	-	-	-	50 m
Lorne Foreshore Transect 1	-	-	-	-	-	20 m
Wongarra Transect 1	-38 42.53	143 44.38	-	-	325	40 m
Wongarra Transect 2	-38 42.53	143 44.38	-	-	232	40 m
Wongarra Transect A	-38 42.53	143 44.38	-	-	235	5 m
Wongarra Transect B	-38 42.53	143 44.38	-	-	235	5 m

Face map Table 1. Face map locations measured for this study, with accompanying GPS coordinates, orientation and length.

Face map Location	GPS Start		GPS End		Orientation of Face map	Length of Face map
	Latitude	Longitude	Latitude	Longitude		
Castle Cove Eocene Sediments Face map	-38 47.011	143 25.757	-38 47.007	143 25.755	092	9 m
Marengo Bay Face map 1	-38 46.737	143 39.964	-38 46.741	143 39.969	305	12 m
Marengo Bay Face map 2	-38 46.748	143 39.971	-38 46.751	143 39.968	225	8 m
Smythes Creek Face map	-38 42.256	143 45.792	-38 42.260	143 45.792	202	5 m
Cape Patton Face map	-38 41.515	143 49.797	-38 41.516	143 49.804	276	11 m
Moonlight Head Face map 1	-38 45.326	143 12.814	-38 45.330	143 12.815	182	5 m
Moonlight Head	-38 45.285	143 12.762	-38 45.288	143 12.771	127	12 m



## Fault and Fracture Networks in the Otway Basin

Face map 2						
Cape Otway Face map 1	-38 51.398	143 30.923	-	-	256	2 m
Cape Otway Face map 2	-38 51.361	143 30.943	-	-	248	2 m

Face map Table 2. Face map locations measured by Holford, Tassone and Bailey, 2012, with accompanying GPS coordinates, orientation and length.

Face map Location	GPS Start		GPS End		Orientation of Face map	Length of Face map
	Latitude	Longitude	Latitude	Longitude		
Castle Cove Face map Proximal to Fault	-38 46.954	143 25.638	-38 46.954	143 25.646	104	8 m
Castle Cove Face map Distal to Fault	-38 46.938	143 25.543	-38 46.936	143 25.546	104	12 m

## STRUCTURAL DATA COLLECTION

Transects - As fractures were encountered along the transect they were numbered and the distance along the transect was recorded. The dip and dip direction of the fracture were measured. If this was not possible, the strike orientation of the fracture was measured. The aperture of the fracture (including if it was open or closed), cement fills (if present), alteration halo (if present) and any cross cutting relationship with other fractures were noted.

Face mapping - Fractures in each face map were drawn numbered. The fracture plane dip and dip direction were measured. If this was not possible, the strike orientation was measured. The aperture of the fracture (including if it was open or closed), cement fills (if present), alteration halo (if present) and any cross cutting relationship with other fractures were noted. The number was then recorded on the sketch next to its corresponding fracture and the data recorded in a notebook.

A list of structural measurements is recorded in Structural Measurements Table.

Structural Measurements Table. List of structural measurements collected and the type of measurement.

Structural Measurement	Type of Measurement
Bedding	Dip and Dip Direction
Fracture Plane	Dip and Dip Direction
Fracture Strike (Where plane was unavailable taken)	Strike

## STRUCTURAL ANALYSIS

In this study, data obtained from the field areas were viewed as rose diagrams and stereonet in order to determine possible fracture sets within the field area and to interpret fracture patterns in the Eumeralla Formation, Otway Basin, Victoria.

Rose Diagrams were created using Roses in JRS Petroleum Suite<sup>®</sup> to plot all strikes take from the field in order to interpret fracture networks in the Eumeralla Formation.

Stereonet were created using Stereonet 8<sup>®</sup> (Allmendinger *et al.* 2012) to plot dip and dip directions of bedding and fracture planes and poles to bedding and poles to fracture planes in order to interpret fracture networks in the Eumeralla Formation.

JRS Method -

JRS Data Entry

1. Enter data into JRS Office Access 2000 file.

a) Under 'Field – Ref' tab, assign Field/s.

## Fault and Fracture Networks in the Otway Basin

	Field	Field Name	Click to Add
+		4 Vic Otway	
+		8 Facemaps	
*		(New)	

b) Under 'Wellinfo' tab, enter field site names (or well) into new rows and assign a number corresponding to the field the well/site belongs to (from previous step)

	UWI	Well Name	Field
+	1	Castle Cove Eumeralla	4
+	2	Castle Cove Eocene	4
+	3	Crayfish Bay	4
+	4	Marengo	4
+	5	Skene's Creek	4
+	6	Smythe's Creek	4
+	7	Cape Patton	4
+	8	Cumberland River	4
+	9	Moonlight Head	4
+	10	Cape Otway	4
+	11	Lorne	4
+	12	Wongarra	4
+	13	Cape Otway Map 1	8
+	14	Cape Otway Map 2	8
+	15	Moonlight Head Map 1	8
+	16	Moonlight Head Map 2	8
+	17	Marengo Map 1	8
+	18	Marengo Map 2	8
+	19	Satellite Test Marengo	0
+	20	Satellite Test Skenes Cree	0
+	21	Castle Cove Map Proximal	8
+	22	Castle Cove Map Distal	8
+	23	CCP Update	8
+	24	CCD Update	8
*		(New)	0

c) Under the 'Frac Colour' tab, assign fracture types to a corresponding 'FracID' number. Then choose frac colour, marker type, line width to each fracture.

FracID	FracType	Frac Colour	Marker Type	Stipple	LineWidth	Factor	Alpha	AzLines	DisplayName
96	Field Fracture	clBlack	2	<input type="checkbox"/>	3	0	0.5	<input type="checkbox"/>	Field Interpreted Fracture
97	Strike Only	clBlack	2	<input type="checkbox"/>	3	0	0.5	<input type="checkbox"/>	Field Interpreted Fracture Strike Only
101	Calcite	clBlack	2	<input type="checkbox"/>	2	0	0.5	<input type="checkbox"/>	
102	Siderite	clBlack	2	<input type="checkbox"/>	2	0	0.5	<input type="checkbox"/>	
103	Quartz	clBlack	2	<input type="checkbox"/>	2	0	0.5	<input type="checkbox"/>	
104	Open Field Fracture	clBlack	1	<input checked="" type="checkbox"/>	3	0	0.5	<input type="checkbox"/>	Field Interpreted Fracture
105	Closed Field Fracture	clBlack	2	<input checked="" type="checkbox"/>	3	0	0.5	<input type="checkbox"/>	Field Interpreted Fracture
*	(New)			<input type="checkbox"/>	0	0	0	<input type="checkbox"/>	

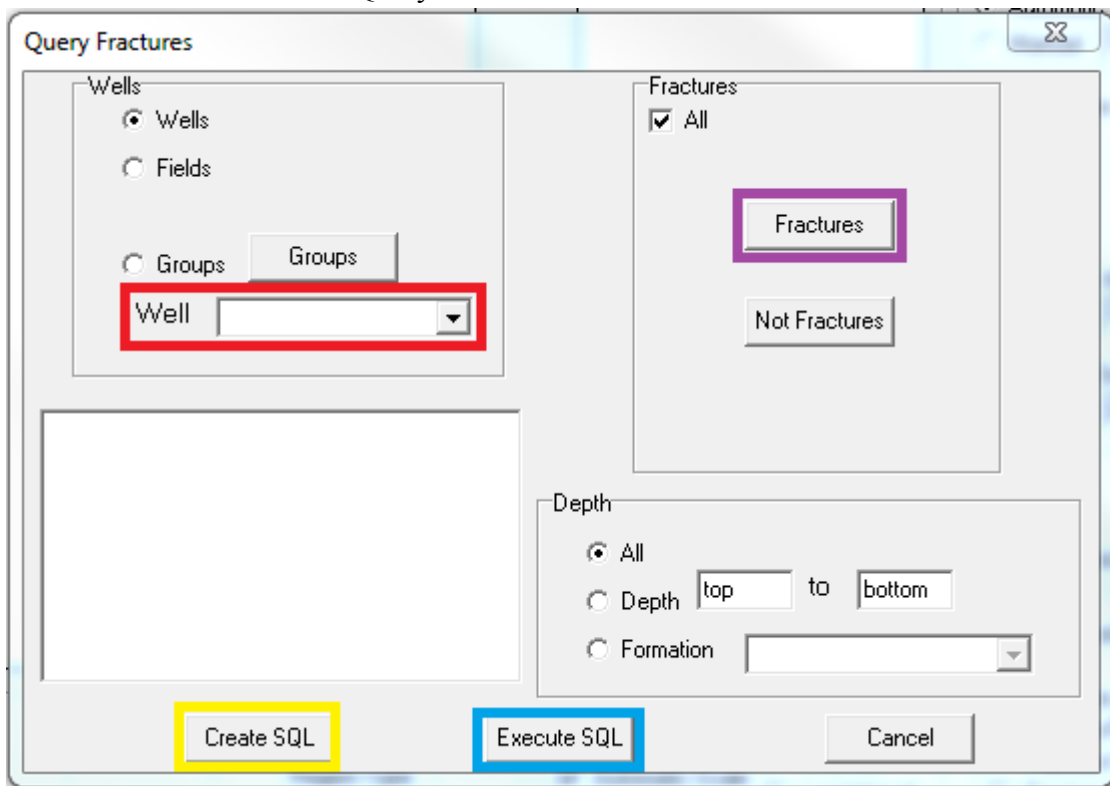
d) Under the 'Fractures – Int' tab, begin to add data. UWI is the assigned UWI from step 1b, FracID is the assigned value from step 1c, Depth the depth at which the fracture was

recorded, and Dip and DipDirn the dip and dip direction of the fracture.

UfracID	UWI	FracID	Depth (m)	Dip	DipDirn
12275	20	97	1	90	314
12276	20	97	1	90	314
12277	20	97	1	90	315
12278	20	97	1	90	315
12279	20	97	1	90	324
12280	20	97	1	90	341
12281	20	97	1	90	342
12282	20	97	1	90	346
12283	20	97	1	90	347
*(New)	0	0			

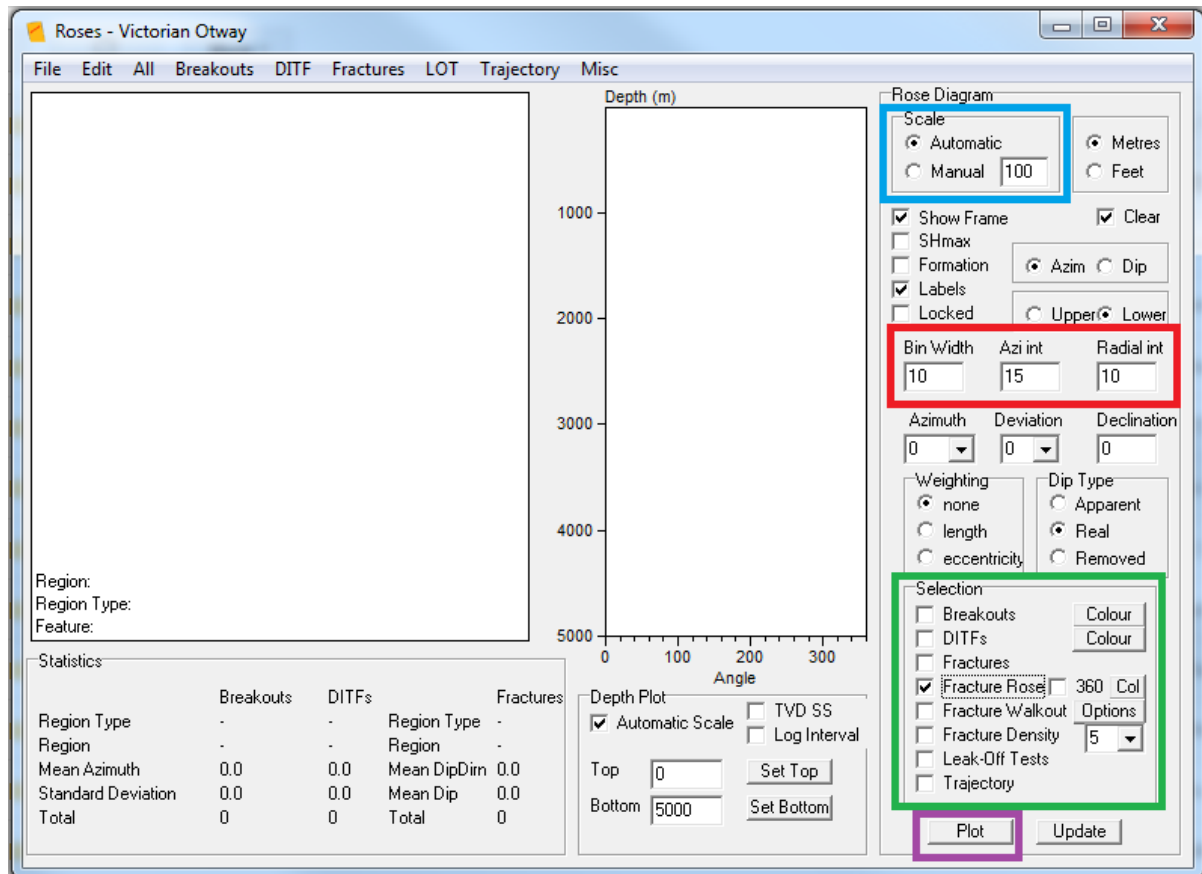
JRS Roses

1. Open 'Roses' and select appropriate field.
2. Under 'Fracture' menu select 'Query'



Choose desired well in 'Well' drop down menu (highlighted red). Select desire fractures to be displayed on rose diagram under menu 'Fractures' (highlighted purple). First select 'Create SQL' (outlined yellow), then select 'Execute SQL' (highlighted blue).

3.

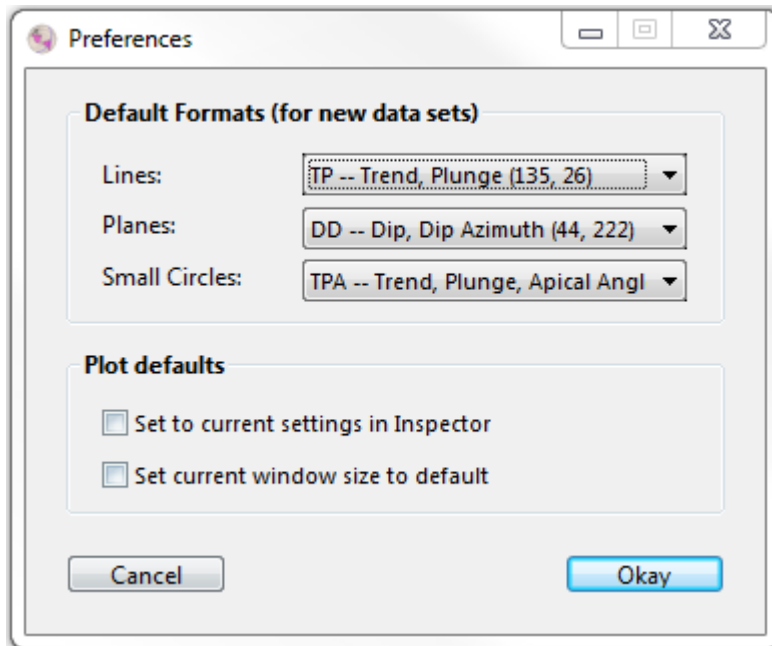


First assign desired scale, either 'Automatic' or 'Manual' (outlined blue). Then assign desired 'Bin Width,' azimuth interval 'Azi int' and radial interval 'Radial int' (outlined red). Select 'Fracture Rose' in selection tab (outlined green) and then select 'Plot' to plot rose diagram.

Stereonet 8<sup>©</sup> method -

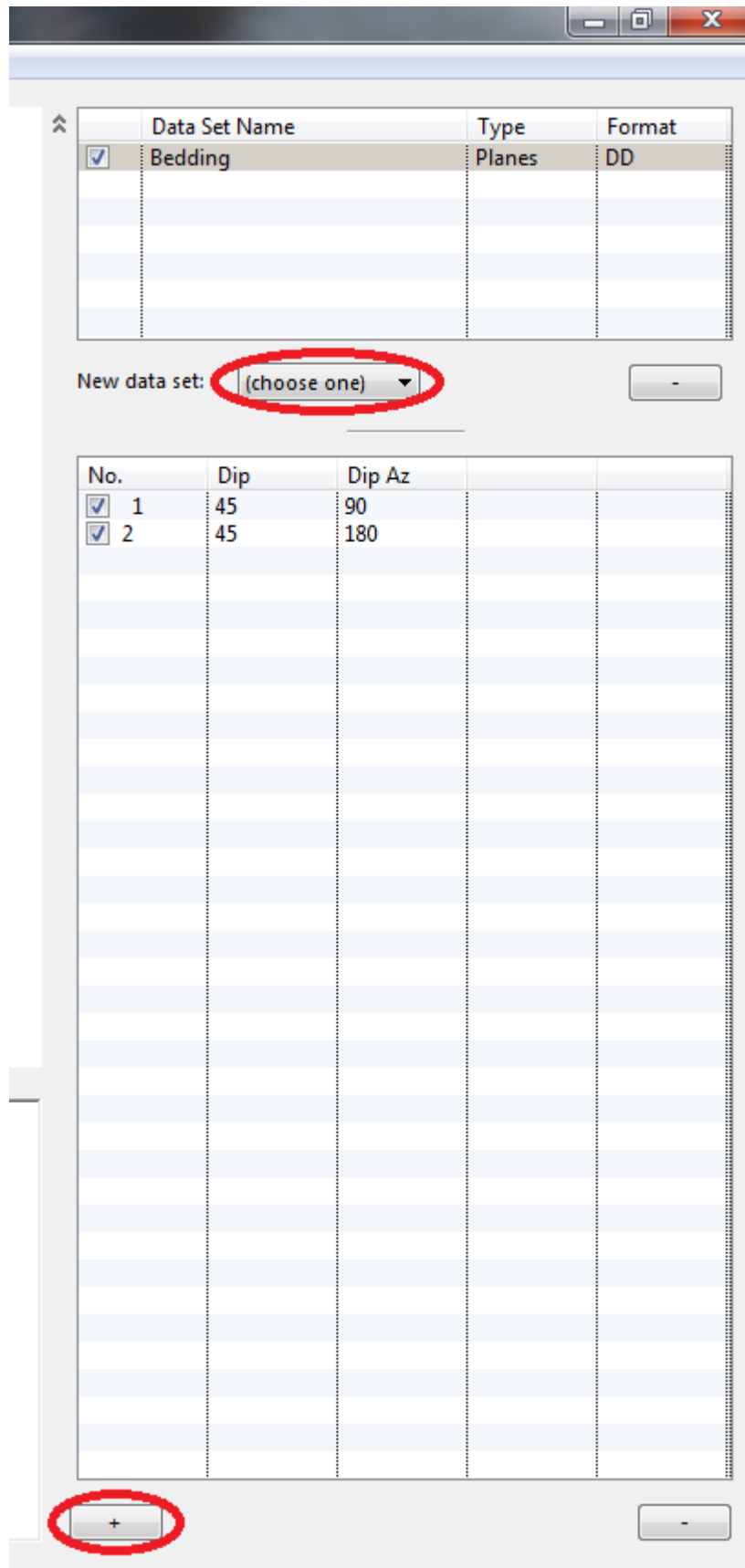
Open Stereonet 8 and select 'New blank window'

1) Under 'Window' tab select 'Preferences'



- Set 'Lines' to TP – Trend, Plunge
- Set 'Planes' to DD – Dip, Dip Azimuth
- Select 'Okay'

2) In the 'choose one' menu select 'planes' to create new data set.  
To add planes, click '+' then enter dip and dip azimuth values



3) To calculate poles to plan, in the 'calculations' drop down menu, select 'poles'

The screenshot shows a software window titled 'Untitled 0' with a menu bar (File, Edit, Data, Calculations, Plot, View, Window). The main area is divided into several sections:

- Stereonet Plot:** A circular plot with a grid. Two great circles are drawn, and two points are plotted on the grid. A central crosshair is visible.
- Data Set Table:**

	Data Set Name	Type	Format
<input checked="" type="checkbox"/>	Bedding	Planes	DD
<input checked="" type="checkbox"/>	poles to Bedding	Lines	TP
- New data set:** A dropdown menu showing '(choose one)' and a '-' button.
- Results Table:**

No.	Trend	Plunge		
<input checked="" type="checkbox"/> 1	270.0	45.0		
<input checked="" type="checkbox"/> 2	000.0	45.0		
- Text Output:**

----- Poles from Planes | 11/09/2013 at 10:02 AM  
 -----  
 calculated from 2 planes from Data set: 'Bedding'

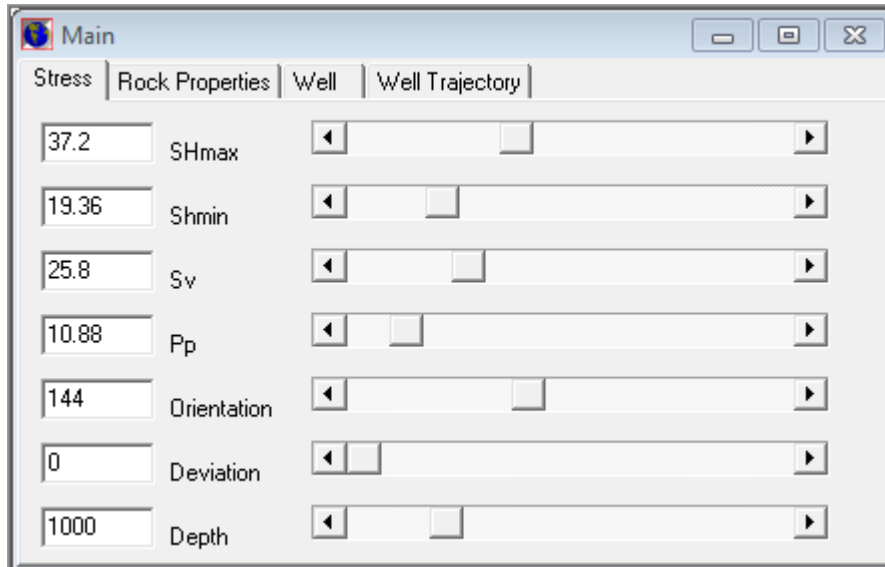


## STRUCTURAL PERMEABILITY

Fracture susceptibility/fault reactivation plots were created using Swift in JRS Petroleum Suite<sup>®</sup> to determine optimal orientations for fractures to be open to fluid flow.

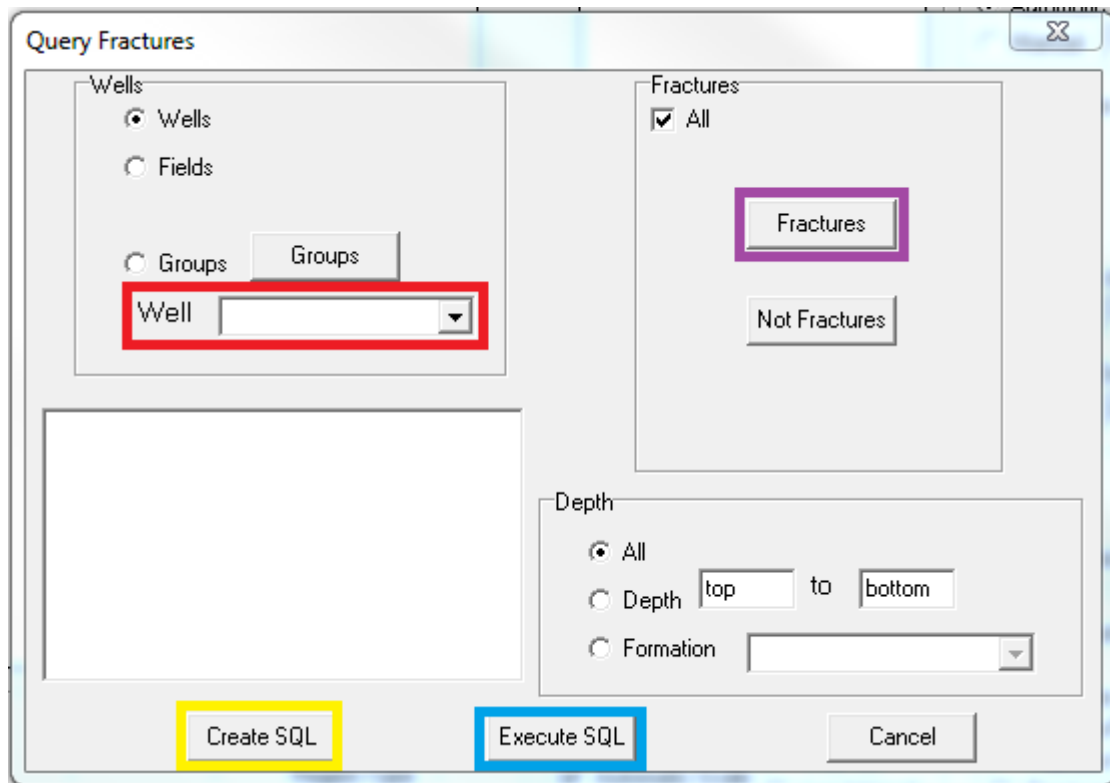
JRS Swift

1. Open 'Swift' and select appropriate project.



Enter appropriate values in 'Main Window' under 'Stress,' 'Rock Properties' and 'Well' tabs.

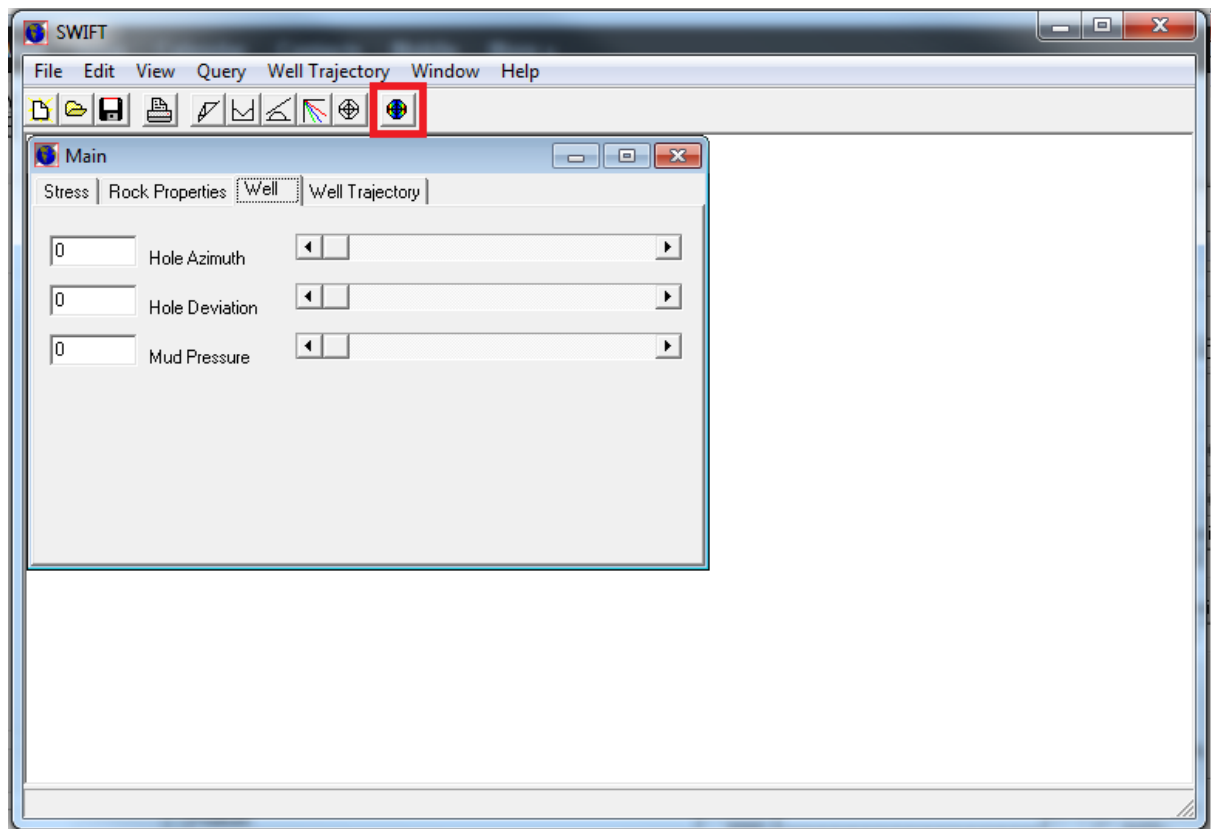
2. Under 'Query' menu, select 'Fracture' menu then select 'Query'



Choose desired well in 'Well' drop down menu (highlighted red). Select desired fractures to be displayed on rose diagram under menu 'Fractures' (highlighted purple). First select

‘Create SQL’ (outlined yellow), then select ‘Execute SQL’ (highlighted blue).

3. Under ‘View’ menu, select ‘Stereonets,’ then ‘StrucPerm’ then ‘Fractures.’
- 4.



Finally select ‘Risk of Reactivation’ icon (outlined red) to display reactivation potential plot with fracture sets.

## SLIDE PREPARATION

Slides used for optical microscopy were prepared from samples taken in the field (Slide Location/Description Table).

Slide Location/Description Table. List of samples taken from the Eumeralla Formation, Victoria

Number	Location	Description
JS-01	Moonlight Head, Face map 1	Calcite Fracture Fill. <1 cm fracture cement fills taken from fine grained sand unit. Show multiple (2?) stages of crystallisation. For mineralogy and porosity of fracture cements.
JS-02	Moonlight Head, Face map 1	Calcite Fracture Fill. <1 cm fracture cement fills taken from fine grained sand unit. Show multiple (3?) stages of crystallisation. For mineralogy and porosity of fracture cements.
JS-03	Moonlight Head, Face map 1	Calcite Fracture Fill. <1 cm fracture cement fills taken from fine grained sand unit. For lithology of fine grained unit and mineralogy and porosity of fracture cements.
JS-04	Moonlight Head, Face map 2	Rock Sample taken from fine to medium grained, cross bedded sands. For lithology and porosity of unit.
JS-05	Moonlight Head, Face map 2	Thick Calcite Fracture Fill with thin siderite rim, 2-3 cm thickness. For mineralogy and porosity of fracture cements.
JS-06	Cape Otway, Face map 1	Rock Sample taken from fine grained sand to silt. For lithology and porosity of unit.
JS-07	Cape Otway, Face map 2	Calcite Fracture Fill. <1 cm fracture cement fills taken from fine grained to silt unit. For mineralogy and porosity of fracture cements.

Using a rock saw the samples were first cut to the rough outline shape of a glass slide, this was dependent on the original size of the sample, but was generally no larger than 6 cm by 2 cm. The thickness of the sample was then reduced down to around 3 to 4 mm. Thin sections were then prepared by Pontifex & Associates Pty Ltd. using the following technique:

- 1) First, a small slab is cut, approximately 25 mm x 55 mm, x 8 mm thick, using a 250 mm diameter rock-cutting saw blade with a continuous diamond rim. Samples were impregnated with blue dyed epoxy to highlight porosity.
- 2) A top surface on the slab, is manually ground flat on a bench-mounted, horizontal diamond grinding wheel Habit-brand, grit size 64.
- 3) The coarse ground top surface is warmed on a hot plate (at 50oC), and the top coarse-ground surface is impregnated with an epoxy mix of Araldite LC191 resin, with HY951 hardener, ratio 8:1. This surface is then manually more finely ground flat using 600 SiC grit, on a zinc-lap or glass plate, using water as a lubricant. This flat

finely ground surface is cleaned, checked manually for “perfection”, (if open porosity is still exposed another veneer of epoxy is applied), is then glued onto a clean, dry glass slide, ground to a known thickness, using a UV curing, cyanoacrylate liquid adhesive “Loctite Impruv 36331”. [Exposure to a UV light of the glued interface through the back of the glass slide cures the adhesive in 2 to 3 minutes. This is a permanent bond, and the rock (or eventual wafer) cannot be ever separated from the glass.

- 4) The block mounted on glass is then cut off using a trim saw with a thin continuous diamond rimmed sawblade (Diatrenn E2-G), to leave a thickness of about 1 mm of the sample slab (glued onto the glass slide), with the top surface exposed for further processing.
- 5) The 1 mm slab thickness is further ground down on a diamond wheel (Habit D76) held within a special jig attachment by vacuum, using water as a lubricant. This reduces the slab thickness stuck on the glass, to a wafer of about 120 micron (0.12 mm).
- 6) The glass slide of known thickness with the glued-on rock wafer is then loaded and held in place on the face of a special jig, and lapped flat on a Logitech machine, to a final petrographic thickness of the rock wafer, of 30 micron, using 600 SiC grit as the grinding abrasive, and water as a lubricant.
- 7) When the Logitech lapping cycle is finished, the quality of the wafer on the glass is assessed, also optically checked for the required 30 micron thickness, and when confirmed as correct, the section is cleaned and covered with a glass coverslip, using the same UV curing adhesive as listed above. Again this is a permanent fix, i.e. the coverslip cannot be removed. The final thin section is then again cleaned and labelled.

## PETROLOGY

Using an optical microscope, thin section slides were examined to determine the mineralogy, structure and porosity of rocks and fracture fills of the Eumeralla Formation. To complete this accurately, optical properties of minerals expected to be encountered were revised according to Kerr and Rogers (1977). All samples were taken from the Eumeralla Formation, a volcanogenic sedimentary rock; therefore quartz, alkali feldspar and plagioclase feldspar were expected (Minerals Table 1). Siderite, calcite and quartz were expected as fracture cements (Minerals Table 1, Minerals Table 2).

Minerals Table 1. Optical properties of minerals expected to be seen in the Eumeralla Formation rock samples collected from the field. (Properties are taken from Kerr & Rogers 1977).

Mineral Name	Colour	Form	Cleavage	Relief	Birefringence	Extinction	Twinning	Comments
Quartz (SiO <sub>2</sub> )	Colourless in thin section. Often contains inclusions	Euhedral prismatic crystals, in veinlets, disseminated grains and as replacement anhedral. Common as pseudomorphs of other crystals.	Usually absent. Sometimes shows in the edge of the slide. Imperfect rhombohedral, almost rectangular in favourable section.	Very low.	Weak.	Parallel in euhedral crystals and symmetrical to cleavage traces. Irregular and wavy extinction is very common. Vein quartz often shows feathered or lamellar extinction.	Rarely shows in thin section.	Usually easy to determine due to its lack of alteration and, absence of cleavage and absence of twinning.
Plagioclase Feldspar (CaAl <sub>2</sub> Si <sub>2</sub> O <sub>8</sub> )	Colourless	Occurs in anhedral, subhedral and anhedral crystals and laths.	2 or 3, weak to moderate.	Low.	Very Low. Interference colours are 1 <sup>st</sup> order pale yellows	Inclined.	Simple twins and occasional multiple twinning.	Distinguishable by polysynthetic twinning.
Alkali Feldspar (KAlSi <sub>3</sub> O <sub>8</sub> )	Colourless	Occurs in phenocrysts, subhedral and anhedral crystals and in spherulites.	2 or 3, weak to moderate. 1 perfect cleavage, 1 less perfect and 1 imperfect.	Very low.	Very Low. Interference colours are 1 <sup>st</sup> order grey to white.	Inclined.	Simple twins in sanidine and microcline. Orthoclase is often untwinned.	Distinguished from plagioclase by the absence of multiple twins. Microcline polymorph is distinguishable by tartan cross-hatch twinning. Orthoclase polymorph similar to quartz but is distinguishable due to its cleavage and biaxial character.

Minerals Table 2. Optical properties of minerals expected to be seen in the fractures in the Eumeralla Formation samples collected from the field. (Properties are taken from Kerr & Rogers 1977).

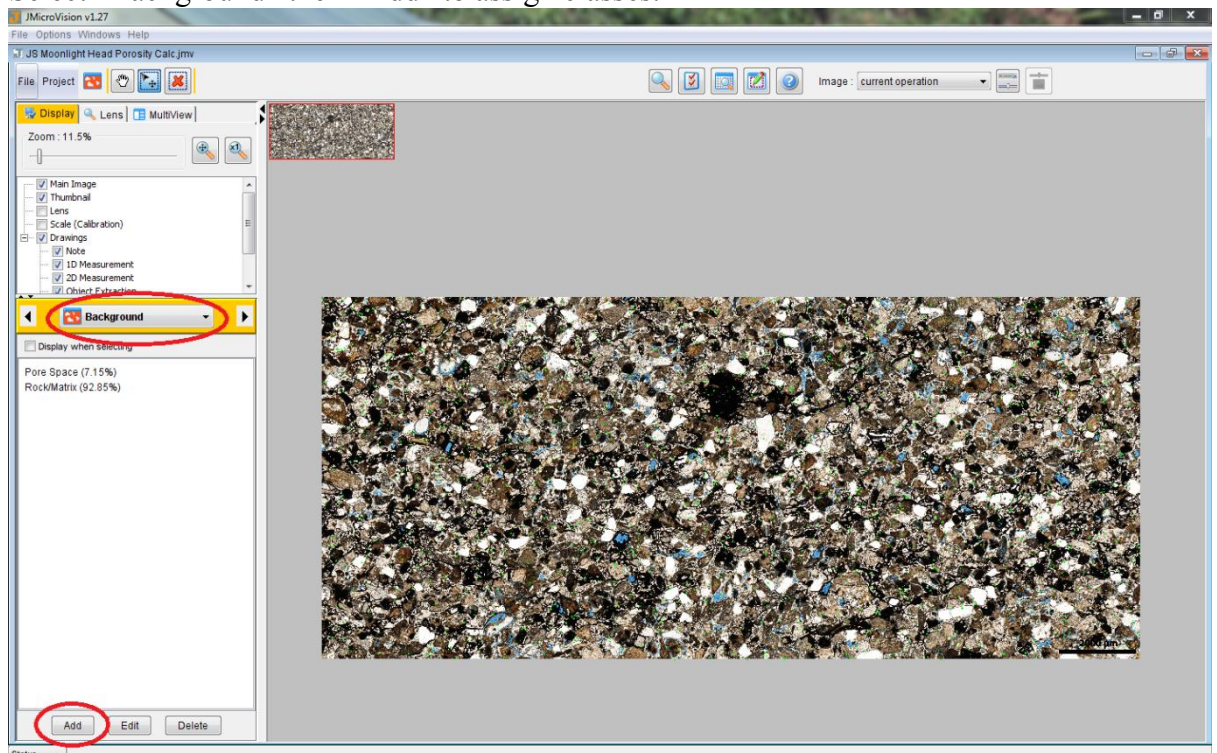
Mineral Name	Colour	Form	Cleavage	Relief	Birefringence	Extinction	Twinning	Comments
Calcite (CaCO <sub>3</sub> )	Colourless in thin section, but often cloudy	Fine to coarse aggregates, usually anhedral. Euhedral crystals are rare.	Perfect rhombohedral, usually shows at two intersecting lines at oblique angles. In fine aggregates cleavage may not show.	Varies with direction, from high to low.	Extreme. Maximum interference colour is pearl grey or white of the higher orders	Symmetrical to cleavage traces	Polysynthetic twinning. Twin lamellae are mostly parallel to the long diagonal.	Often mistake with dolomite and siderite. Dolomite is usually subhedral to euhedral and has lamellae parallel to the short diagonal. Siderite has iron stains around grain borders and relief is not low in any position.
Siderite (FeCO <sub>3</sub> )	Colourless to grey, sometimes with yellowish or brown spots around edges.	Fine to coarse aggregates of anhedral to euhedral crystals.	Perfect rhombohedral, usually shows at two intersecting lines at oblique angles. In fine aggregates cleavage may not show.	Varies with direction, from high to moderate.	Extreme. Maximum interference colour is pearl grey or white of the higher orders. Brighter colours may show on the edge of the slide.	Symmetrical to cleavage traces	Twin lamellae parallel to the long diagonal are occasionally observed.	Distinguished by brown staining around grain boundaries. Chief occurrence of siderite is in veins or replacement deposits.

## POROSITY

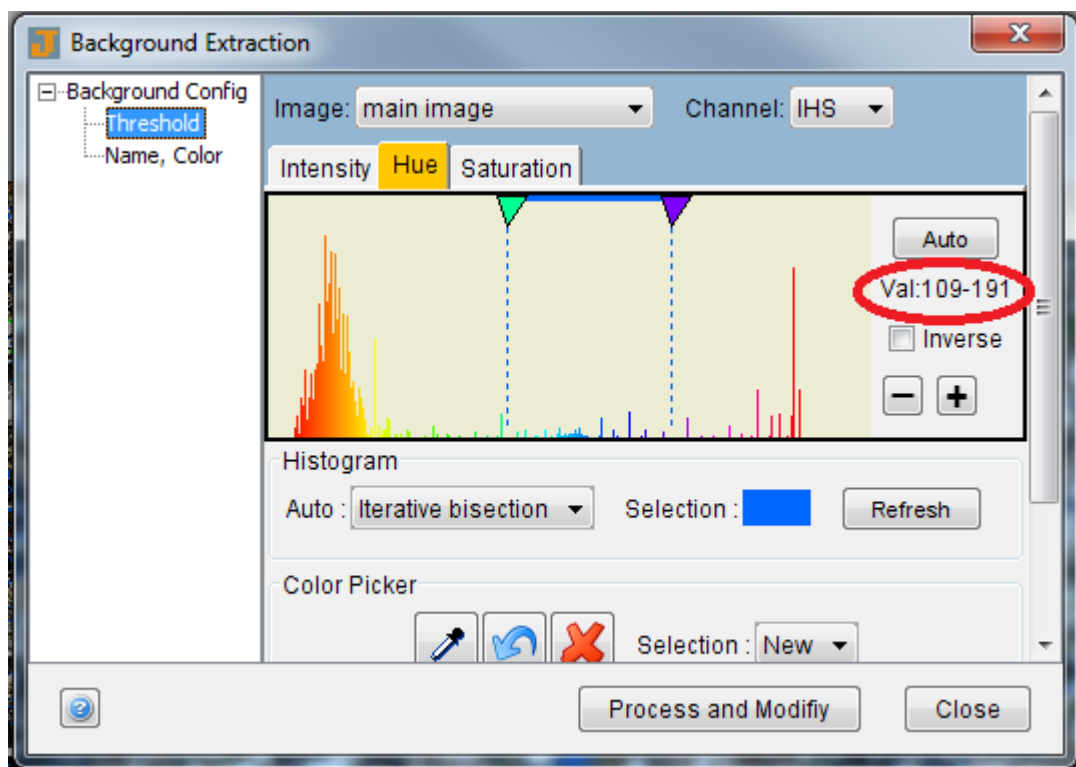
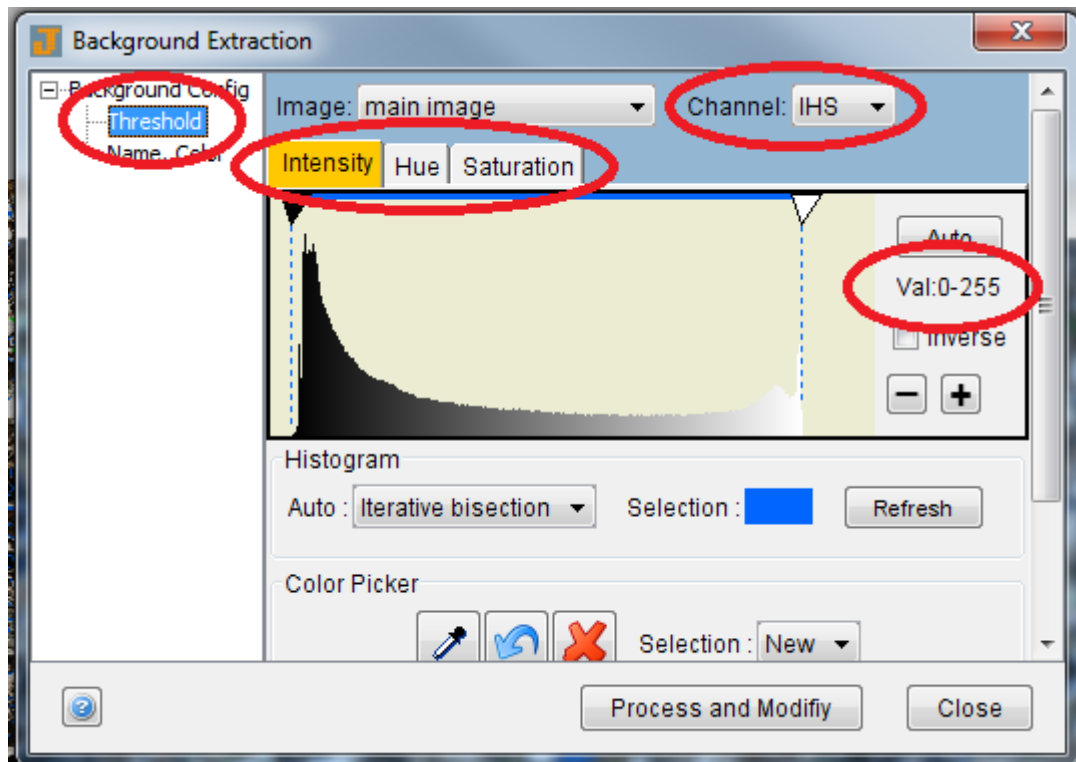
Using JMicroVision© V1.27, the image analysis technique was used to determine the porosity of 2 thin sections from the Otway Basin. The technique used is outline below.

Image Analysis –

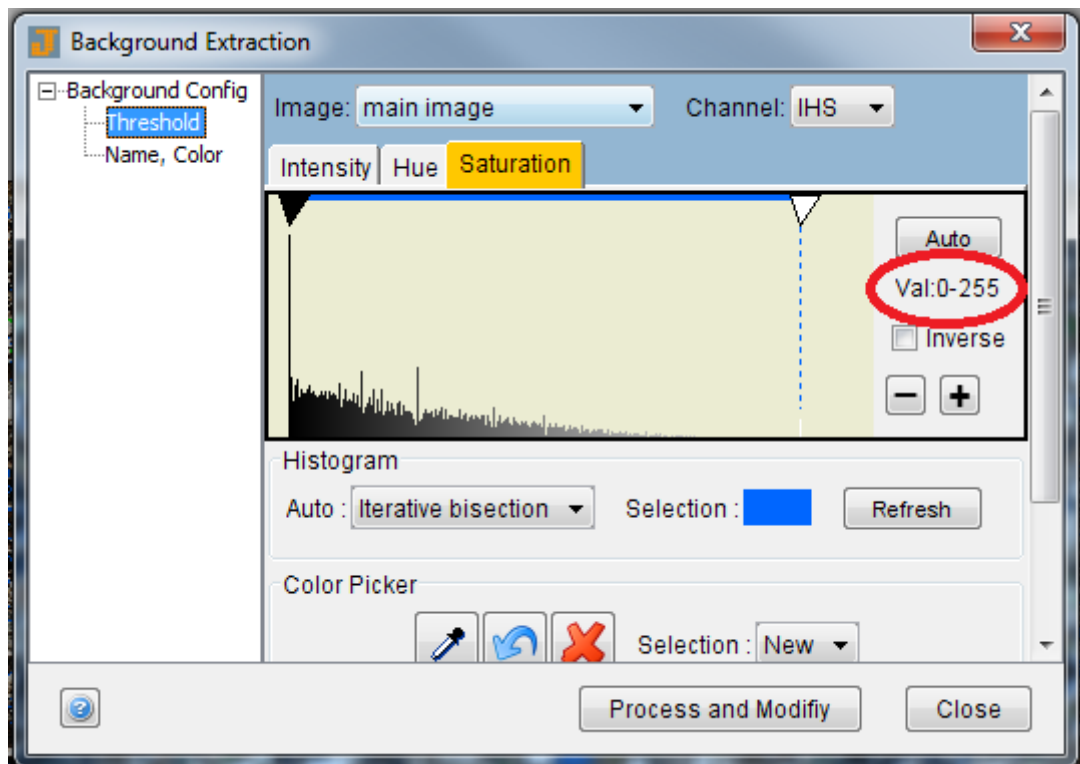
- 1) Load image into JMicroVision (Ctrl+I)
- 2) Select “Background” then “Add” to assign classes.



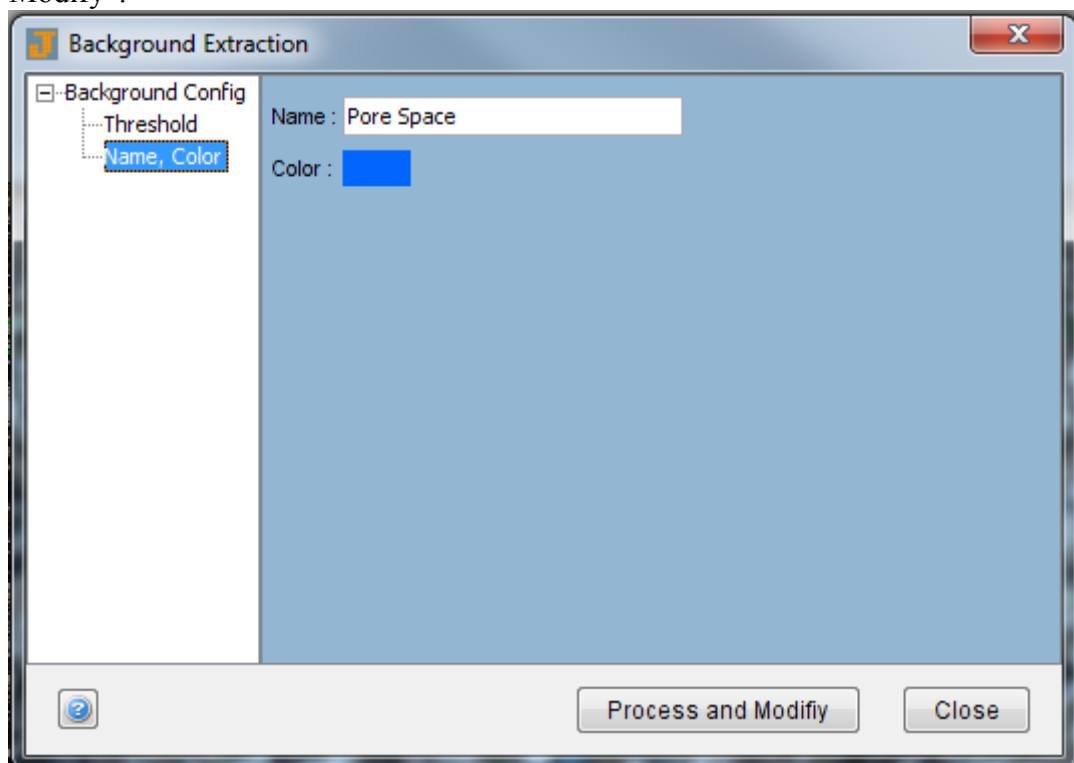
- 3) Under “Threshold” menu, choose “channel” as “HIS.” Set desired Intensity, Hue and Saturation.



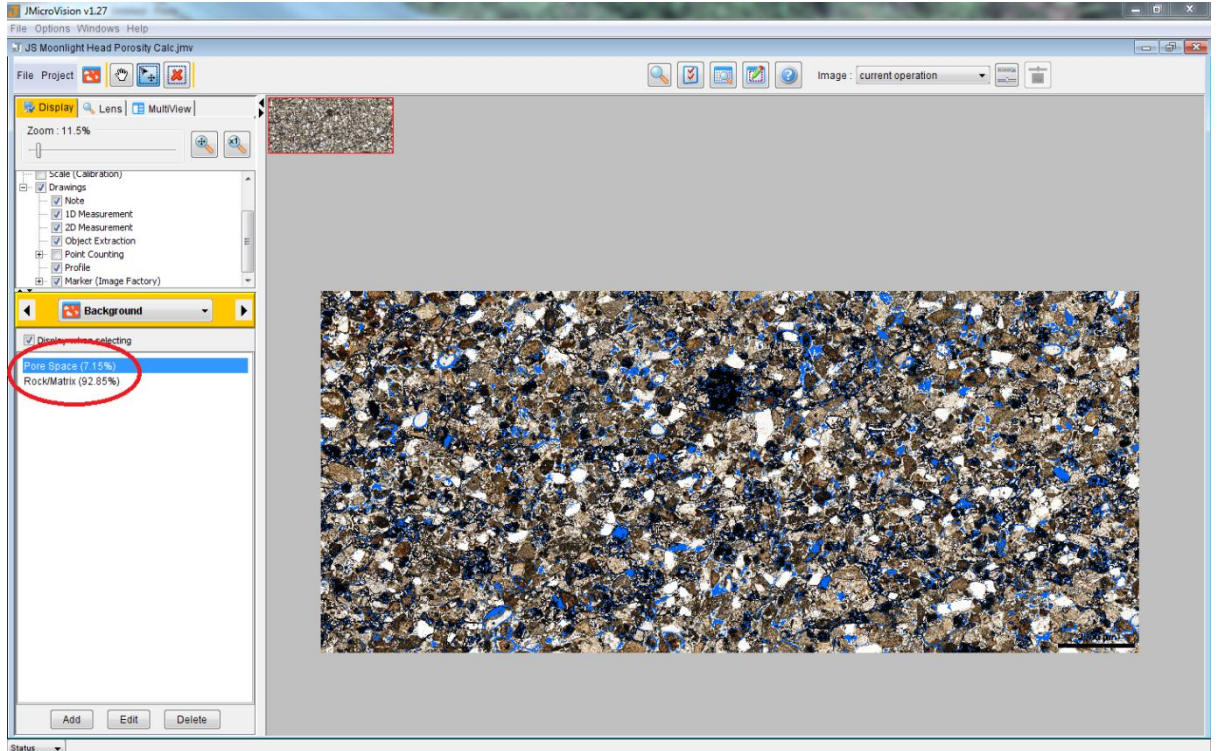




- 4) Under “Name, Colour” Assign a name and colour. Then select “Process and Modify”.



5) Repeat for all desired classes.



Results for image analysis are given as a percentage with corresponding class.

## WYLLIE TIME AVERAGE CALCULATIONS

Wyllie Time Average Equation:

$$\phi = \frac{\Delta t_{\log} - \Delta t_{ma}}{\Delta t_{fl} - \Delta t_{ma}}$$

Where:

$\phi$  = porosity (JS-07 porosity = 0.36)

$\Delta t_{\log}$  = change in time in log ( $\mu\text{s}/\text{ft}$ )

$\Delta t_{ma}$  = change in time in matrix (typical shale value used = 62.5) ( $\mu\text{s}/\text{ft}$ )

$\Delta t_{fl}$  = change in time in fluid (typical saline water value used = 189) ( $\mu\text{s}/\text{ft}$ )

$$.0036 = \frac{\Delta t_{\log} - 62.5}{189 - 62.5}$$

therefore:

$$\Delta t_{\log} = 62.96 \text{ } (\mu\text{s}/\text{ft})$$

## **APPENDIX B: FACE MAPS AND TRANSECTS**

Below are digitised copies of all field maps and transects from this study from the Otway Basin. All face map and transect locations are given in Transect Table 1 & 2 and Face map Table 1 & 2. Included on all face maps are stereonet of all fractures recorded, with open fractures (solid black triangles) and closed fractures (solid black circles) represented.

Cape Patton face map - A-B (Map 1 of 3)

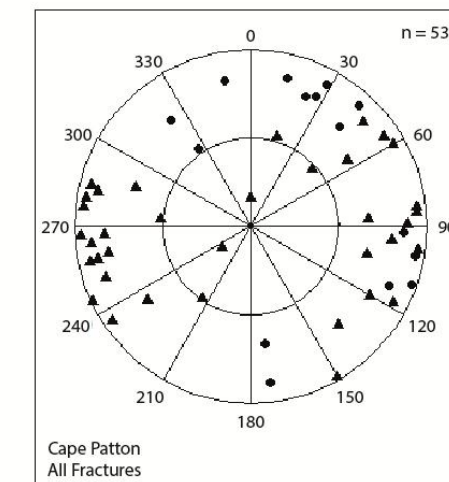
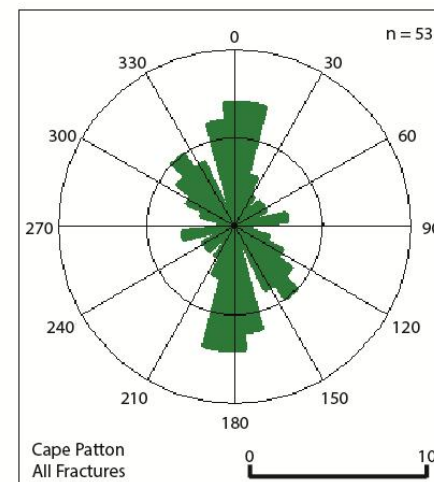
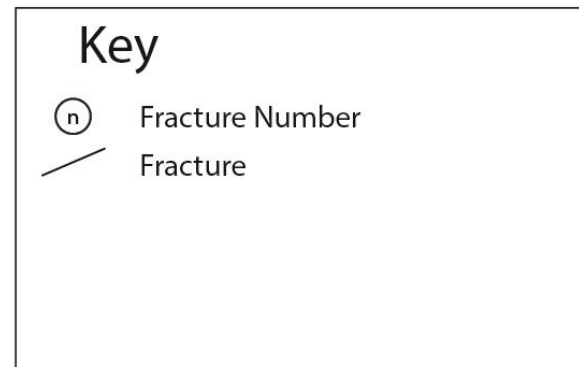


A

Transect Start S 38° 41.515'  
E 143° 49.797'  
Transect End S 38° 41.516'  
E 143° 49.804'

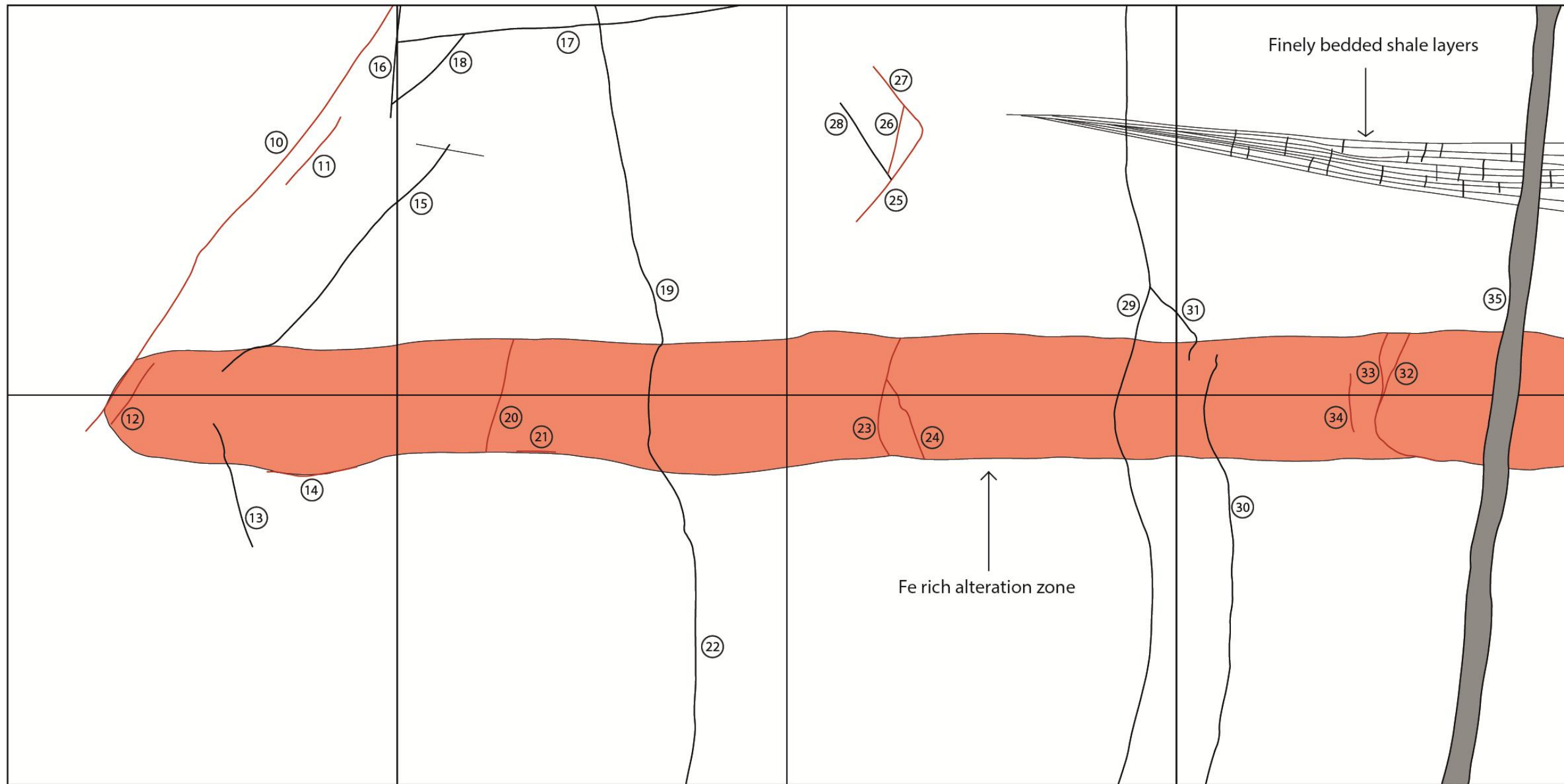


Facing North  
Bearing along face - 276°



B

Cape Patton face map - B-C (Map 2 of 3)

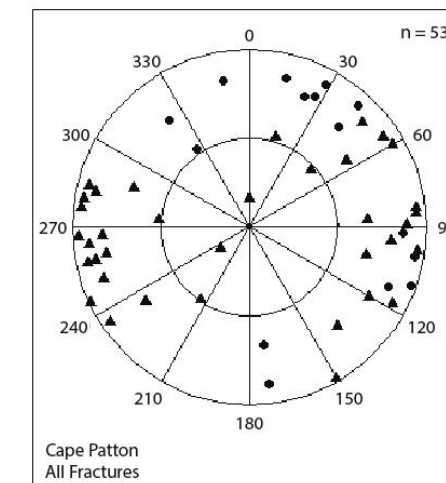
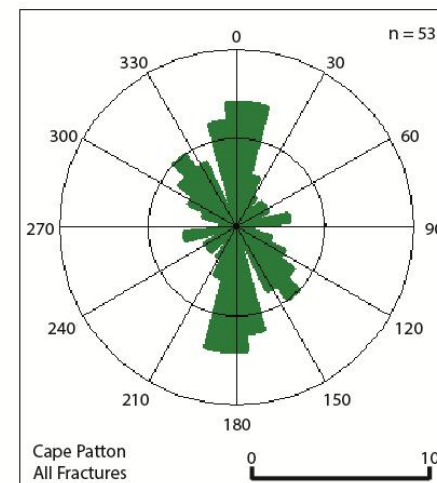
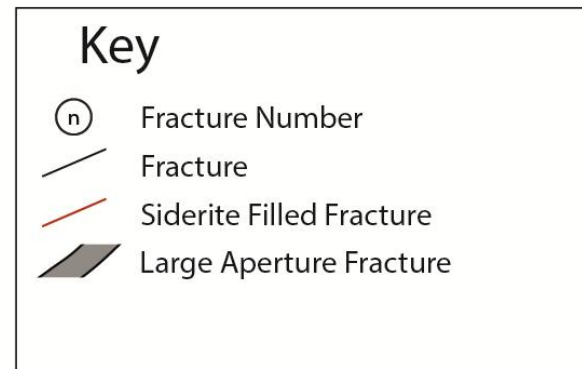


B

Transect Start S 38° 41.515'  
E 143° 49.797'  
Transect End S 38° 41.516'  
E 143° 49.804'



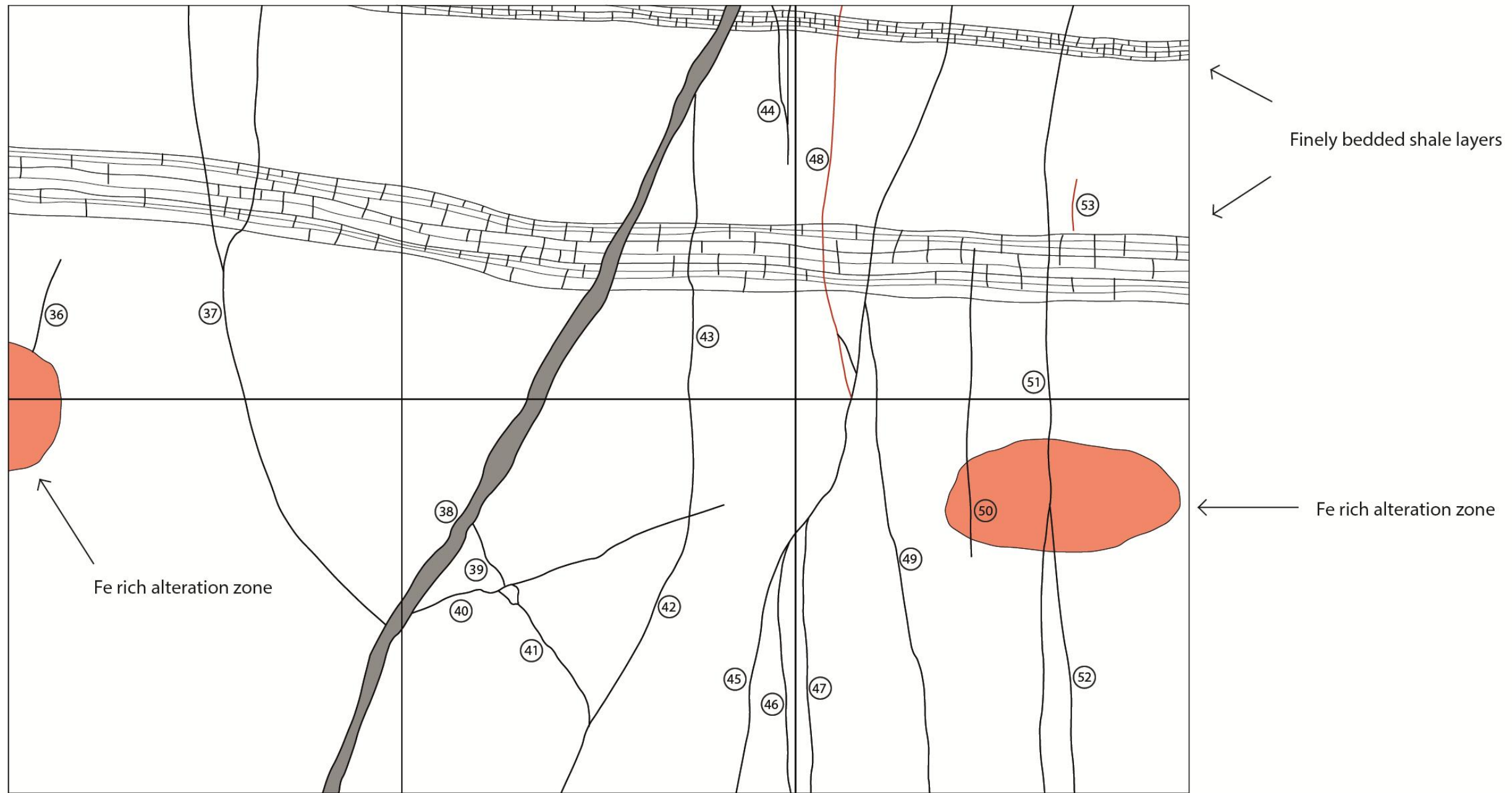
Facing North  
Bearing along face - 276°



C



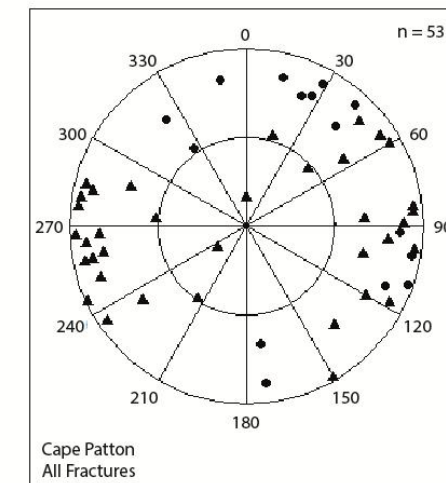
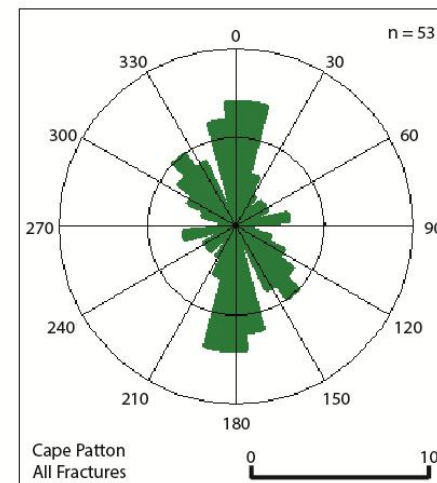
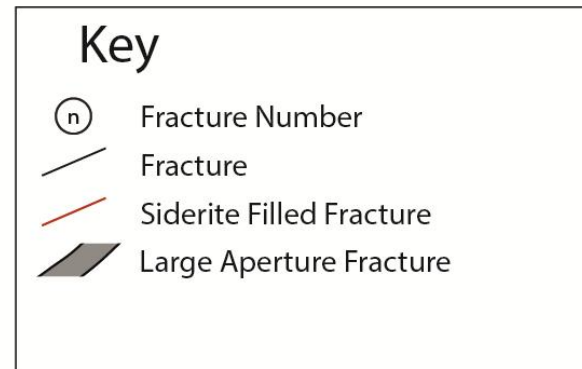
Cape Patton face map - C-D (Map 3 of 3)



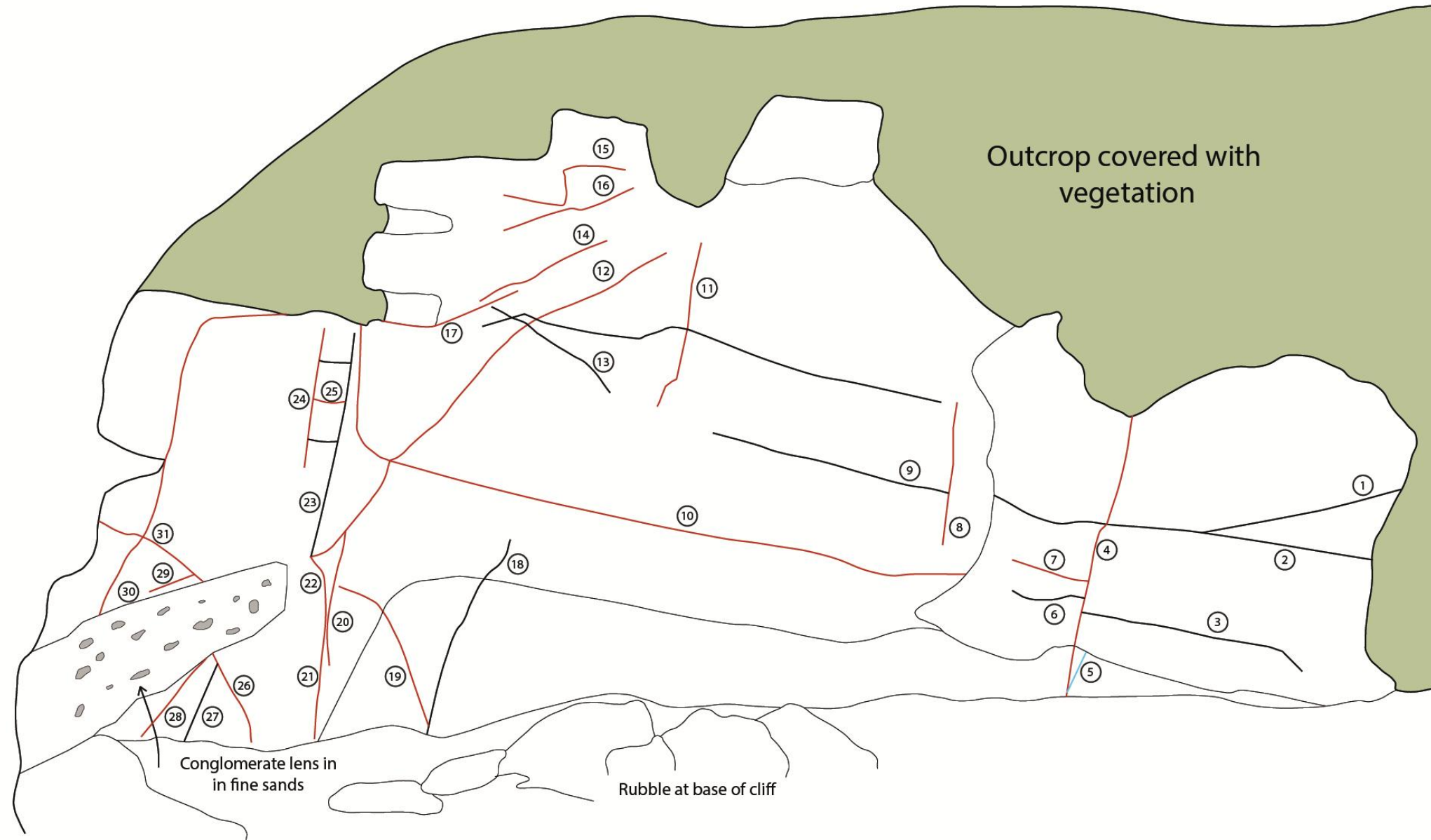
C  
 Transect Start S 38° 41.515'  
 E 143° 49.797'  
 Transect End S 38° 41.516'  
 E 143° 49.804'

0 10 20 30 40 50cm

Facing North  
 Bearing along face - 276°



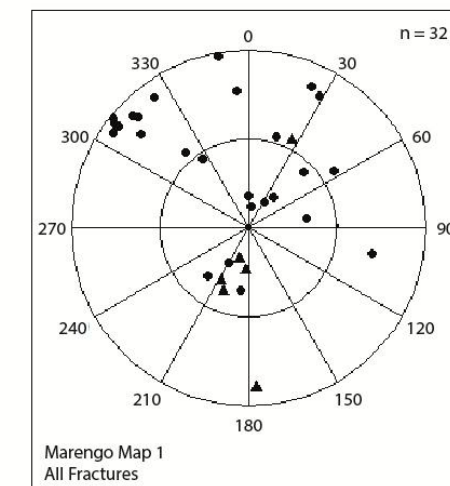
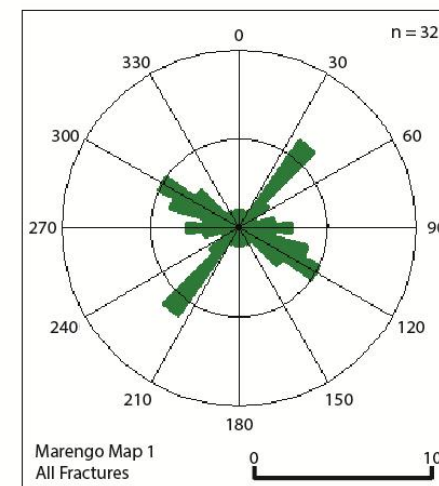
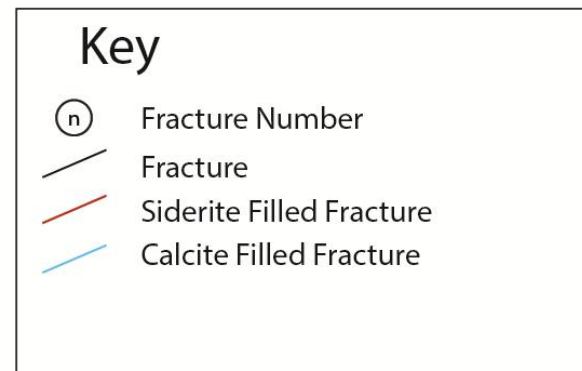
Marengo Bay face map 1



Transect Start S 38° 46.737  
E 143° 39.964'  
Transect End S 38° 46.741'  
E 143° 39.969'

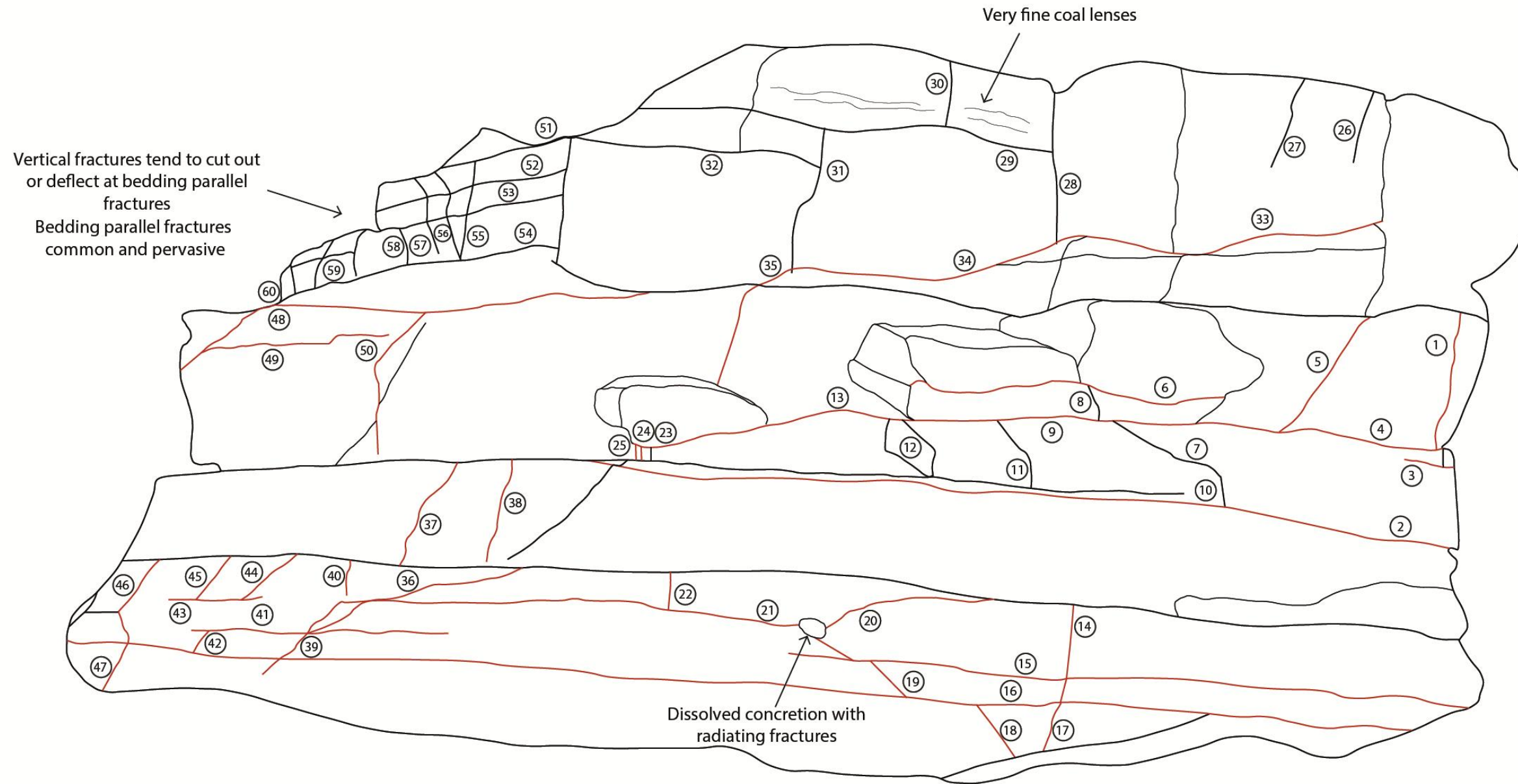


Facing West  
Bearing along face - 305°

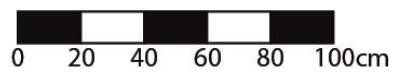




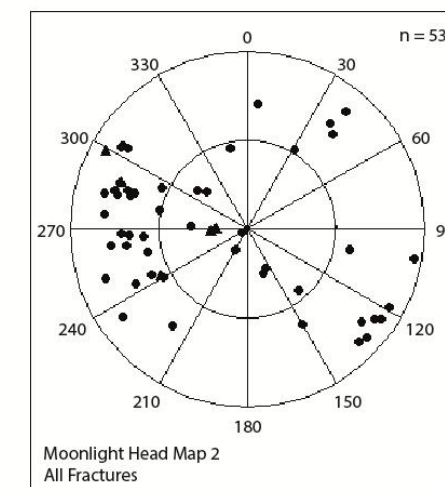
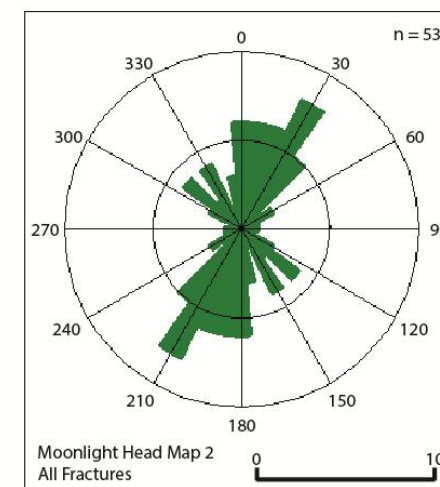
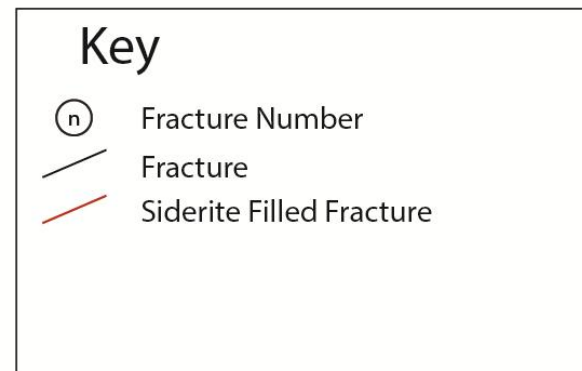
### Marengo Bay face map 2



Transect Start S 38° 46.748  
E 143° 39.971'  
Transect End S 38° 46.751'  
E 143° 39.968'

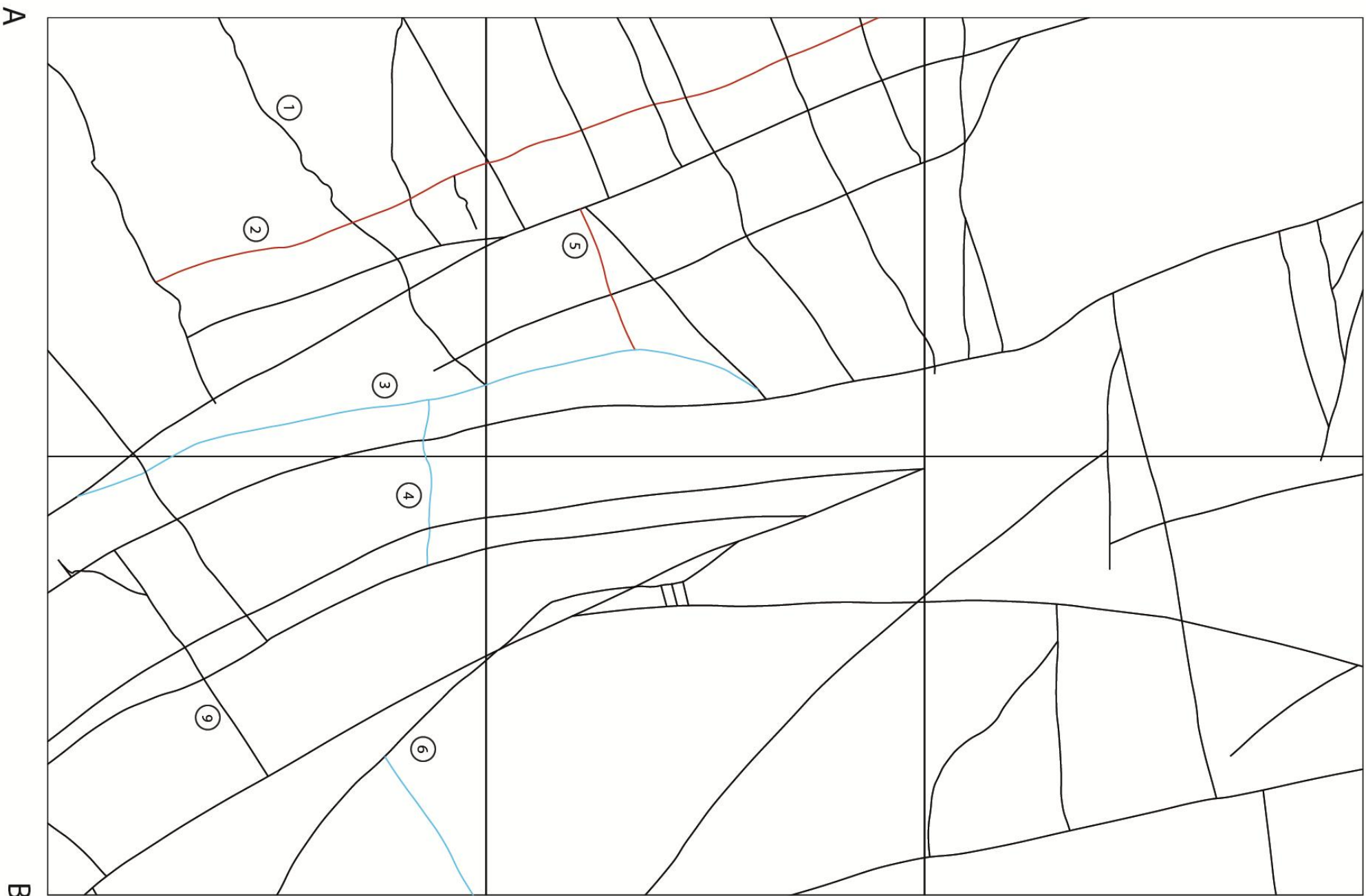


Facing North West  
Bearing along face - 225°





Moonlight Head face map 1 - A-B (Map 1 of 3)

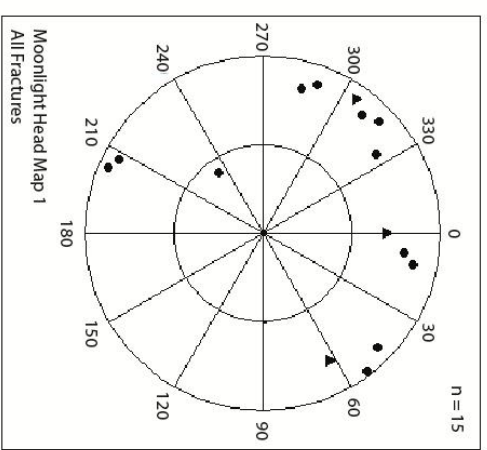
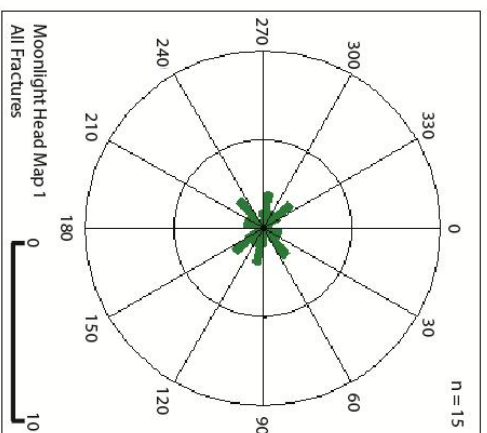
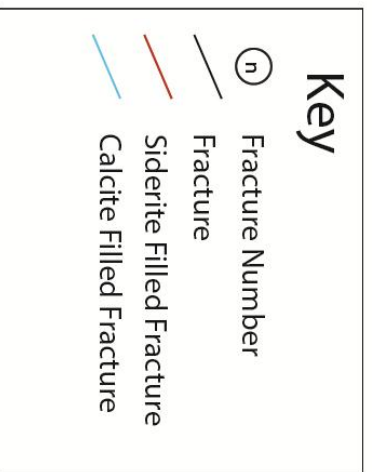


Transect Start S 38° 45.326'  
E 143° 12.814'

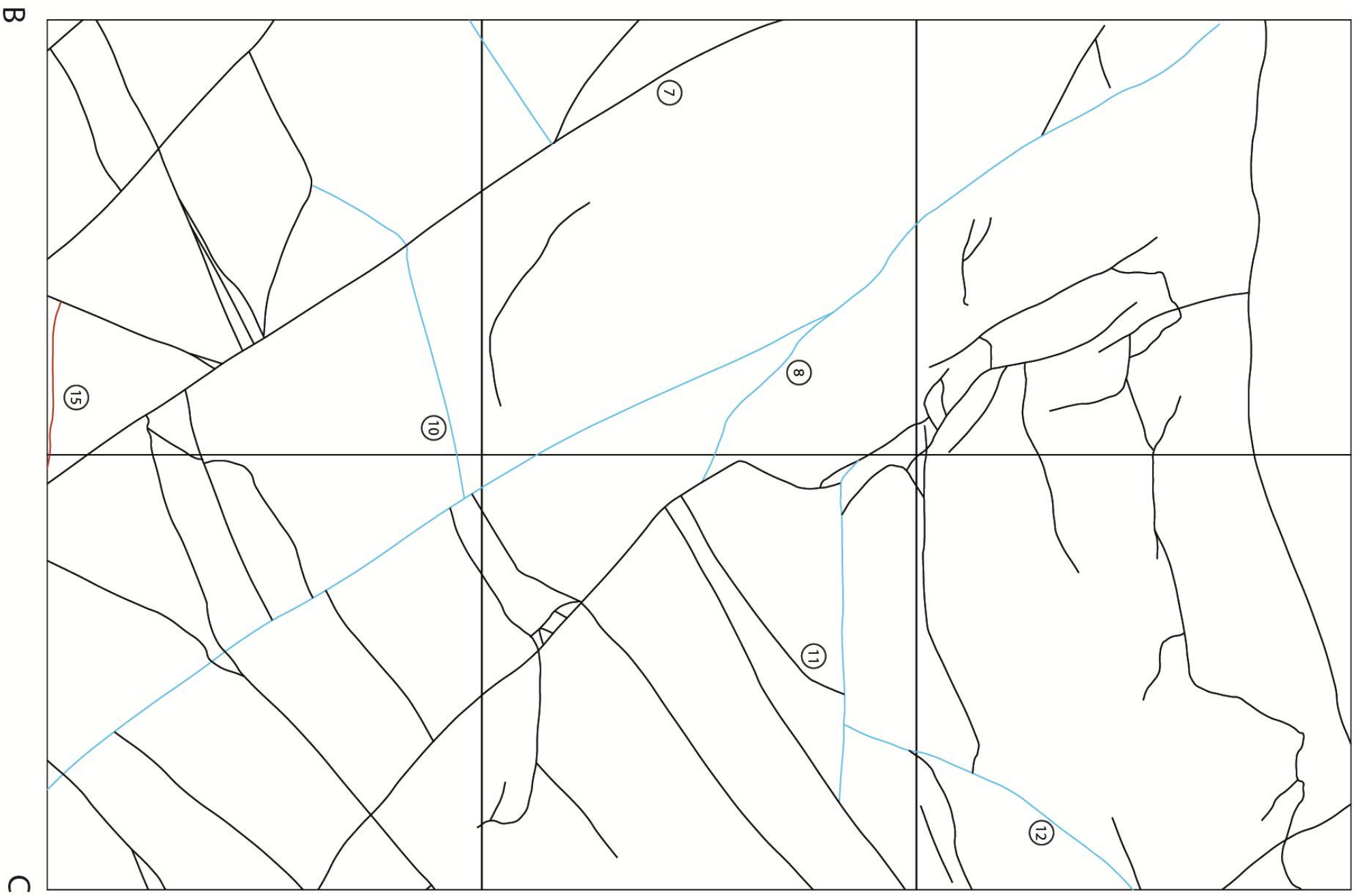
Transect End S 38° 45.330'  
E 143° 12.815'

0 10 20 30 40 50cm

**Facing North**  
Bearing along face - 152



Moonlight Head face map 1 - B-C (Map 2 of 3)

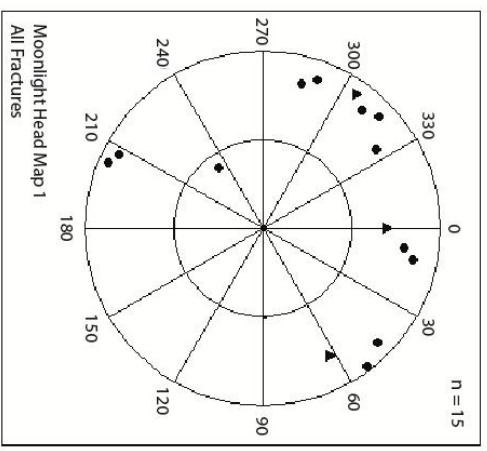
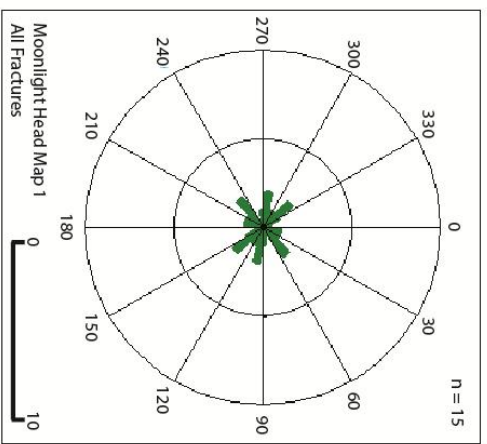
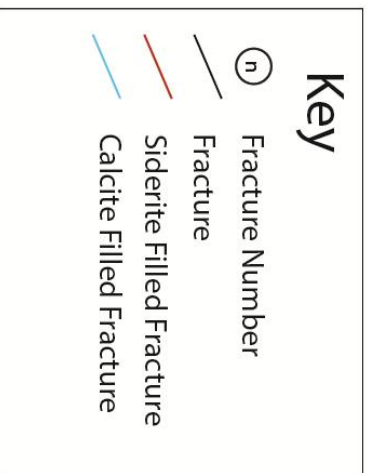


Transect Start S 38° 45.326'  
E 143° 12.814'

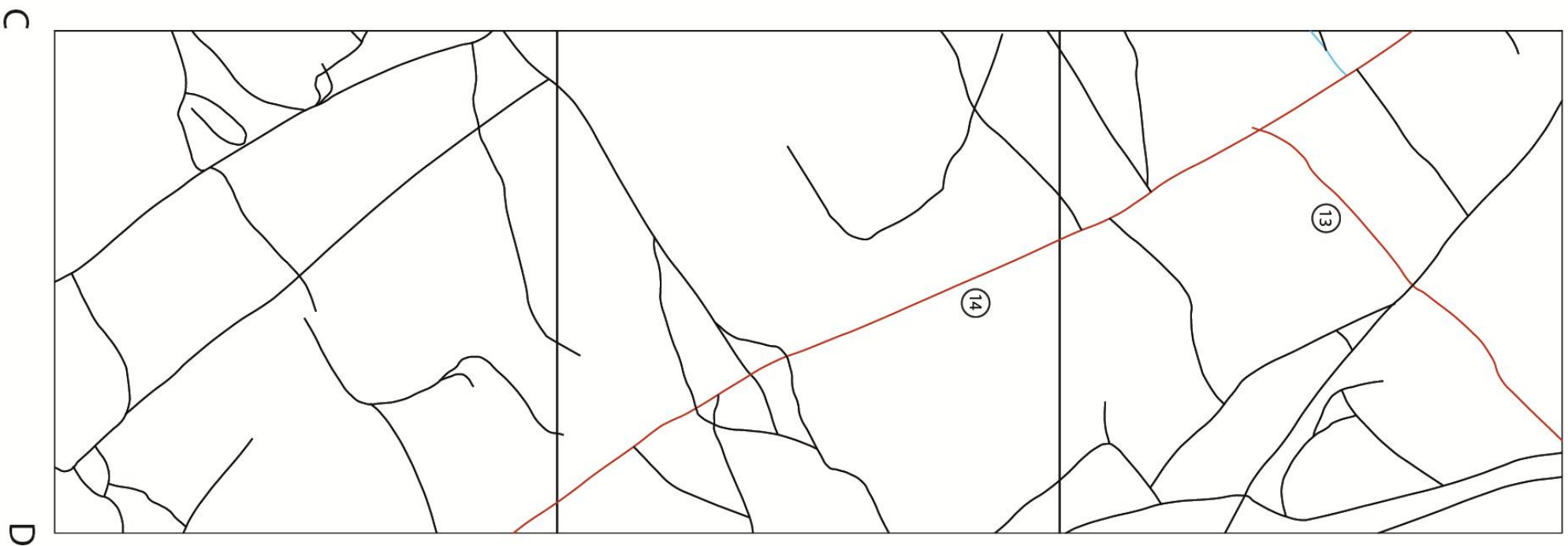
Transect End S 38° 45.330'  
E 143° 12.815'

0 10 20 30 40 50cm

Facing North  
Bearing along face - 152



Moonlight Head face map 1 - C-D (Map 3 of 3)

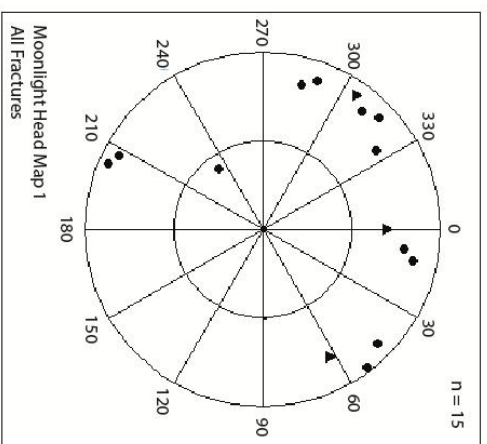
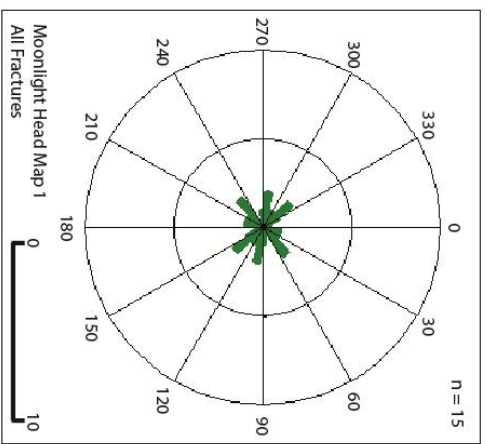
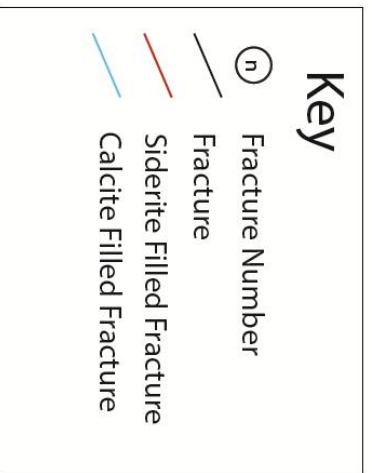


Transect Start S 38° 45.326'  
E 143° 12.814'

Transect End S 38° 45.330'  
E 143° 12.815'

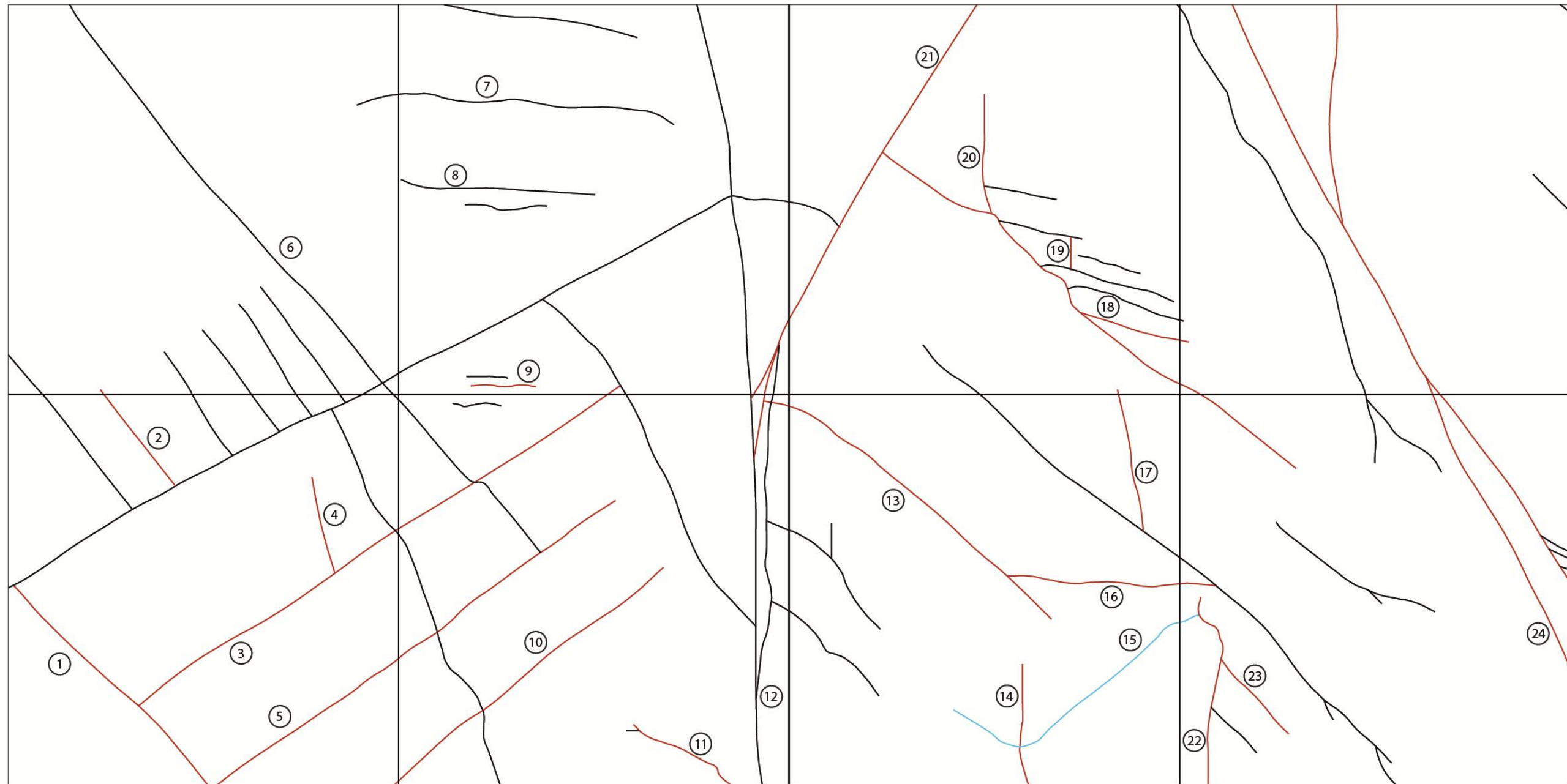
0 10 20 30 40 50cm

Facing North  
Bearing along face - 152





Moonlight Head face map 2- A-B (Map 1 of 3)

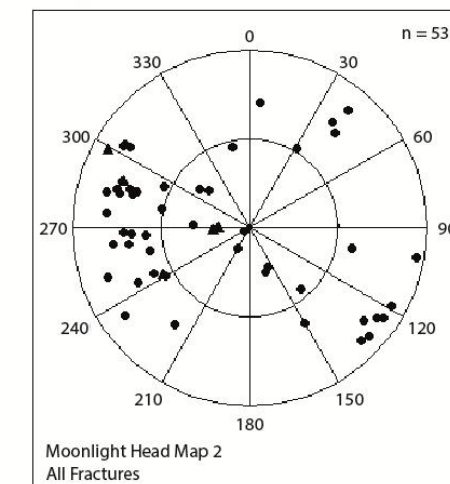
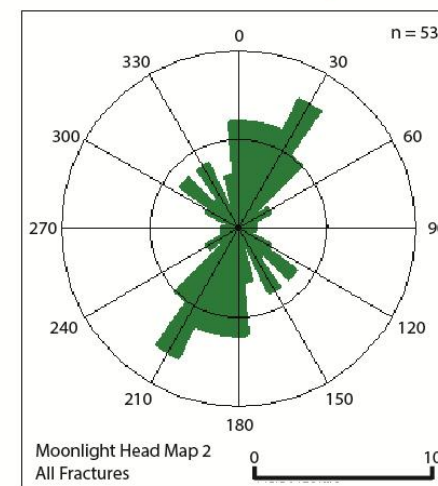
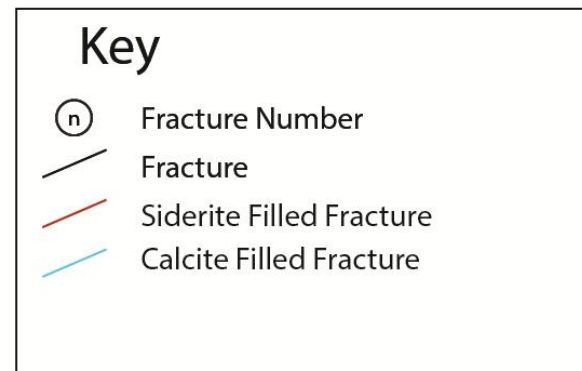


A

Transect Start S 38° 45.285'  
E 143° 12.762'  
Transect End S 38° 45.288'  
E 143° 12.771'

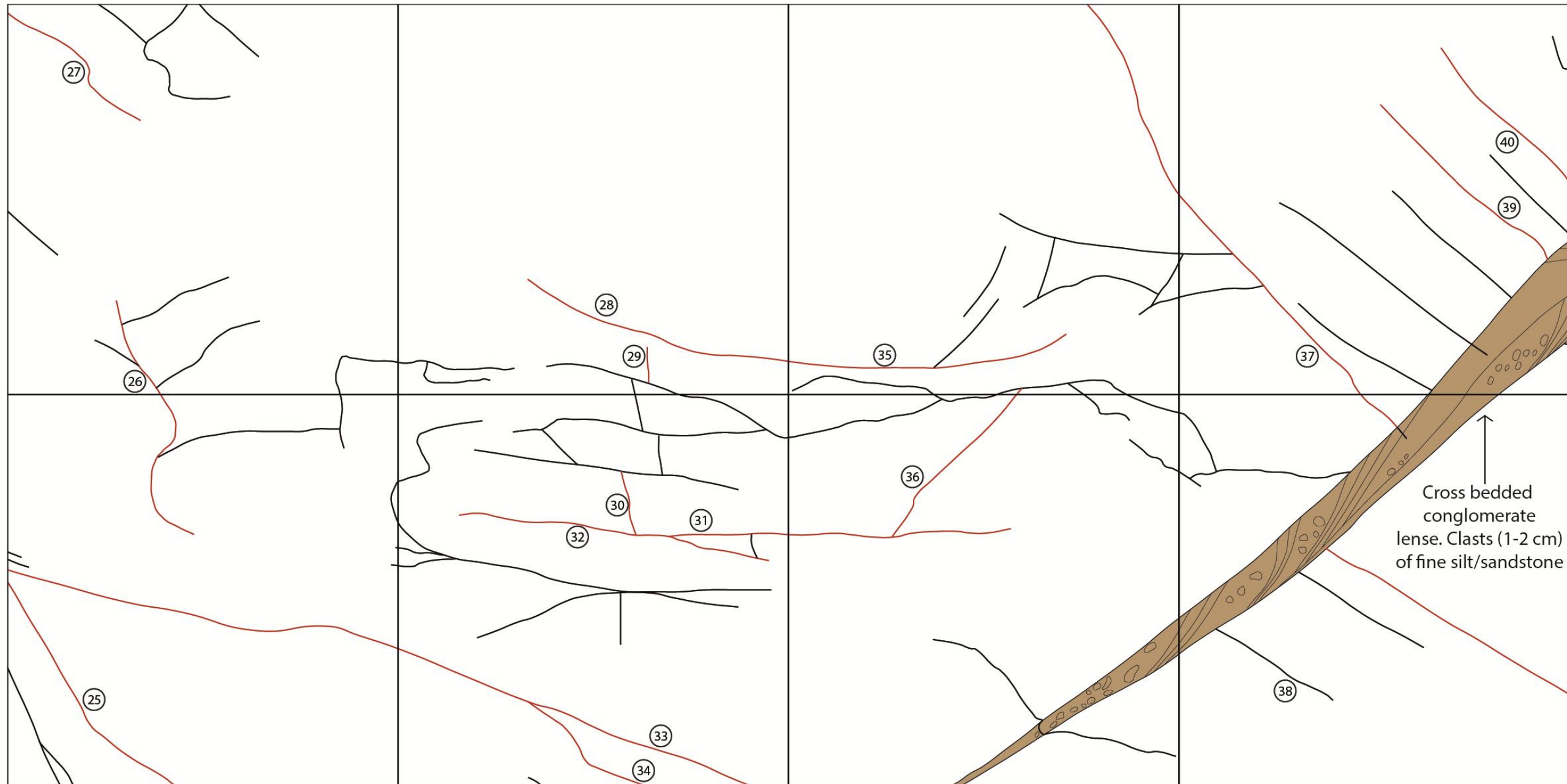


Facing North  
Bearing along face - 127°



B

Moonlight Head face map 2- B-C (Map 2 of 3)

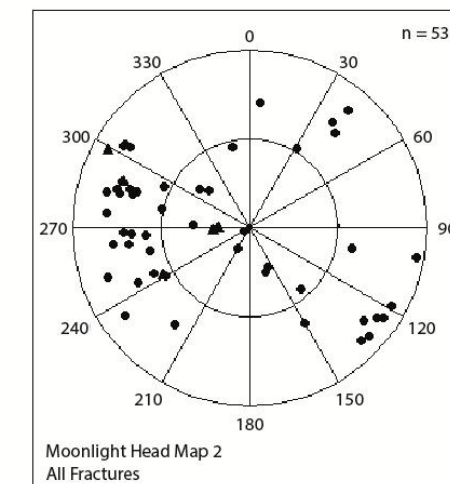
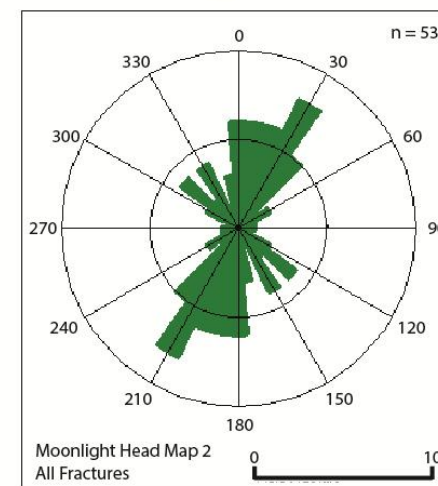
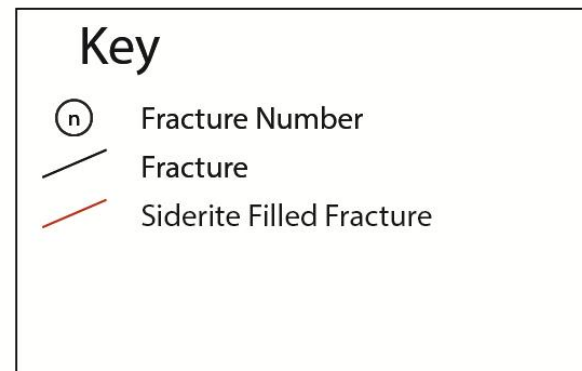


B

Transect Start S 38° 45.285'  
E 143° 12.762'  
Transect End S 38° 45.288'  
E 143° 12.771'



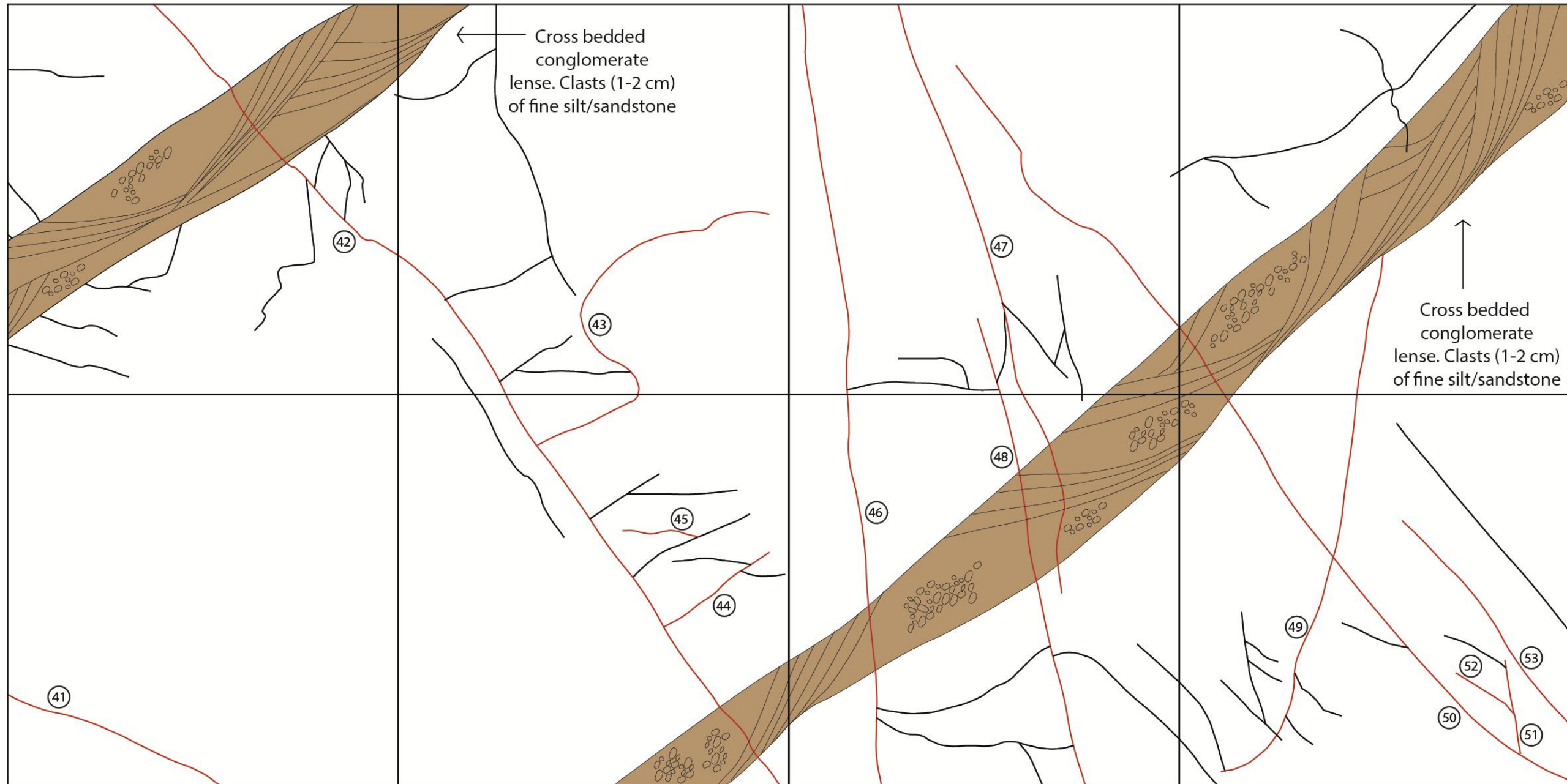
Facing North  
Bearing along face - 127°



C



Moonlight Head face map 2- C-D (Map 3 of 3)

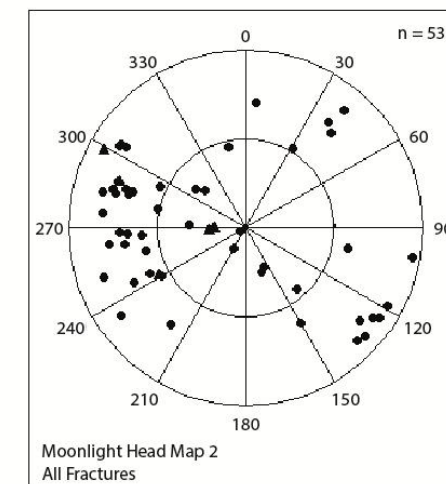
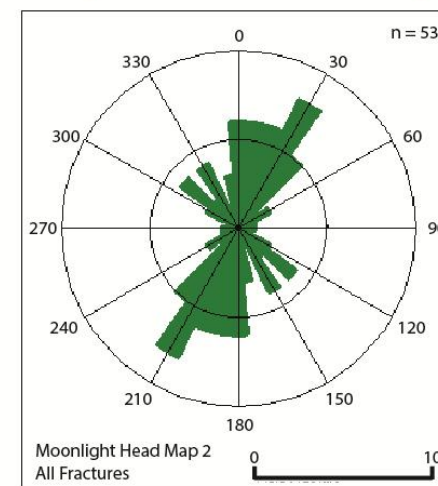
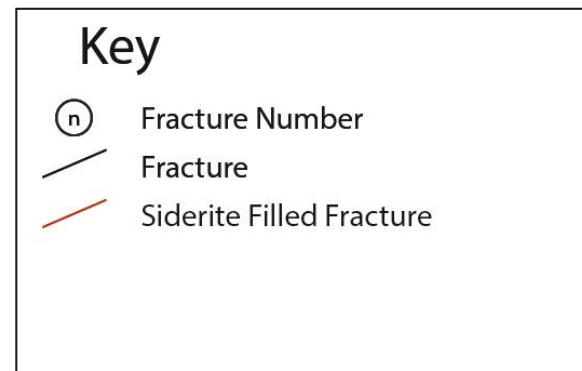


C

Transect Start S 38° 45.285'  
E 143° 12.762'  
Transect End S 38° 45.288'  
E 143° 12.771'



Facing North  
Bearing along face - 127°



D

Smythes Creek face map - A-B (Map 1 of 3)



A

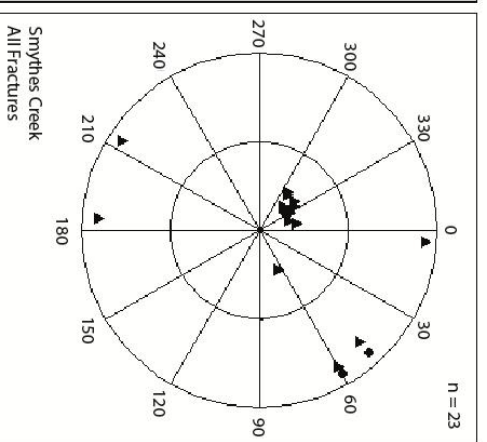
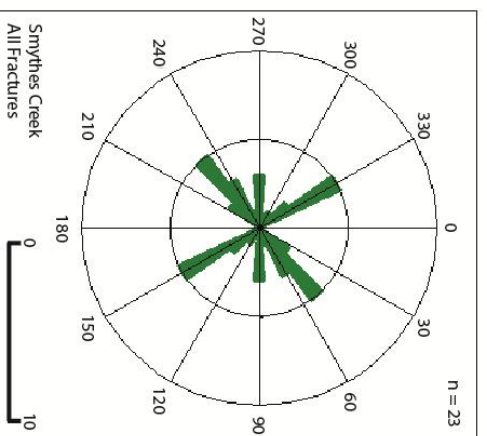
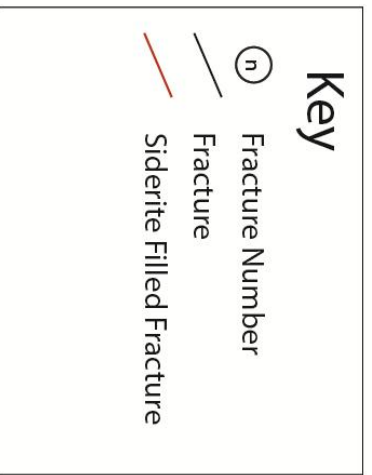
B

Transect Start S 38° 42.256'  
E 143° 45.792'

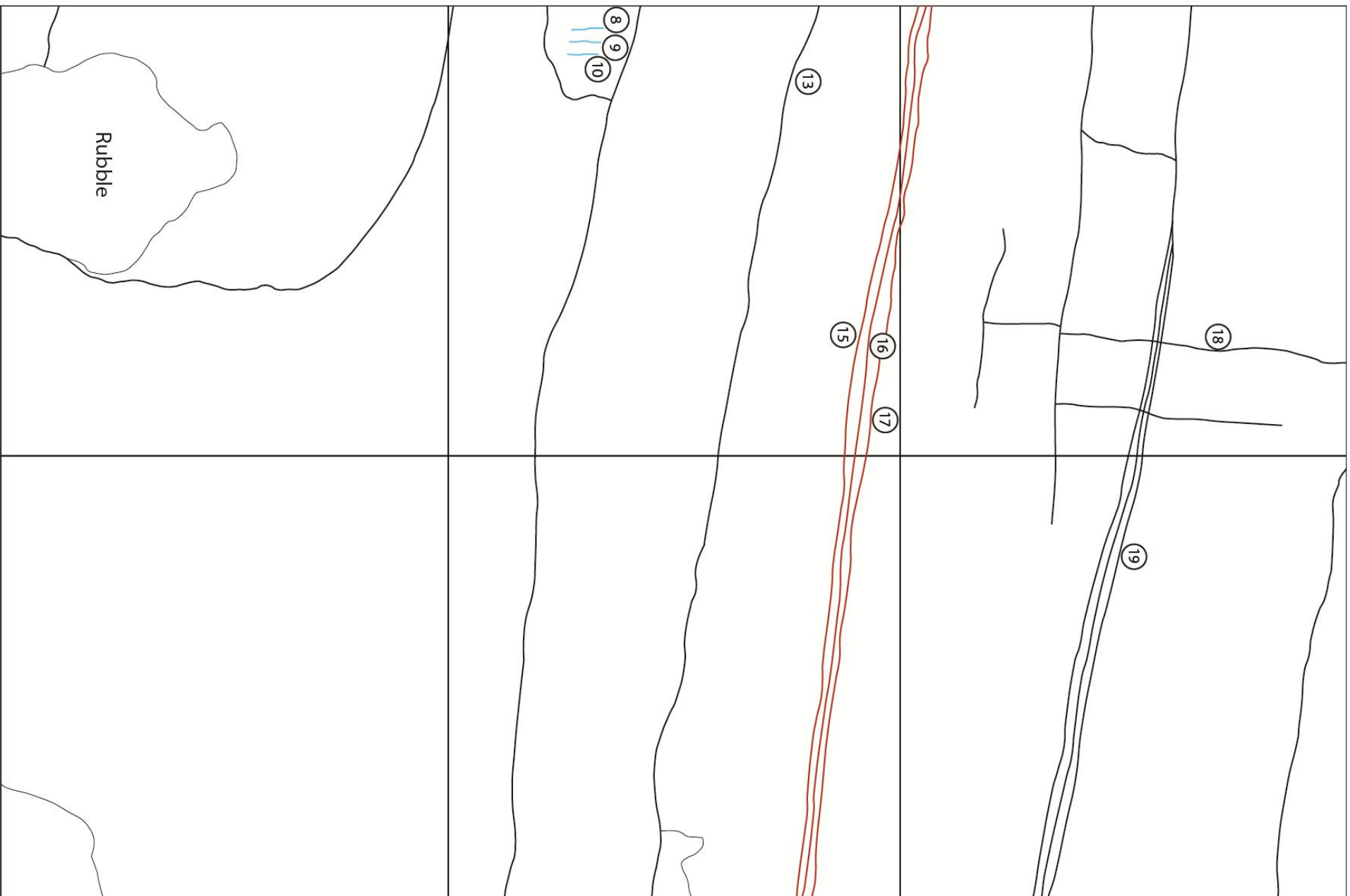
Transect End S 38° 42.260'  
E 143° 45.792'

0 10 20 30 40 50cm

Facing East  
Bearing along face - 202



Smythes Creek face map - B-C (Map 2 of 3)



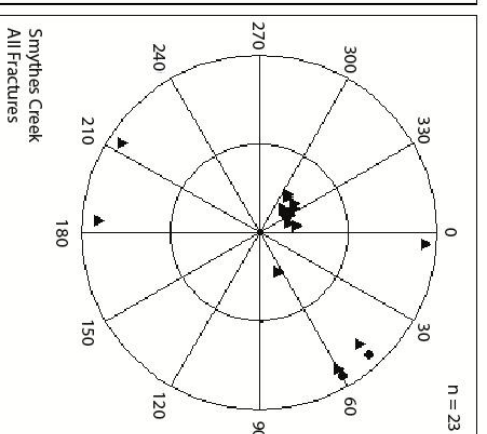
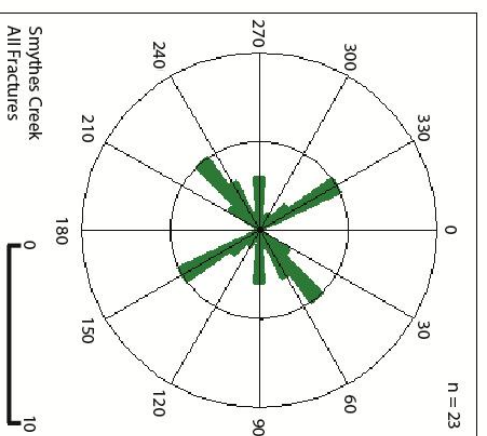
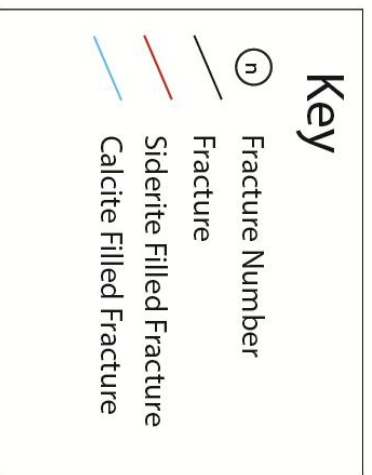
B

C

Transect Start S 38° 42.256'  
 E 143° 45.792'  
 Transect End S 38° 42.260'  
 E 143° 45.792'

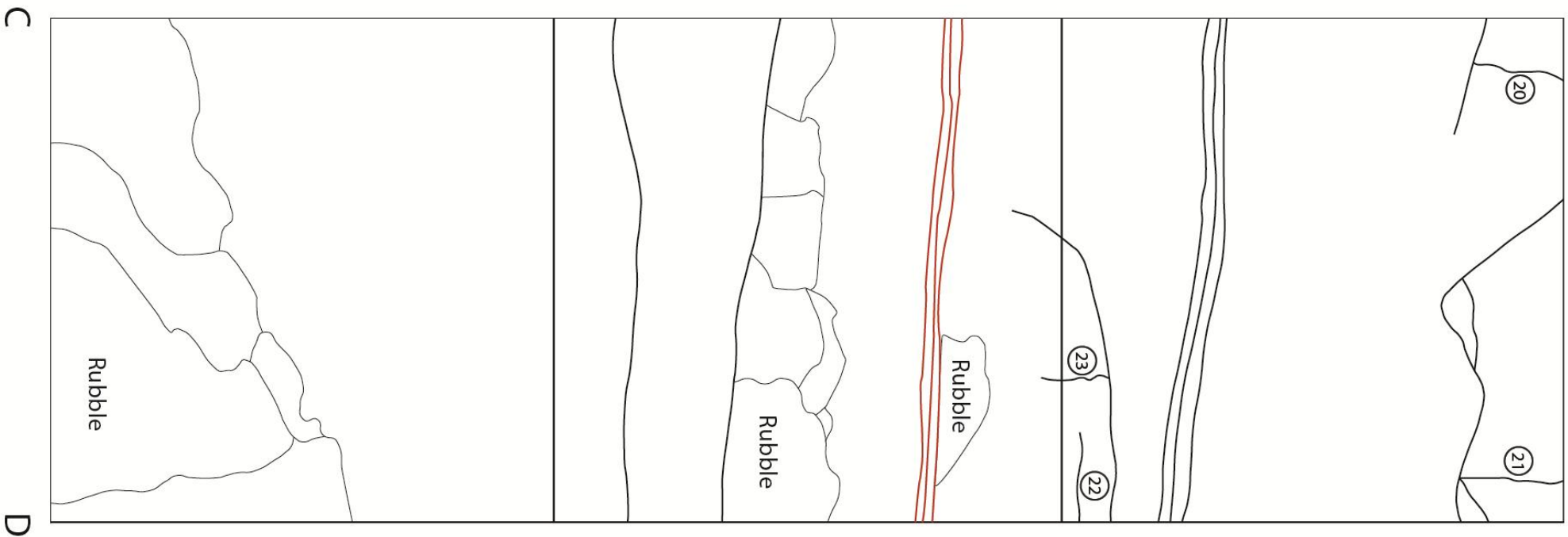


Facing East  
 Bearing along face - 202





Smythes Creek face map - C-D (Map 3 of 3)

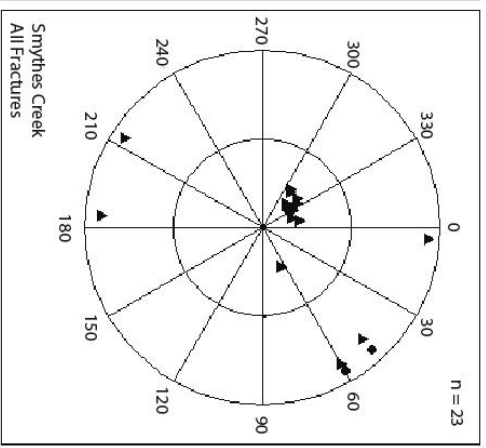
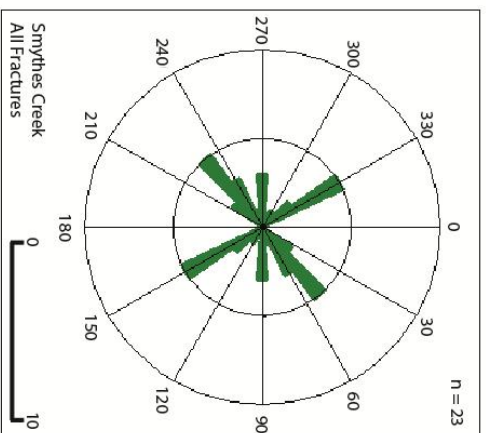
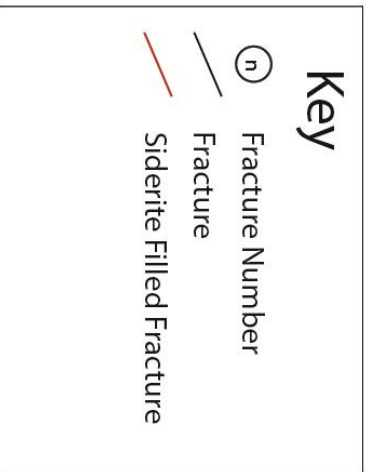


Transect Start S 38° 42.256'  
E 143° 45.792'

Transect End S 38° 42.260'  
E 143° 45.792'

0 10 20 30 40 50cm

Facing East  
Bearing along face - 202



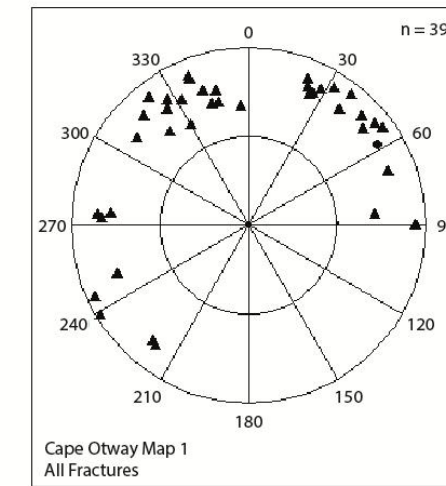
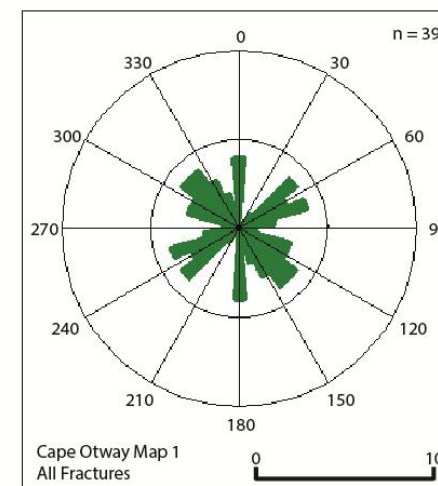
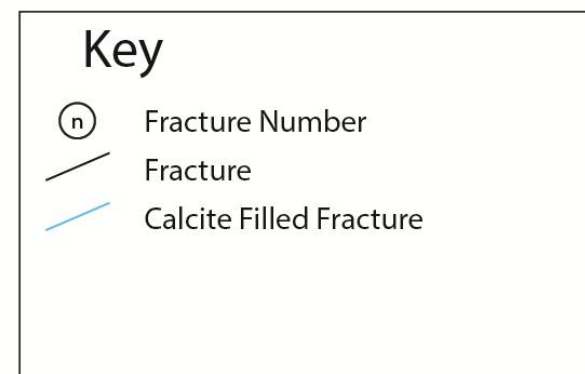
Cape Otway face map 1



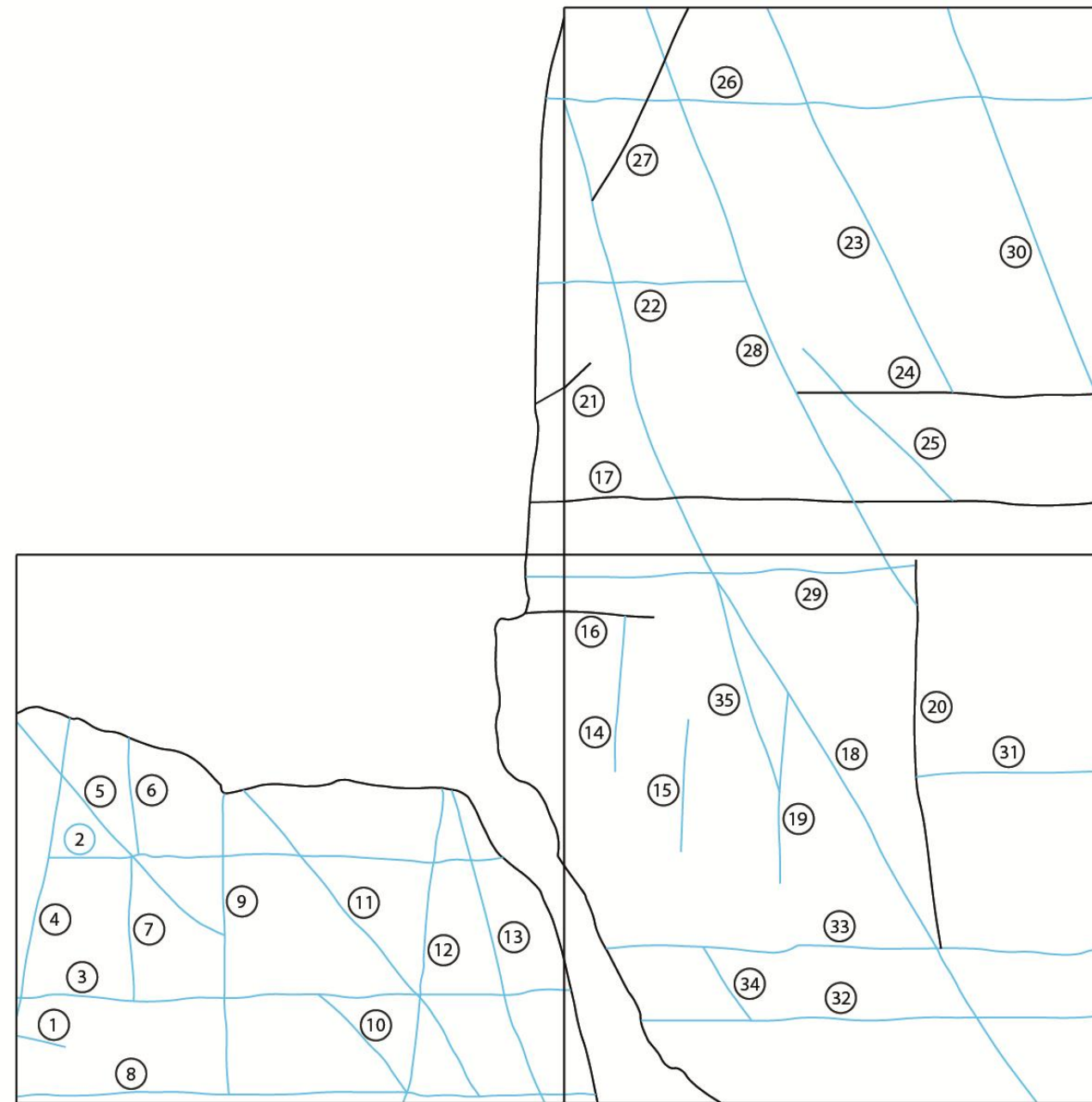
Transect Start S 38° 51.398'  
E 143° 30.923'  
Transect End S 38° 51.398'  
E 143° 30.923'



Facing South East  
Bearing along face - 256



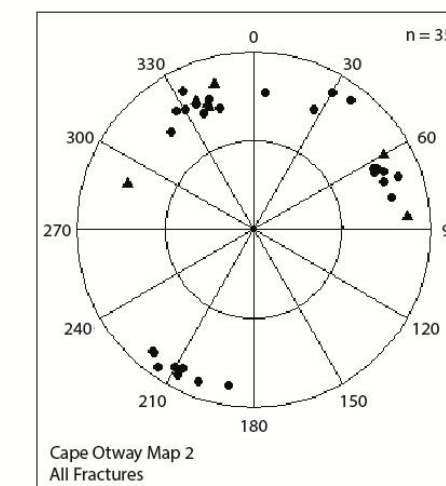
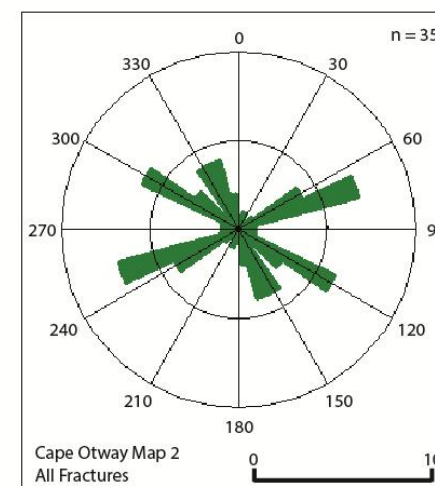
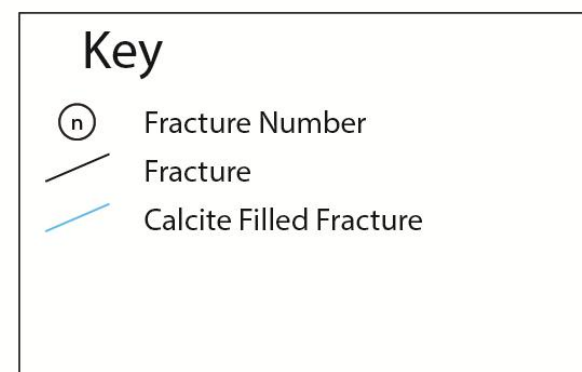
Cape Otway face map 2



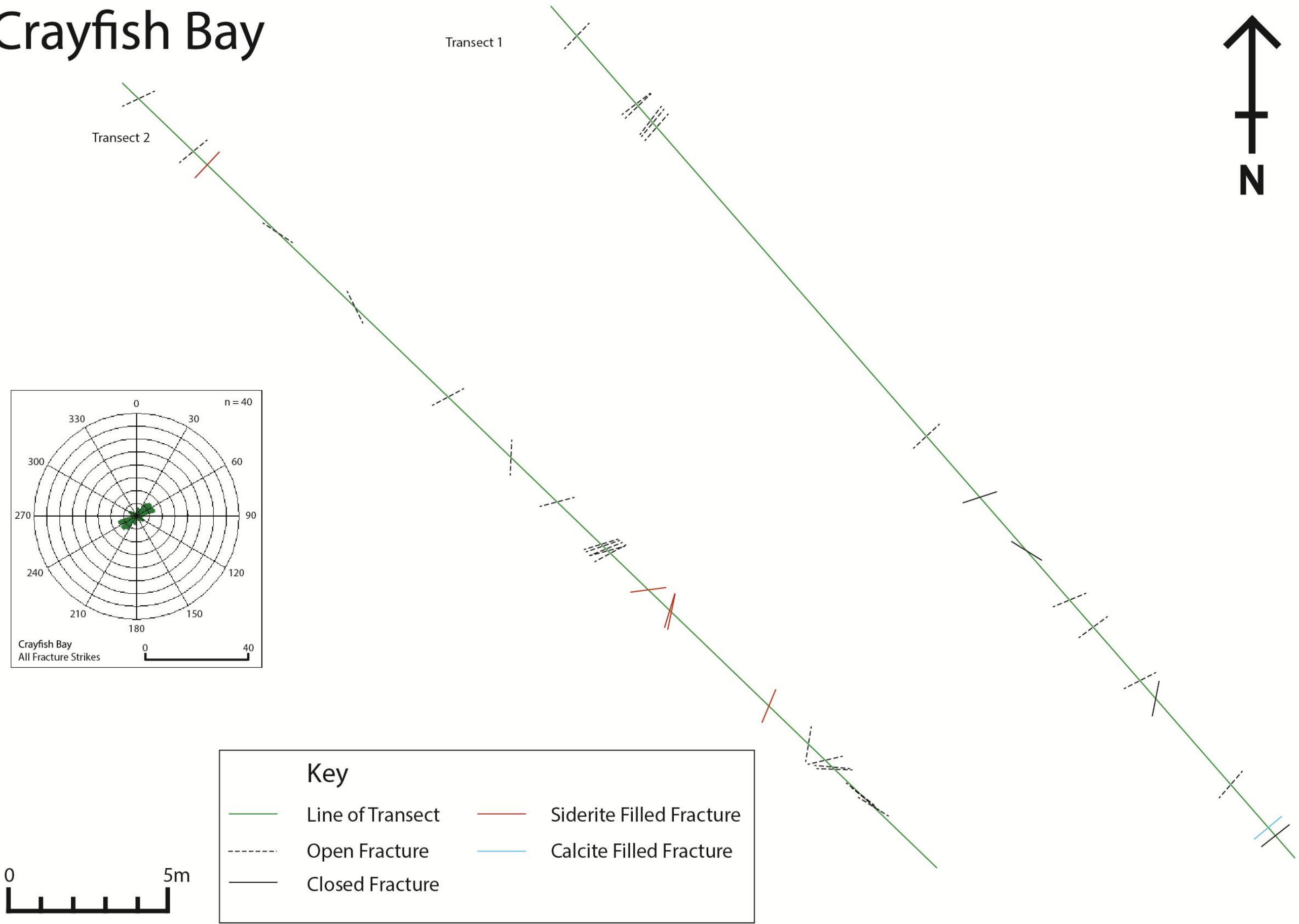
Transect Start S 38° 51.361'  
E 143° 30.943'  
Transect End S 38° 51.361'  
E 143° 30.943'



Facing South East  
Bearing along face - 248

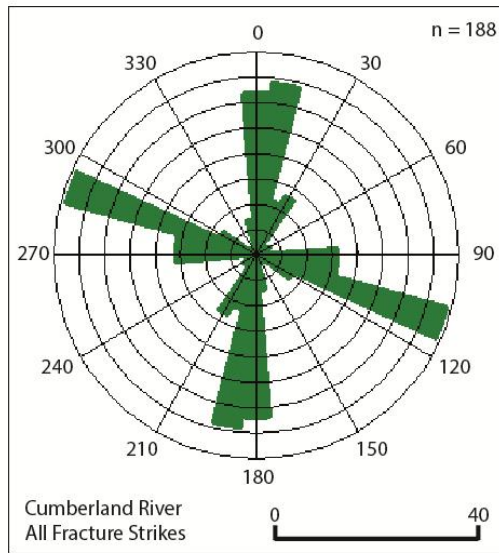
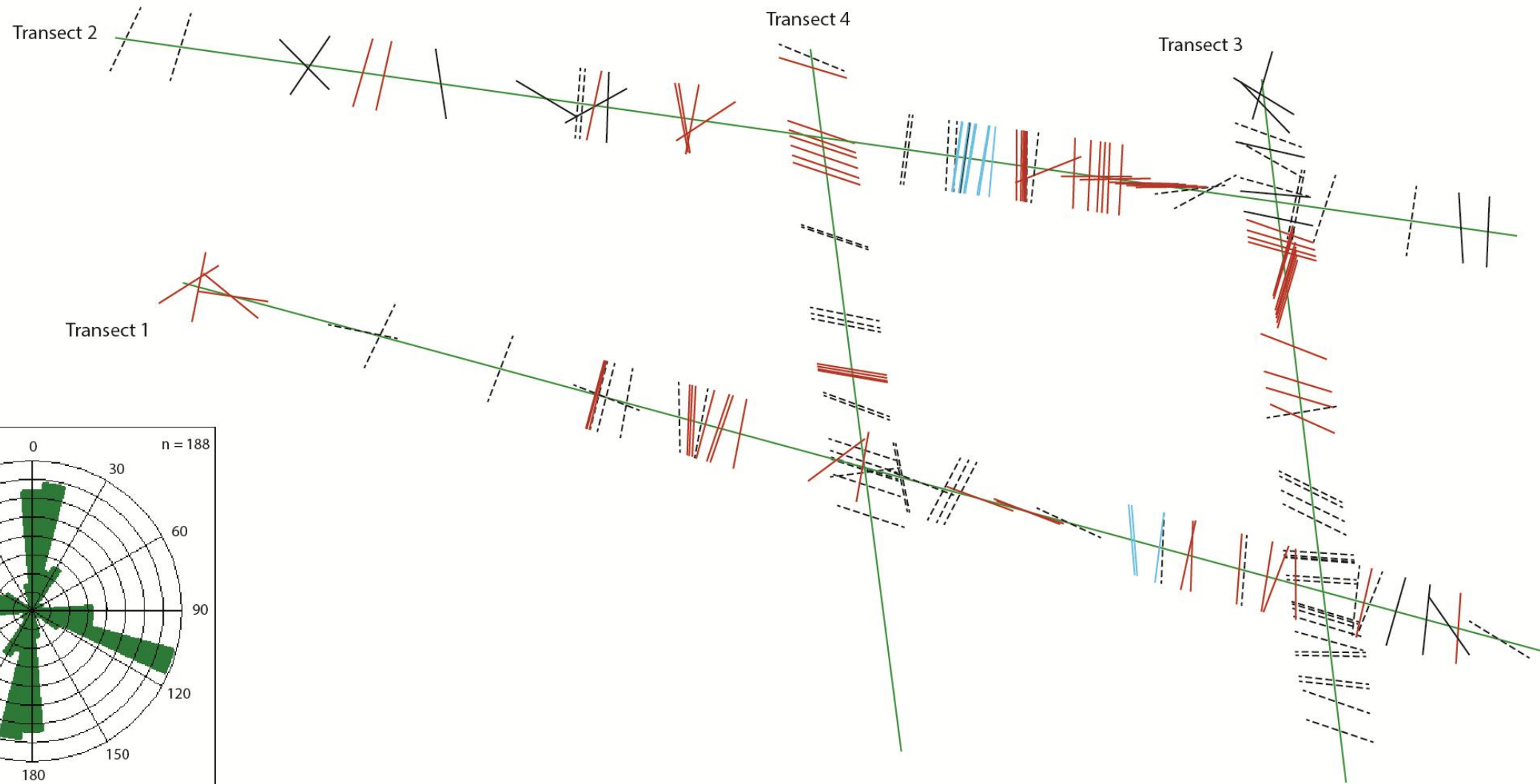


# Crayfish Bay



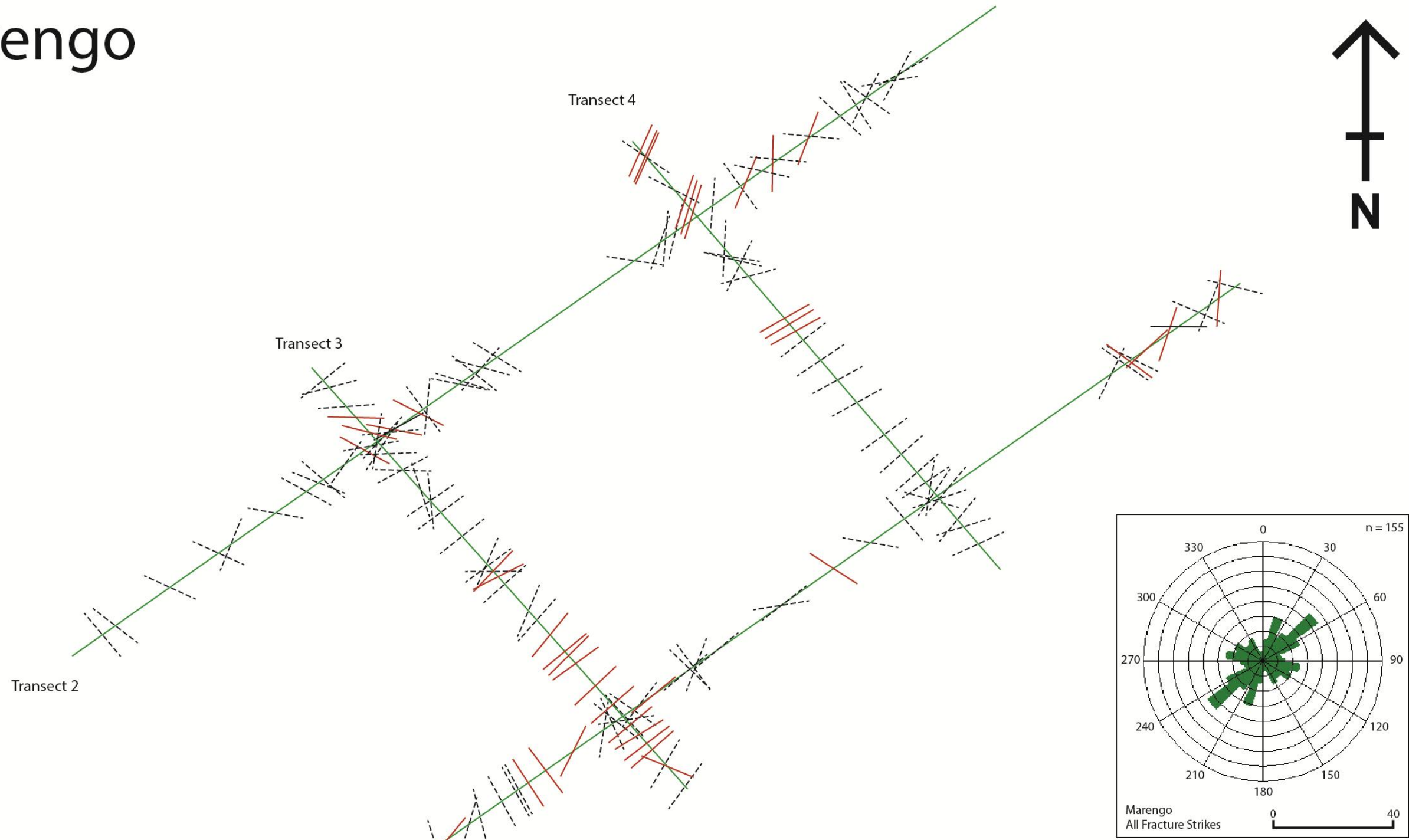


# Cumberland River



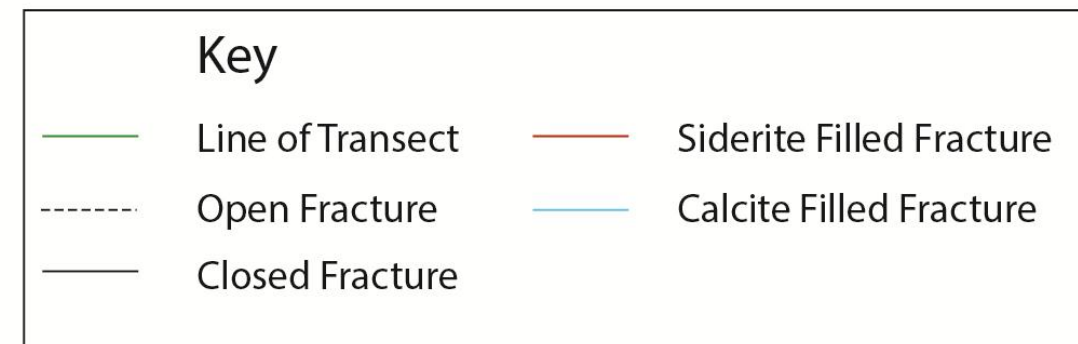
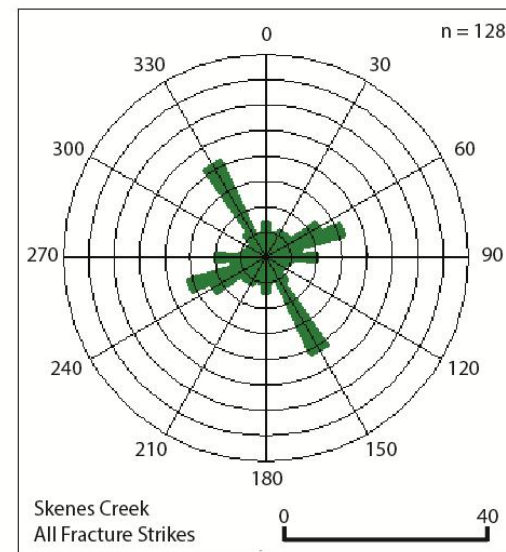
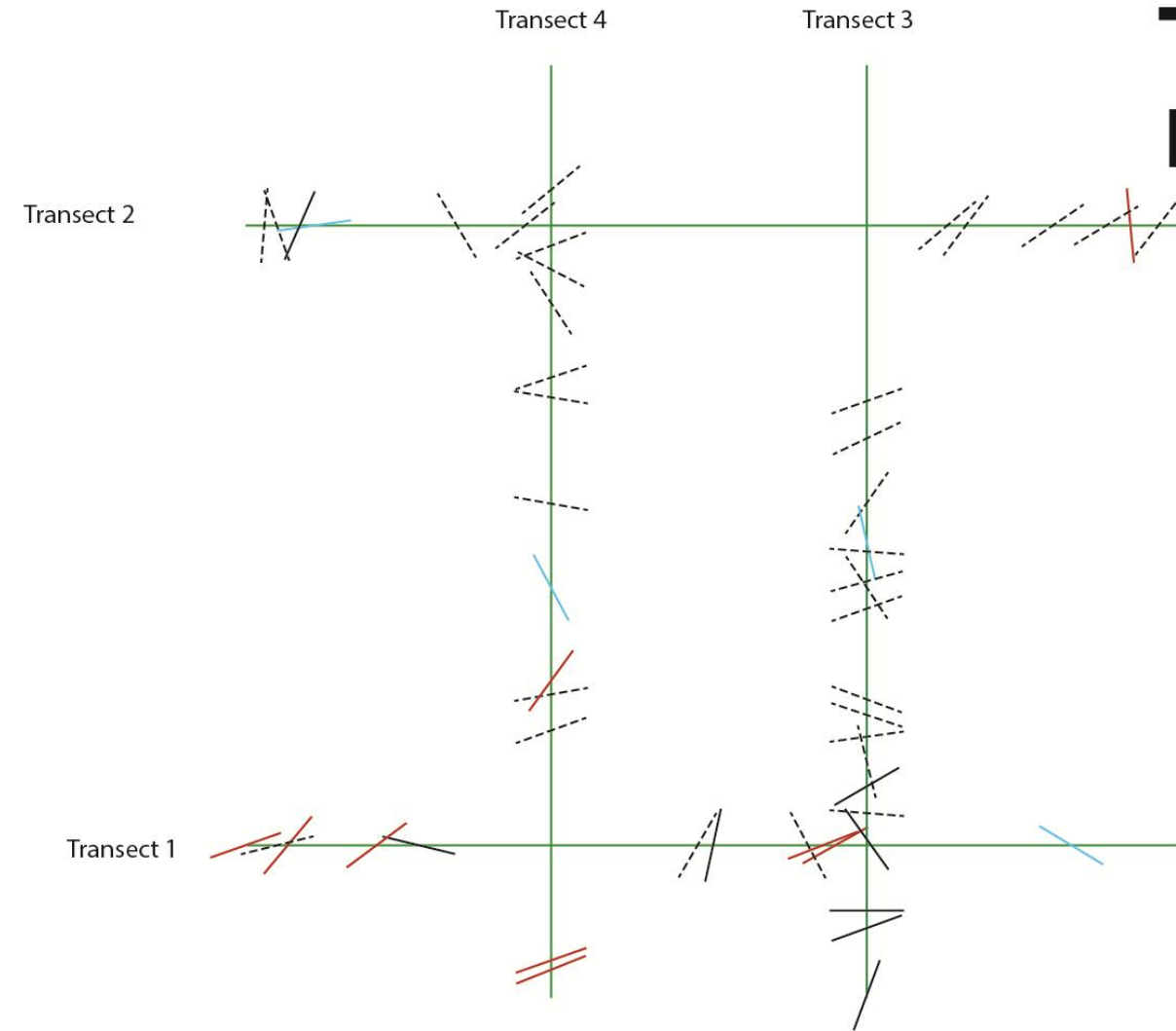
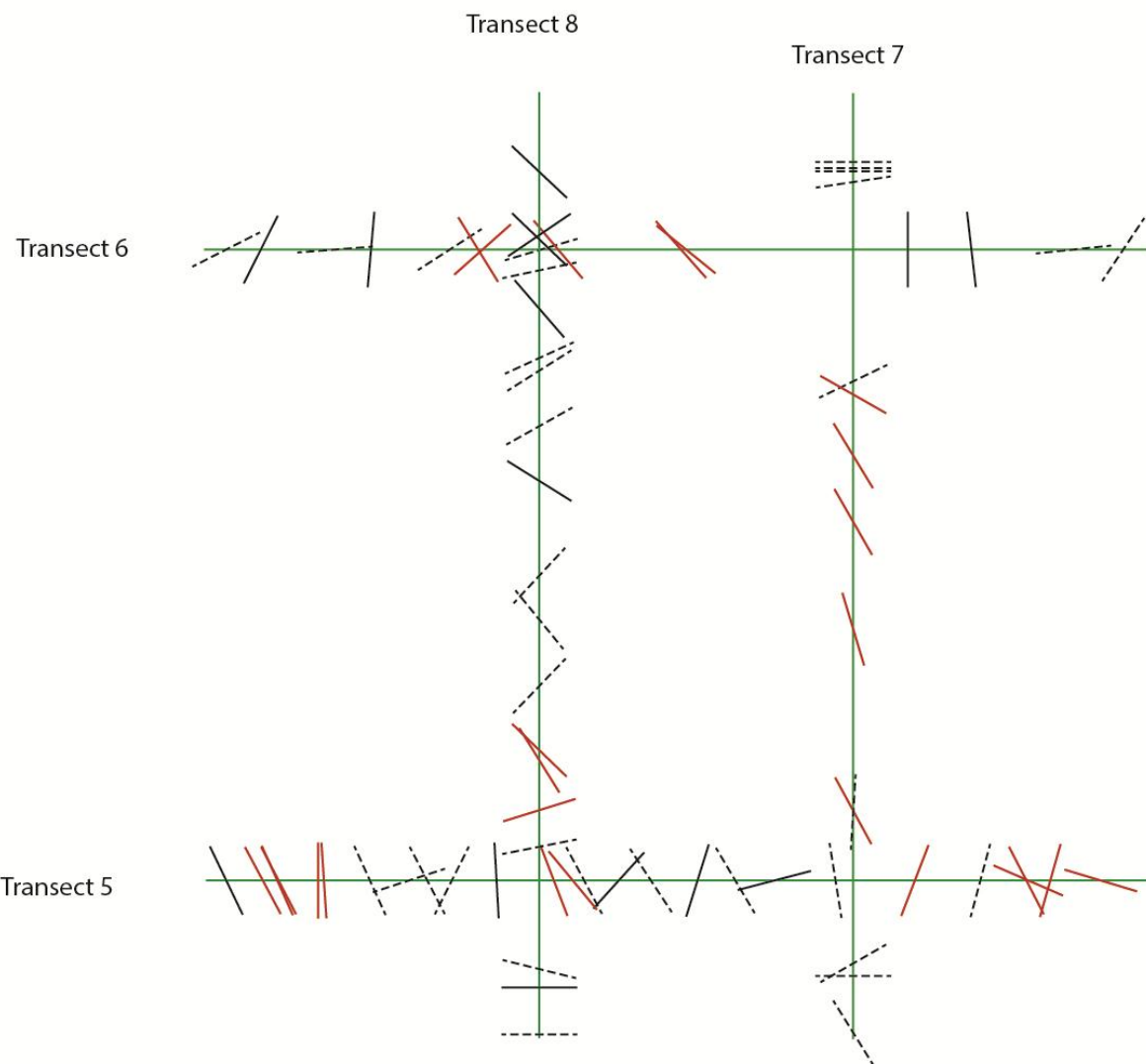
Key			
	Line of Transect		Siderite Filled Fracture
	Open Fracture		Calcite Filled Fracture
	Closed Fracture		

# Marengo



Key	
— (Green)	Line of Transect
- - - (Black)	Open Fracture
— (Black)	Closed Fracture
— (Red)	Siderite Filled Fracture
— (Blue)	Calcite Filled Fracture

# Skenes Creek

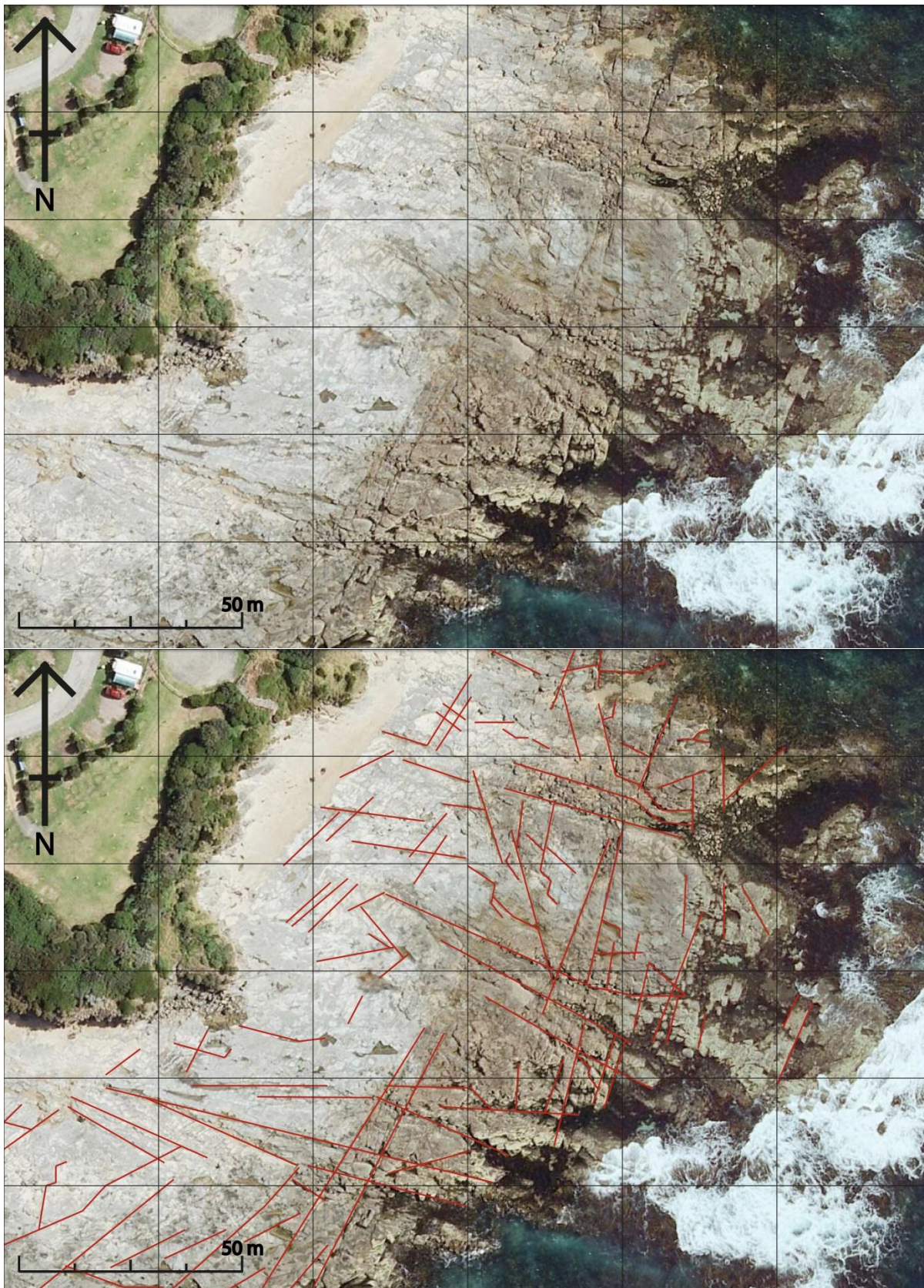


### **APPENDIX C: SATELLITE IMAGES**

Below are satellite images from this study before and after fractures were interpreted in the Otway Basin. Locations of field sites used for comparison with these images are shown in Figure Location Map. All fracture strikes were measured from grid north using the Line Tool in Adobe Illustrator CS6.



MARENGO





SKENES CREEK

